

COMPOSITE ELECTRODE FOR ELECTROCHEMICAL SUPERCAPACITORS

COMPOSITE ELECTRODE FOR ELECTROCHEMICAL SUPERCAPACITORS

By

XIAOFEI LI, B. A. Sci.

A Thesis

Submitted to the School of Graduate Studies

In Partial Fulfillment of the Requirements

For the Degree

Master of Science

McMaster University

© Copyright by Xiaofei Li, August 2012

MASTER OF APPLIED SCIENCE (2010)
(Material Science & Engineering)

McMaster University
Hamilton, Ontario

TITLE: Composite Electrode for Electrochemical Supercapacitors

AUTHOR: Xiaofei Li, B. A. Sci., (University of Windsor, Ontario, Canada)

SUPERVISOR: Professor I. Zhitomirsky

NUMBER OF PAGES: XII, 114

Abstract

The development of all-electric or plug-in hybrid vehicles requires the use of advanced energy storage devices with high power. Dedicated for energy storage, electrochemical supercapacitors (ES) offer the advantage of high power density. High power ES can provide load-leveling for batteries and fuel cells during starting, acceleration, hill climbing and braking. ES are important for reducing cycling of batteries, thus extending their lifetime by energy storage and delivery during fast transient operations such as in braking (storage) or start up and acceleration (supply).

The interest in polypyrrole (PPY) for the application in ES is attributed to the high specific capacitance (SC) of this material. The possibility of PPY deposition on stainless steel substrates is important for the practical applications of PPY films in ES, using low cost stainless steel current collectors. The important task is to avoid anodic dissolution of the substrates during PPY electropolymerization. Polypyrrole (PPY) films were electrochemically deposited on stainless steel substrates or Ni plaque from aqueous pyrrole solutions containing anionic additives. The method resulted in the formation of adherent and uniform films. The deposition yield was investigated at galvanostatic conditions. It was found that anionic additives can be used for the dispersion of multiwall carbon nanotubes (MWCNTs) and fabrication of composite PPY-MWCNT films. The deposition yield was studied under galvanostatic conditions. The mechanism of PPY-MWCNTs deposition was discussed. The incorporation of MWCNTs into the PPY during electropolymerization resulted in the formation of porous films. The films were investigated for the application in electrodes of electrochemical supercapacitors.

Electrochemical testing in the 0.5M Na₂SO₄ electrolyte solutions showed a capacitive behaviour in a voltage window of -0.5 to +0.4 V versus a saturated calomel electrode. The results indicated that the PPY–MWCNT films deposited on the stainless steel and nickel plaque substrates are promising electrode materials for ES.

Acknowledgement

I hereby sincerely acknowledge the support of many people without whom I would never have been able to complete this thesis.

First, I am greatly indebted to my supervisor, Dr. Igor Zhitomirsky, who has gone beyond a mere thesis supervisor by providing me with intellectual challenges, constant encouragements, and an appropriate research environment.

I would like to thank Chao Shi, who has introduced me to the electrochemical supercapacitors in the beginning of my research.

I would also thank all my group mates in the lab, Xin Pang, Yaohui Wang, Yanchao Sun, Deepark Komarappa, Lijia Yang, Mustafa Ata, Imran Deen, for their friendship and for rescuing me whenever I need help.

I am very thankful for the financial support from the Natural Science and Engineering Research Council of Canada (NSERC).

Table of Contents

Abstract.....	I
Acknowledgement	III
Table of Contents.....	IV
List of Figures	VII
List of Tables	XII
1 Introduction.....	1
2 Literature Review.....	3
2.1 Energy Storage Devices Development.....	3
2.2 Advantages of Supercapacitor Technology	4
2.3 Application of Electrochemical Supercapacitors	7
2.4 Principles of Energy Storage in Electrochemical Supercapacitors	9
2.4.1 Electric double layer supercapacitors (EDLCs).....	9
2.4.2 Pseudo-supercapacitors	11
2.5 Materials for Electrodes of Supercapacitors	13
2.5.1 Carbon-based Materials	14
2.5.2 Redox Pseudo-Capacitive Materials	19
2.5.3 Composite Materials	29
2.6 Electrolytes	31
2.6.1 Aqueous Electrolytes	32
2.6.2 Organic Electrolytes.....	32
2.6.3 Ionic liquid electrolytes.....	33
2.7 Problems Formulation.....	34
3 Objectives	35
4 Approach and Methodology.....	36

4.1 Novel Additives	36
4.2 Suggested Complexation Mechanism	38
5 Experimental Procedures	39
5.1 Materials Preparation	39
5.2 Electrodeposition Equipments	39
5.3 Electropolymerization procedures	40
6 Characterization	43
6.1 Electrochemical Characterization	43
6.2 Investigation of deposition yield.....	44
6.3 Scanning electron microscopy (SEM)	44
6.4 Film Adhesion Test.....	44
7 Results and Discussion.....	46
7.1 Electropolymerization of PPy using GA as an Anionic Dopant	46
7.1.1 Deposition Yield	46
7.1.2 Electrochemical Studies	47
7.1.3 Specific Capacitance	48
7.2 Electropolymerization of PPy using SSA as an Anionic Dopant.....	49
7.2.1 Cyclic Voltammograms for Electropolymerization of PPy	49
7.2.2 Galvanostatic Electropolymerization of PPy	50
7.2.3 Characterizations of PPy Film Prepared Using SSA	52
7.2.4 Corrosion Performance of PPy Coated Stainless Steel	59
7.3 Pulse Deposition of PPy films using SSA as an Anionic Dopant.....	62
7.3.1 Deposition Yield	63
7.3.2 Electrochemical Studies	64
7.3.3 Specific Capacitance	66

7.3.4 Morphology Characterization	67
7.3.5 Electrochemical Impedance Spectra	69
7.4 Electro-Co-Deposition of PPy/SWCNTs from aqueous SSA/PPE solutions	70
7.4.1 The Influence of PPE on Dispersion of SWCNTs	71
7.4.2 Electrochemical Studies	72
7.4.3 Specific Capacitance	73
7.4.4 Morphology Characterization	74
7.4.5 Electrochemical Impedance Spectra	77
7.5 Electropolymerization of PPy using PV as an Anionic Dopant.....	78
7.5.1 Cyclic Voltammograms for Electropolymerization of PPy	78
7.5.2 Galvanostatic Electropolymerization of PPy	79
7.5.3 Characterizations of PPy Film Prepared Using PV	81
7.6 Electro-Co-Deposition of PPy/MWCNTs from aqueous PV solutions	87
7.6.2 Deposition Yield of MWCNT.....	88
7.6.3 Morphology Characterization	92
7.7 Electro-Co-Deposition of PPy/MWCNTs from aqueous PV solutions on Nickel plaques .	94
7.7.1 Electrochemical Studies	94
7.7.2 Specific Capacitance	96
7.7.3 Electrochemical Impedance Spectra	97
7.7.4 Morphology Characterization	99
7.8 Pulse Deposition of PPy/MWCNTs from aqueous PV solutions on Nickel Plaques	100
7.8.1 Characterizations of PPy/MWCNTs Film	100
7.8.2 Morphology Characterization	103
8 Conclusions.....	107
References.....	109

List of Figures

Figure 2 - 1 Ragone plot for various energy storage and conversion devices [8]	5
Figure 2 - 2 Typical configuration of an EDLC cell [4]	10
Figure 2 - 3 Schematic diagram of the pore size network of an activated carbon grain [23]	15
Figure 2 - 4 Conceptual diagrams of SWCNT (A) and MWCNT (B) [36]	18
Figure 2 - 5 Polyaniline (PANI) structure [46]	24
Figure 2 - 6 Formation of cation radical [54].....	25
Figure 2 - 7 Resonance form of cation radical [54]	25
Figure 2 - 8 Formation of the dihydromer dication [54]	25
Figure 2 - 9 Formation of the aromatic dimer [54]	26
Figure 2 - 10 Formation of cation radical [54].....	26
Figure 2 - 11 Formation of trimer [54]	26
Figure 2 - 12 Formation of final PPy conducting polymer [54].....	27
Figure 2 - 13 Composite material to improve both energy and power densities [8]	29
Figure 4 - 1 Chemical structures of novel additives (a) GA, (b) SSA and (c) PV	37
Figure 4 - 2 Chemical structure of PPE polymer	37
Figure 4 - 3 Chelate complexes formed with Fe^{2+} by (a) GA, (b) SSA and (c) PV	38
Figure 5 - 1 Electrochemical cell (L: Platinum; M: Stainless steel; R: Platinum)	39
Figure 5 - 2 Scheme of PPy film preparation on SSt	40
Figure 5 - 3 Scheme of PPy/CNT composite fabrication process by using SSA	41
Figure 5 - 4 Scheme of PPy/CNT composite fabrication process by using PV	42
Figure 6 - 1 Classification of Adhesion Test results [74]	45
Figure 7 - 1 PPy/GA film mass versus deposition time at 1 mAcm^{-2}	46
Figure 7 - 2 CV for the $211 \mu\text{gcm}^{-2}$ film deposited from the 0.2 M pyrrole solution containing 0.05 M GA on stainless steel in 0.5 M Na_2SO_4 electrolyte at scan rate of (a) 2, (b) 5 and (c) 10 mVs^{-1}	47

Figure 7 - 3 SC versus scan rates for the $211 \mu\text{gcm}^{-2}$ film deposited from the 0.2 M pyrrole solution containing 0.05 M GA on a stainless steel	48
Figure 7 - 4 Cyclic voltammograms at a scan rate of 20 mVs^{-1} from solution containing 0.01 M SSA and 0.1 M pyrrole	49
Figure 7 - 5 Galvanostatic behavior of PPy deposit on stainless steel from a 0.10 M pyrrole solution in the presence of 0.01 M (a) PTSA and (b) SSA at a current density of 1 mA cm^{-2} . Inset shows the chemical structure of (a) PTSA and (b) SSA.	51
Figure 7 - 6 PPy/SSA film mass versus deposition time at 1 mA cm^{-2}	53
Figure 7 - 7 Cyclic voltammetry data at scan rates of a (a) 2 mV s^{-1} , (b) 10 mV s^{-1} , (c) 50 mV s^{-1} for $208 \mu\text{g cm}^{-2}$ film prepared at a current density of 1 mA cm^{-2} from 0.1M pyrrole solution containing 0.01 M SSA.....	54
Figure 7 - 8 Cyclic voltammetry data at scan rate of 2 mV s^{-1} for the films of different mass: (a) $108.85 \mu\text{g cm}^{-2}$, (b) $160.42 \mu\text{g cm}^{-2}$, (c) $263.54 \mu\text{g cm}^{-2}$ prepared at a current density of 1 mA cm^{-2} from 0.1 M pyrrole solution containing 0.01 M SSA.	55
Figure 7 - 9 Limited depth of ion penetration	56
Figure 7 - 10 Specific capacitance versus scan rate for the films of different mass: (a) $108.85 \mu\text{g cm}^{-2}$, (b) $160.42 \mu\text{g cm}^{-2}$, (c) $263.54 \mu\text{g cm}^{-2}$ prepared at current density of 1 mA cm^{-2} from 0.1 M pyrrole solution containing 0.01 M SSA.	57
Figure 7 - 11 SEM image of surface for PPy/SSA on stainless steel foil substrate.	58
Figure 7 - 12 SEM images for the PPy/SSA film on a stainless steel mesh. Inset is the surface image in the circle area at high magnification.	59
Figure 7 - 13 OCP-time curve recorded for (a) bare stainless steel and (b) PPy coated stainless steel in aqueous 0.5 M Na_2SO_4 solution.	60
Figure 7 - 14 Potentiodynamic polarization curves for (a) bare stainless steel and (b) PPy coated stainless steel recorded in a 0.5 M Na_2SO_4 solution.	61
Figure 7 - 15 Deposit mass versus charge passed for deposition from 0.1 M pyrrole solution containing 0.01 M SSA using (a) galvanostatic method, and (b) pulse deposition with ON/OFF times of 0.5 s.	63
Figure 7 - 16 Cyclic voltammetry data at a scan rate of 2 mVs^{-1} for 0.2 mg cm^{-2} films prepared from 0.1 M pyrrole solution containing 0.01 M SSA using (a) galvanostatic method and (b,c) pulse deposition method with ON/OFF times of (b) 0.5 and (c) 1.5 s.	64

Figure 7 - 17 Cyclic voltammetry data at a scan rate of 5 mVs^{-1} for 0.2 mg cm^{-2} films prepared from 0.1 M pyrrole solution containing 0.01 M SSA using (a) galvanostatic method and (b,c) pulse deposition method with ON/OFF times of (b) 0.5 and (c) 1.5 s .	65
Figure 7 - 18 Cyclic voltammetry data at a scan rate of 10 mVs^{-1} for 0.2 mg cm^{-2} films prepared from 0.1 M pyrrole solution containing 0.01 M SSA using (a) galvanostatic method and (b,c) pulse deposition method with ON/OFF times of (b) 0.5 and (c) 1.5 s .	66
Figure 7 - 19 SC versus scan rate for 0.2 mg cm^{-2} films prepared from 0.1 M pyrrole solution containing 0.01 M SSA using (a) galvanostatic method and (b,c) pulse deposition method with ON/OFF times of (b) 0.5 and (c) 1.5 s .	67
Figure 7 - 20 SEM images of films prepared from 0.1 M pyrrole solution containing 0.01 M SSA using (A) galvanostatic method, and (B) pulse deposition with ON/OFF times of 0.5 s .	68
Figure 7 - 21 Nyquist plots of complex impedance $Z^* = Z' - iZ''$ for 0.2 mg cm^{-2} films prepared from 0.1 M pyrrole solution containing 0.01 M SSA using (a) galvanostatic method and (b) pulse deposition method with ON/OFF times of 0.5 s .	70
Figure 7 - 22 Aqueous PPE (left), SWCNT (middle), PPE and SWCNT (right).	71
Figure 7 - 23 Cyclic voltammetry data at a scan rate of 20 mVs^{-1} for $160 \text{ } \mu\text{g cm}^{-2}$ films prepared at current density of 1 mA cm^{-2} from 0.1 M pyrrole solution containing 0.01 M SSA using (a) without additives and (b) containing 0.1 gL^{-1} PPE and 0.1 gL^{-1} SWCNTs.	72
Figure 7 - 24 SC versus scan rate in a $0.5 \text{ M Na}_2\text{SO}_4$ solution for $160 \text{ } \mu\text{g cm}^{-2}$ films prepared at a current density of 1 mA cm^{-2} from 0.1 M pyrrole solution containing 0.01 M SSA: (a) without additives and (b) containing 0.1 gL^{-1} PPE and 0.1 gL^{-1} SWCNT.	73
Figure 7 - 25 SEM image of film prepared at a current density of 1 mA cm^{-2} from 0.1 M pyrrole solution containing 0.01 M SSA.	75
Figure 7 - 26 SEM image of film prepared at a current density of 1 mA cm^{-2} from 0.1 M pyrrole solution containing 0.01 M SSA containing 0.1 gL^{-1} PPE and 0.1 gL^{-1} SWCNT.	76
Figure 7 - 27 SEM image of film prepared at a current density of 1 mA cm^{-2} from 0.1 M pyrrole solution containing 0.01 M SSA, 0.1 gL^{-1} PPE and 0.1 gL^{-1} SWCNT at higher magnification. ...	76
Figure 7 - 28 Nyquist plots for $160 \text{ } \mu\text{g cm}^{-2}$ films prepared at a current density of 1 mA cm^{-2} from 0.1 M pyrrole solution containing 0.01 M SSA: (a) without additives (b) containing 0.1 gL^{-1} PPE and 0.1 gL^{-1} SWCNT and an equivalent circuit.	77
Figure 7 - 29 CV at a scan rate of 20 mVs^{-1} at a current density of 1 mA cm^{-2} for 6.7 gL^{-1} pyrrole solution, containing 0.1 gL^{-1} PV.	78
Figure 7 - 30 Potential versus time for 6.7 gL^{-1} pyrrole solution, containing 0.1 gL^{-1} PV.	80

Figure 7 - 31 Potential versus time from pyrrole solution containing oxalic acid [86].	80
Figure 7 - 32 Chemical structure of (A) Pyrocatechol violet (PV); (B) m-Cresol Purple sodium salt (CP); (C) complex formed by chemisorption of PV on metal (Fe) surface.	81
Figure 7 - 33 Deposit mass versus time at a current density of 1 mAcm^{-2} for 6.7 gL^{-1} pyrrole solution, containing 0.1 gL^{-1} PV.	82
Figure 7 - 34 CV for the $160 \text{ } \mu\text{g cm}^{-2}$ film deposited from the 6.7 gL^{-1} pyrrole solution containing 1 gL^{-1} PV on a stainless steel substrate at scan rate of (a) 2, (b) 5 and (c) 10 mV s^{-1} .	84
Figure 7 - 35 SC for the (a) $222 \text{ } \mu\text{g cm}^{-2}$, (b) $160 \text{ } \mu\text{g cm}^{-2}$ film deposited from the 6.7 gL^{-1} pyrrole solution containing 1 gL^{-1} PV on a stainless steel substrate at current density 1 mA cm^{-2} .	85
Figure 7 - 36 Nyquist plot in a $0.5\text{M Na}_2\text{SO}_4$ solution for 160 mgcm^{-2} film prepared at a current density of 1 mAcm^{-2} from 6.7 gL^{-1} pyrrole solution containing 1 gL^{-1} PV on SS substrate.	86
Figure 7 - 37 Aqueous PV (left), MWCNT (middle), PV and MWCNT (right).	87
Figure 7 - 38 Deposit mass versus PV concentration in 1 gL^{-1} MWCNT suspension at a deposition voltage of 20V and deposition time of 6 min.	89
Figure 7 - 39 Deposit mass versus deposition time for 1 gL^{-1} MWCNT suspension, containing 1 gL^{-1} PV at a current density of 1 mAcm^{-2} .	90
Figure 7 - 40 SEM images of films prepared at a current density of 1 mAcm^{-2} : (A) PPY, deposited from 6.7 gL^{-1} pyrrole solution, containing 1 gL^{-1} PV (B) MWCNT, deposited from 1 gL^{-1} MWCNT suspension, containing 1 gL^{-1} PV (C) composite PPY-MWCNT, deposited from 6.7 gL^{-1} pyrrole solution, containing 1 gL^{-1} PV and 0.1 gL^{-1} MWCNT, and corresponding pictures of the films on stainless steel substrates (D)(a) PPY, (b) MWCNT and (c) PPY-MWCNT.	93
Figure 7 - 41 CVs for 350 mg cm^{-2} composite PPY-MWCNT film deposited at a current density of 1 mAcm^{-2} from 6.7 gL^{-1} pyrrole solution containing 1 gL^{-1} PV and 0.1 gL^{-1} CNTs on nickel plaque substrate at scan rate of (a) 2, (b) 10 and (c) 20 mV s^{-1} .	95
Figure 7 - 42 CVs for $660 \text{ } \mu\text{g cm}^{-2}$ composite PPY-MWCNT film deposited at a current density of 1 mAcm^{-2} from 6.7 gL^{-1} pyrrole solution containing 1 gL^{-1} PV and 0.1 gL^{-1} CNTs on nickel plaque substrate at scan rate of (a) 2, (b) 10 and (c) 20 mV s^{-1} .	96
Figure 7 - 43 SC versus scan rate, (a) $350 \text{ } \mu\text{gcm}^{-2}$, (b) $660 \text{ } \mu\text{gcm}^{-2}$ films prepared at a current density of 1 mAcm^{-2} from 6.7 gL^{-1} pyrrole solution containing 1 gL^{-1} PV and 0.1 gL^{-1} CNTs on nickel plaque substrate.	97
Figure 7 - 44 Nyquist plots in a $0.5\text{M Na}_2\text{SO}_4$ solution for (a) $350 \text{ } \mu\text{gcm}^{-2}$, (b) $660 \text{ } \mu\text{gcm}^{-2}$ films prepared at a current density of 1 mAcm^{-2} from 6.7 gL^{-1} pyrrole solution containing 1 gL^{-1} PV and 0.1 gL^{-1} CNTs on nickel plaque substrate.	98

Figure 7 - 45 SEM image at X1000 magnifications of as-received plaques.....	99
Figure 7 - 46 SEM image at X10000 magnifications of as-received plaques.....	99
Figure 7 - 47 CVs at a scan rate of 20 mVs^{-1} for 1 mgcm^{-2} PPy-MWCNT films prepared at (a) a constant current density of 1 mAcm^{-2} (b) a pulse current density of 1 mAcm^{-2} with 0.5s time interval from 6.7 gL^{-1} pyrrole solution containing 1 gL^{-1} PV and 0.1 gL^{-1} CNTs on nickel plaque substrate.	101
Figure 7 - 48 SC versus scan rate for 1 mgcm^{-2} PPy-MWCNT films prepared at (a) a constant current density of 1 mAcm^{-2} (b) a pulse current density of 1 mAcm^{-2} with 0.5s time interval from 6.7 gL^{-1} pyrrole solution containing 1 gL^{-1} PV and 0.1 gL^{-1} CNTs on nickel plaque substrate...	102
Figure 7 - 49 Nyquist plots for 1 mgcm^{-2} PPy-MWCNT films prepared at (a) a constant current density of 1 mAcm^{-2} (b) a pulse current density of 1 mAcm^{-2} with 0.5s time interval from 6.7 gL^{-1} pyrrole solution containing 1 gL^{-1} PV and 0.1 gL^{-1} CNTs on nickel plaque substrate.	103
Figure 7 - 50 SEM images of the film prepared on nickel plaques substrates at a constant current density of 1 mAcm^{-2} from 0.1M pyrrole solution containing 1g/L Pyrocatechol violet and 0.1g/L CNTs.....	105
Figure 7 - 51 SEM images of the film prepared on nickel plaques substrates at a pulse current density of 1 mAcm^{-2} and 0.5s time interval from 0.1M pyrrole solution containing 1g/L Pyrocatechol violet and 0.1g/L CNTs.....	106

List of Tables

Table 2 - 1 Comparison of the properties of battery, conventional capacitor and ES [9]	6
Table 2 - 2 Double-layer capacitance and pseudocapacitance compared [18].....	12
Table 2 - 3 Summary of the carbon-based electrode materials investigated [9]	13
Table 2 - 4 Summary of transition metal oxide electrode materials investigated [9]	13
Table 2 - 5 Summary of the conductive polymer electrode materials investigated [9].....	14
Table 2 - 6 Some common conducting polymers properties [49]	23

1 Introduction

Electrochemical Supercapacitors (ES) are currently under investigation for an advanced energy storage technology. They can complement or replace batteries in electrical energy storage and harvesting applications, when high power delivery or uptake is needed. A notable improvement in performance has been achieved through the development of advanced nanostructured electrode materials, such as high surface area carbon, transition metal oxides and conducting polymers.

The growing interest in application of polypyrrole (PPY) for electrodes of electrochemical supercapacitors (ES) is attributed to high specific capacitance (SC), relatively large voltage window, high electrical conductivity, low cost, advanced chemical and mechanical properties of this material. The high SC of PPY results from redox reactions, which allow charge storage in the bulk of the electrode material. Many fundamental investigations have been conducted with the objective to investigate the charging mechanism of PPY in different electrolytes and to utilize high theoretical SC of PPY (620 Fg^{-1}) in electrodes of ES. The fabrication of PPY films by electropolymerization is an attractive technique that allows the pyrrole monomer, dissolved in a solvent, containing an anionic dopant, to be oxidised at the electrode surface by the applied anodic potential, forming a polymer film. Despite the impressive progress achieved in the fabrication of PPY and composite electrodes of ES by electropolymerization, there is a need for further development of this method. One of the major challenges of electrochemical polymerisation of pyrrole involves formation of

adherent PPY films on non-noble metal substrates, as oxidation and dissolution of the substrates during anodic electropolymerization occurs readily.

Recent studies highlighted the importance of high active material loadings for the fabrication of efficient ES. However, the increase in material loading usually results in increased resistance and reduced SC. This problem can be addressed by the use of special current collectors, such as Ni foams or plaques. The Ni plaque based electrodes offer significant benefits, especially at high charge-discharge rates. Another strategy is based on the fabrication of PPY-CNT composites. CNT are usually added to active materials in order to increase the electronic conductivity of the composite electrodes and improve the power density of ES. The use of CNT as conductive additives offers benefits of their high surface area and low percolation threshold. However, the specific capacitance of CNT is low. Therefore, the fabrication of PPY-CNT electrodes requires efficient dispersion of CNT in the PPY matrix and optimization of the CNT content in the composites. In order to achieve this goal, CNT must be well dispersed and negatively charged in the pyrrole solutions and incorporated into the growing PPY films. Therefore, the goal of this research was to find perfect anodic additives for electrochemical fabrication of PPY film or composite PPY electrodes using stainless steel and Ni plaque current collectors.

2 Literature Review

2.1 Energy Storage Devices Development

It is now essential to move towards renewable and sustainable resources, in response to needs of climate change and the decreasing availability of fossil fuels concerns [1]. As a result, the modern society is observing an increasing in renewable energy productions, such as the sun, wind, water, significant interest has been generated in the development of electrical vehicles and hybrid vehicles with low CO₂ emissions. Energy storage systems are starting to play a major role in modern lives since many limitations mainly related to reliability and sustainability for these renewable energy productions [2]. Hence, many studies have focused on the development of new electrical energy storage system to meet higher requirements of future systems, ranging from portable electronics to hybrid electric vehicles and large industrial equipment [3]. Electrochemical supercapacitors are currently under development for advanced energy storage systems.

In 1957, the practical use of supercapacitors, for the storage of electrical charge, was demonstrated and patented by Becker [4]. The patent described electrical energy storage by means of the charge, held in the interfacial double layer at a porous carbon material and an aqueous electrolyte. After Becker, in 1969, the Sohio Corporation, also utilized the high-area carbon double-layer capacitance, but in a non-aqueous solvent. Such systems allowed higher operating voltages, they can accommodate higher charge densities and provide larger specific energy storage. A different principle was utilized and developed in period of 1975-1981 by Conway in Ottawa, which was named

pseudocapacitors. It arises from the electro-sorption or redox reaction which occurs at the electrodes through Faradaic or non-Faradaic process. RuO₂ films in aqueous H₂SO₄ showed pseudocapacitance associated with solid oxide redox system. Such system exhibited almost ideal capacitive behavior, which has a large degree of reversibility between charge and discharge, and long cyclability [5]. In 1990s, electrochemical supercapacitors became important for application in hybrid electric vehicles. Different materials such as various carbon materials, mixed metal oxides and conducting polymers, have been developed as supercapacitor electrode materials. Today several companies such as Maxwell Technologies, NEC, Panasonic and several other others invest in electrochemical supercapacitor development [6].

2.2 Advantages of Supercapacitor Technology

Energy density and power density are two main fundamental parameters for describing the behavior of energy storage devices. Energy density is the energy stored per unit mass and is proportional to voltage squared, which can be defined as:

$$W = \frac{1}{2}CV^2 \quad (2-1)$$

Where C is the specific capacitance, V is the operating voltage. Power density describes the amount of energy delivered per unit time. It is given as [7]:

$$P = \frac{1}{4R}V^2 \quad (2-2)$$

Where R is the equivalent series resistance (ESR), V is the initial voltage.

The reason why electrochemical supercapacitors became popular is visualized in Figure 2-1 where various energy storage and conversion devices are presented in the ‘Ragone Plot’ [8] in terms of their specific energy and power density.

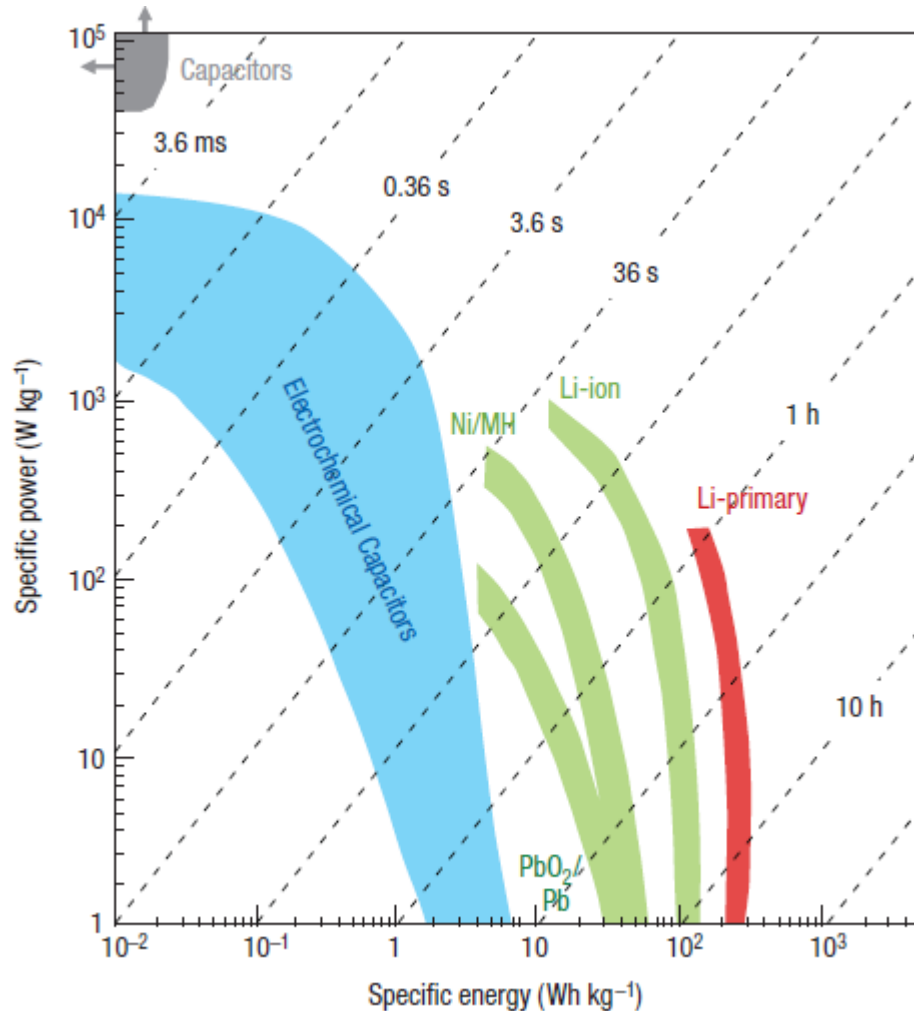


Figure 2 - 1 Ragone plot for various energy storage and conversion devices [8]

Batteries and low temperature fuel cells are typical high energy devices (about 10-1000 Wh kg^{-1}), where they are able to store a large amount of energy but take a long time to charge or discharge due to their low power delivery. Conventional capacitors such as

electrolytic capacitors or metallized film capacitors may have high power density of $> 10^6$ W kg⁻¹ [6]; however, they suffer very low energy stored to meet requirement of long duration. Either case is not suitable to meet the needs of today's market.

Electrochemical Supercapacitors currently fill in the gap between batteries and conventional capacitors. They can store hundreds or thousands of times more charge than the conventional capacitors, because of a much larger surface area available for charge storage. They also are able to hold a very high charge which can be released in a controlled manner. Hence, electrochemical supercapacitors may improve battery performance in terms of power density or may improve capacitor performance in terms of energy density when combined with the respective device. In addition, electrochemical capacitors are expected to have a much longer cycle life than batteries. The comparison of the properties of battery, conventional capacitor and electrochemical capacitor was recently published by Y. Zhang and shown in Table 2-1 [9].

Table 2 - 1 Comparison of the properties of battery, conventional capacitor and ES [9]

	Battery	Capacitor	ES
Discharge time	0.3-3 h	10^{-3} to 10^{-6} s	0.3-30 s
Charge time	1-5 h	10^{-3} to 10^{-6} s	0.3-30 s
Energy density (Wh/kg)	10-100	<0.1	1-10
Specific power (W/kg)	50-200	>10,000	≈1000
Cycle life	500-2000	>500,000	>100,000

2.3 Application of Electrochemical Supercapacitors

Electrochemical Supercapacitors are electrochemical energy sources with high power delivery and an exceptional cycle life. They are used when high power demands are needed, such as for power buffer and power saving units, but are also of great interest for energy recovery [8]. Recent articles from Miller et al [7]. Present an overview of the opportunities for electrochemical supercapacitors in a variety of applications. Three main applications are summarized such as energy management applications, day-night storage applications and power tools applications.

Electrochemical supercapacitors are successfully used in hybrid diesel/electric cranes to load and unload container ships at major seaports in the Far East [10]. The most important function of capacitors in this application is to capture and store regenerative energy during load lowering that is then used to help raise the next load, resulting in improved efficiency and greatly reduced air emissions. Moreover, electrochemical supercapacitors are among the most promising energy storage technologies currently used or being considered for heavy hybrid vehicles [10]. They can supply pulse power for batteries in engine starting, acceleration, and also can store energy during braking within a short time. The stored energy can be reused when the vehicle starts moving again. Hence they are well suited for city transit buses with stop-and-go driving, in trash trucks, which can experience as many as a thousand start/stop cycles during a day.

Electrochemical supercapacitors have been proposed for bulk energy storage to store off peak electricity from the utility grid at night, when it is abundant and low cost for use during the day (it may be in short supply and more costly) [10]. This application is

particularly interesting for hot summer days, when there are heavy air conditioning loads. It would involve one single cycle (night storage/day use) per day, which means that the energy storage system designed to last for ten years would require fewer than 5,000 cycles [10]. Such number is readily attainable for electrochemical supercapacitors but is a challenge for most batteries. This application has advanced in recent years to where it now appears technically ready for commercialization [11].

For power tools applications, the cordless electric screwdriver with electrochemical supercapacitor, which is fully charged in only 90 seconds, was recently introduced. Compared to traditional batteries in powering this product, electrochemical supercapacitors are advantageous in their power delivery performance, cycle life, and fast charge capability. Although batteries can store considerably more energy, they generally have charge/discharge time issue, which are too long and thus only a fraction of their stored energy can be used effectively. Another cordless tool example is a power tubing cutter produced by the Superior Tool Co. for cutting copper tubing. It has electrochemical supercapacitor wired in parallel with the rechargeable battery to increase its cutting efficiency, which makes it possible for a substantially greater number of tubes to be cut on each battery charge [12].

Despite electrochemical supercapacitors have high level of performance, they are simply too expensive to compete against the other available systems. It is the primary reason why they are not the energy storage technology of choice for many applications today. For some applications, potential users find energy density of electrochemical

supercapacitors is too low to use. Hence increasing energy density and lowering cost are primary challenges facing developers and researchers [10].

2.4 Principles of Energy Storage in Electrochemical Supercapacitors

According to the charge storage mechanism as well as the active materials used, the electrochemical supercapacitors can be classified in two types: electric double layer supercapacitors (EDLCs) and pseudo-supercapacitors.

2.4.1 Electric double layer supercapacitors (EDLCs)

EDLCs are defined as electrochemical devices, which store the electric energy directly in the double-layer at the electrode/electrolyte interface [5]. The EDLC has a pair of polarizable electrodes with current collectors, a separator, and an electrolyte solution. Figure 2-2 shows the configuration of a typical EDLC cell [4]. The capacitor is charged and the electrical energy stored when electric charges are accumulated on the electrode surfaces and ions of opposite charge are arranged on the electrolyte side. The capacitor is discharged at loads when the accumulated ions are released from the electrode surfaces and moved back into the bulk of the electrolyte [13]. The capacitance of EDLCs is analogous to a conventional capacitor and can be described as:

$$C_{dl} = \frac{\epsilon_r \epsilon_0 A}{d} \quad (2-3)$$

where ϵ_r is the relative dielectric constant in the double layer; ϵ_0 is the permittivity of free space; d represents the effective thickness of double layer with surface area A . Compared

to a conventional capacitor, an EDLC has much smaller thickness “d” (5-10Å) which is resulting in significantly higher capacitance values.

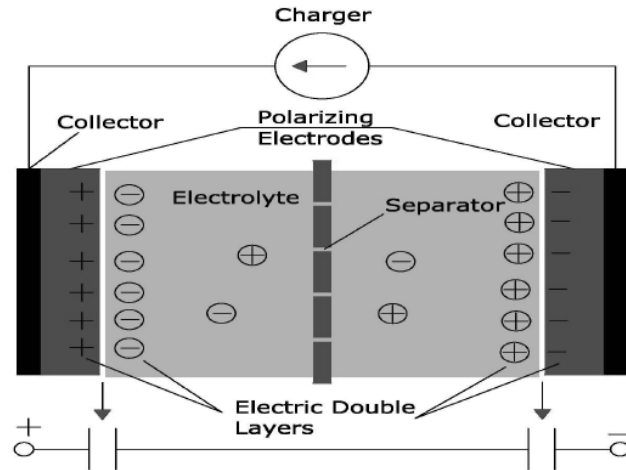


Figure 2 - 2 Typical configuration of an EDLC cell [4]

As a result of the electrostatic charge storage mechanism involved, there is no faradaic reaction at EDLC electrodes. EDLCs allow very fast energy uptake and delivery, and exhibit better power performance compared to batteries. Hence, highly reversible charging/discharging and millions of cycle life are achievable for EDLCs, whereas batteries survive a few thousand cycles at best. In addition, the solvent of the electrolyte is not involved in the charge storage mechanism, unlike in Li-ion batteries where it contributes to the solid-electrolyte interphase [8]. This does not limit the choice of solvents, and electrolytes with high power performance at low temperature can be designed for EDLCs. Moreover, high capacitance EDLCs are also achieved by increasing electrode surface area, which can be additionally increased by using porous materials such as carbon fabrics, fibres, nanotubes etc. However, because the electrostatic surface

charging mechanism, EDLCs still suffer from a limited energy density. Therefore, today's EDLC research is largely focused on increasing their energy performance and widening the temperature limits into the range where batteries cannot operate [14].

2.4.2 Pseudo-supercapacitors

The second type of electrochemical supercapacitor is called pseudocapacitor, in which the energy storage mechanism is much more complex than that of EDLC. Instead of electrostatic charge storage mechanism used in EDLCs, pseudocapacitors use fast, reversible redox reactions at the surface of active materials, such as metal oxides and electronically conducting polymers. The pseudo-capacitive behavior of ruthenium oxide, RuO_2 , is widely studied. According to the Equation (2-4), the electrochemical reaction of RuO_2 electrodes can be described as a fast, reversible electron transfer together with an electro-adsorption of protons on the surface of RuO_2 particles.



where $0 \leq x \leq 2$. Specific capacitance of more than 600 Fg^{-1} has been reported [15], but Ru-based aqueous electrochemical capacitors are extremely expensive, the high cost limits their commercial applications. Academic institutions have focused on searching for other cheaper materials instead of RuO_2 , such as other transition metal oxides and conducting polymers.

Conway has been proposed three types of charge transfer processes within pseudocapacitance, including surface adsorption of ions from the electrolyte, redox reactions and doping/de-doping of active conducting polymers [16]. The first two

processes are highly dependent on the surface area of electrode material while the third process is a bulk process, which is less dependent on surface area although the electrodes require micro-pores for ion transfer [17].

It should be noted that the EDLC and pseudocapacitor storage mechanisms usually co-exist in supercapacitor system. Generally, one of the storage mechanisms dominates in the system, another one is relatively in small portion (2%~5%). To distinguish between these two mechanisms, a comparison of EDLC and pseudocapacitance is summarized by Conway shown in Table 2-2 [18].

Table 2 - 2 Double-layer capacitance and pseudocapacitance compared [18]

Double-layer capacitance
1. Non-faradaic
2. 20-50 $\mu\text{F cm}^{-2}$
3. C fairly constant with potential, except through the p.z.c.
4. Highly reversible charging/discharging
5. Has restricted voltage range (contrast non-electrochemical electrostatic capacitor)
6. Exhibits mirror-image voltammograms
Pseudocapacitance
1. Involves faradaic process
2. 2000 $\mu\text{F cm}^{-2}$ for single-state process; 200-500 $\mu\text{F cm}^{-2}$ for multi-state, overlapping processes
3. C fairly constant with potential for RuO_2 ; for single-state process, exhibits marked maximum
4. Can exhibit several maxima for overlapping, multi-state processes, as for H at Pt
5. Quite reversible but has intrinsic electrode-kinetic rate limitation
6. Has restricted voltage range
7. Exhibits mirror-image voltammograms

2.5 Materials for Electrodes of Supercapacitors

Supercapacitors can be made from a variety of materials whose selection depends largely on the type of capacitance to be utilized, such as materials utilizing double-layer capacitance, pseudocapacitance and combination of double-layer and pseudocapacitance. With respect to electrode materials there are three main categories: carbon-based, transition metal oxides, and conductive polymers. A comprehensive review of these different classes of materials are given by Yong and summarized in Table 2-3, 2-4 and 2-5 [9].

Table 2 - 3 Summary of the carbon-based electrode materials investigated [9]

Carbon-based	Electrolyte	Working voltage (V)	S. C. (F/g)
Activated carbon	1M Et ₄ NBF ₄ +PC	1.5	40
Graphite	1M Et ₄ NBF ₄ +PC	3.0	12
Carbon aerogels	1.5M Et ₃ MeNBF ₄ +PC	3.0	160
AC fiber cloth	6 mol/L KOH	1.0	208
Sing-walled CNTs	EMITFSI	2.3	50
Multi-walled CNTs	1.96M TEMABF ₄ +PC	2.5	13
Mesoporous carbon	30wt% KOH	0.9	180

Table 2 - 4 Summary of transition metal oxide electrode materials investigated [9]

Metal oxide	Electrolyte	Working voltage (V)	S. C. (F/g)
RuO ₂ H ₂ O	0.5M H ₂ SO ₄	1.0	650
H _{0.2} RuO _{2.1} nH ₂ O	0.5M H ₂ SO ₄	1.2	390
MnO ₂	0.5M K ₂ SO ₄	0.8	261
Ni(OH) ₂	3% KOH	0.8	578
Mo ₂ N/Ta ₂ O ₅	3.5mol/L H ₂ SO ₄	0.8	106
MnFe ₂ O ₄	1M LiPF ₆ +EC/EMC	2.5	126
TiN	1M KOH	0.2	238
V ₂ O ₅	2M KCl	0.7	262

Table 2 - 5 Summary of the conductive polymer electrode materials investigated [9]

Conductive polymers	Electrolyte	Working voltage (V)	S. C. (F/g)
Poly(3-methylthiophene)	PYR ₁₄ TFSI	3.6	25
Polypyrrole/AC	0.5M Pyrrole/ β -NSA	0.9	345
PANI/MnO ₂	0.1M Na ₂ SO ₄	1.2	715
PANI/AC	6M KOH	0.9	588

2.5.1 Carbon-based Materials

Carbon-based materials can be obtained by an activation pre-treatment of existing carbon materials made initially from thermal carbonization of coal, pitch, wood, coconut shells or polymers [5]. The most commonly used pre-treatments are hot nitrogen [19], hydrogen [20], carbon dioxide or steam flux [21], through which high surface area and pore accessibility are achieved [22]. Carbon-based materials in various modifications (carbon aerogels, graphites, CNTs, carbon nanofibers and nano-sized carbon) exhibit a large and stable double-layer capacitance due to their good conductivity, large specific area, high chemical stability, easy processability, relatively low cost and wide temperature range of stability.

Activated carbons are the most widely used active materials for EDLC applications, because of their high surface area and relatively low cost. Activated carbons are derived from carbon-rich organic precursors by heat treatment in inert atmosphere followed by selective oxidation process in water, CO₂, or KOH, to obtain the high SSA and pore volumes [23]. The activation process results in a porous network in the bulk of the carbon particles; micropores (< 2 nm), mesopores (between 2 and 50 nm), and macropores (larger than 50 nm size), shown in Figure 2-3 [23].

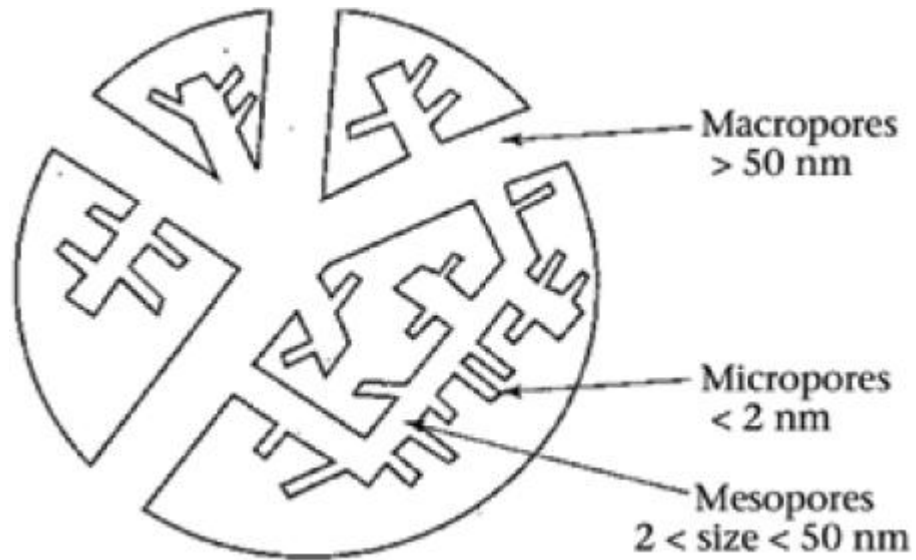


Figure 2 - 3 Schematic diagram of the pore size network of an activated carbon grain [23]

According to the storage mechanism of EDLCs, the specific surface area of carbon-based materials plays an important role. Theoretically, the specific capacitance of carbon materials is proportional to their specific area. However, the problem of activated carbons is that not all the surface area is electrochemically accessible when in contact with electrolyte [24]. It is more difficult to adsorb large solvated ions in micropores than in mesopores, and that is more difficult with a higher rate of charge-discharge. Therefore, it has become the most important task to investigate meso and macroporous carbon materials in order to develop high performance EDLC electrode materials. Moriguchi et al. [25] synthesized bimodal porous carbons with both micropores and meso- or macropores by SiO_2 colloidal crystal-templating process. The specific capacitance per surface area of the samples was estimated to be about $20 \mu\text{F}/\text{cm}^2$, which was much larger than that of commercial. Recently, Zhao et al. [26] synthesized ordered

meso/macroporous carbon monoliths using SiO₂ opal and Pluronic F127 as templates by a facile method. The specific capacitance was about 130 F/g at a constant current density of 10 mA/cm², which is much larger than those of commercially available activated carbons. All these improvements are probably attributed to the novel structure of the sample, which could make full use of the inner surface of the materials.

Activated carbon fibers are popular materials for the electrodes of EDLC due to their large specific surface area and high electrical conductivity. Compared to activated carbon powders, they do not require any binder addition and can be directly used as active material films. Activated carbon fibers can be obtained from polymeric fibers, such as rayon and polyacrylonitrile. Once activated, the surface area is comparable to activated carbons and most of the porosity being developed in the mesoporous range. Kim et al. [27] developed activated carbon fibers with exposed graphite edges for use as the electrode materials of ECs and showed the largest capacitance of 149 F/g. Xu et al. [28] prepared activated carbon fiber cloth electrodes with high double-layer capacitance and good rate capability from polyacrylonitrile fabrics by CO₂ activation. However, the cost of these activated carbon fibers is high, which restrict their use in EDLCs to very specific applications.

Carbon aerogels have a monolithic three-dimensional porous network consisting of carbon nanoparticles, which exhibit a high electrical conductivity, controllable pore structure, and relatively high accessible surface area [29]. Carbon aerogels can be prepared by the pyrolysis of organic aerogels based on resorcinol-formaldehyde or phenol-furfural precursors through sol-gel process in which particles sizes, pore shape

and density can be controlled [30]. Zhu's [31] group has used carbon aerogels as electrode materials and conducted relevant research regarding to this subject. The specific capacitance of samples prepared by their method, was up to 78 F/g at a current density 1 mA/cm² using 30% KOH aqueous electrolyte. When the sample was activated for 2 h at 900 °C, the highest specific capacitance of 146 F/g was achieved. However, further investigations revealed that although a large increase of BET surface area was achieved by thermal activation, the accompanying increase of capacitance was relatively small. In Pandolfo's research [32], the capacitance was decreased from 18 μF/cm² of activated sample to 8 μF/cm² of inactivated sample, and this was attributed to an increase of inaccessible pores volume after activation.

Recently, carbon nanotubes (CNTs) have attracted great attention due to their good mechanical strength, high electric conductivity, good electrolyte accessibility, good chemical and thermal stability. CNTs can be conceptualized as seamless hollow tubes rolled up from two-dimensional graphene sheets with diameters in the nanometer range and lengths usually on the micron scale [33]. Depending on the number of tube walls, CNTs can be classified into two forms: multi-walled CNTs (MWNTs) and single-walled CNTs (SWNTs) [34]. MWCNTs are made up of coaxial cylindrical carbon layers with an interlayer distance of 0.36 nm and a diameter typically on the order of 10-20 nm [35]. SWCNTs are usually 1-2 nm in diameter and tens of microns in length. The structural characteristics of an SWCNT, namely its diameter and chirality, are usually described by a pair of indices (n, m).

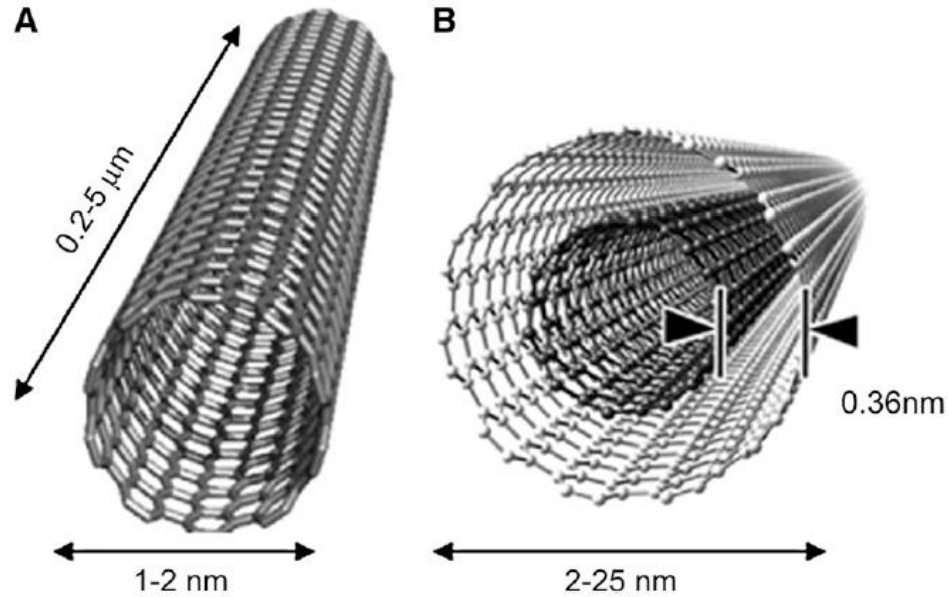


Figure 2 - 4 Conceptual diagrams of SWCNT (A) and MWCNT (B) [36]

For purified CNT powders, specific capacitance is not high, typically in the range of 20 to 80 F/g. This has been mainly attributed to the hydrophobic property of CNT surface. Surface functionalization by introducing pseudocapacitance contribution through oxidation treatments leads to significant improvement of the specific capacitive behaviour [23]. Specific capacitance 130 F/g was achieved by oxidative (acid) treatment reported by Frackowiak [37]. The activated CNTs have 3 times higher BET specific surface area and 1.5 times higher pore volume than the original CNTs. The electrochemical capacitance of the activated CNTs was 2 times that of the original CNTs. However, the cycling life tends to be limited after the activation. Thus, many efforts are recently focused on the development of a dense, nano-ordered, aligned CNT forest perpendicular to the current collector that could help to increase the capacitance by fine-tuning the inter-tube distance [23].

2.5.2 Redox Pseudo-Capacitive Materials

The specific pseudo-capacitance exceeds the capacitance of carbon materials due to fast, reversible redox reactions at the surface. Some pseudo-capacitive materials such as metal oxides and electronically conducting polymers have been extensively studied in the past decades.

2.5.2.1 Transition Metal Oxides

Transition metal oxides present an attractive alternative as the best candidate materials for electrochemical capacitors because of their high specific capacitance coupled with relatively low resistance, resulting in a high specific power, which makes them very important for commercial application [38]. Among the transition metal oxides, ruthenium oxide (RuO_2) is the most beneficial metal oxide due to its high specific capacitance, high rate capability, good electrochemical reversibility, high conductivity, as well as its long cycle life [39]. The pseudo-capacitive behavior of RuO_2 in acidic solutions was described as a fast, reversible electron transfer together with an electro-adsorption of protons on the surface of RuO_2 particles, according to the equation (2-4), where Ru oxidation states can change from (II) up to (IV) [8]. Very high specific capacitance of up to 750 F/g was reported for RuO_2 prepared at relatively low temperatures [40]. Such high specific capacitance combined with low resistance resulted in very high specific powers. However, the rarity of ruthenium in the earth's crust and hence the high market price of RuO_2 limits applications mostly in military and aerospace, where cost is presumably less of an issue than it is for commercial ventures [16].

Academic institutions have focused on searching for other cheaper transition metal oxides instead of RuO_2 [4].

Less expensive metal oxides, such as iron, vanadium, nickel and cobalt have been tested, but none of them has been investigated as much as manganese oxide (MnO_2) [41]. The charge storage mechanism is based on surface adsorption of electrolyte cations C^+ as well as proton incorporation and can be described as:



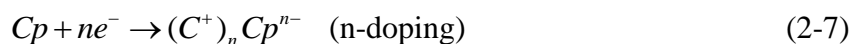
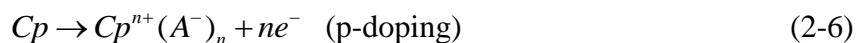
the pseudocapacitance of MnO_2 is attributed to the redox transitions of interfacial oxyanion species in various oxidation states. These redox transitions of hydrous manganese oxides include the transitions from Mn(III) to Mn(II), from Mn(IV) to Mn(III) and from Mn(VI) to Mn(IV). Most of the MnO_2 reported in the literature showed specific capacitance as high as 600 F/g for thin films and 150-300 F/g for powder based electrodes in aqueous electrolytes. Miura and Prasad [42] reported a capacitance value between 400 and 621 F/g for amorphous electrolytic manganese dioxide and MnO_2 -based mixed oxides. Recently, Yang et al. [43] prepared porous MnO_2 with pore sizes from 5 nm to 30 nm by organic-aqueous interfacial method. The MnO_2 synthesized under optimum conditions shows a capacitance of 261 F/g and exhibits good cyclic stability. Accordingly, there is limited interest in MnO_2 electrodes for symmetric devices, because there are no oxidation states available at less than 0 V. However, it is suitable for a pseudo-capacitive positive electrode in hybrid system [8].

Nickel oxide is another potential candidate as metal oxides electrode material in pseudocapacitors. However, the only drawback of Ni(OH)_2 cathode is the specific capacitance decreased dramatically when current density was increased. Zhao et al. [44] electrodeposited a hexagonal nanoporous Ni(OH)_2 film, and a maximum specific capacitance of 578 F/g was achieved, but its long-term cyclic stability is poor, which is approximately 4.5% loss of specific capacitance after 400 cycles. Wu et al. [38] electrochemically deposited nickel oxide films, which exhibited highly porous morphology with interconnected nanoflakes. Specific capacitance of the sample significantly depends on the applied potential window in 1 M KOH solution. When the upper limit potential is higher than 0.35V, the cyclic voltammetry (CV) exhibits rectangular mirror image and the specific capacitance is increased due to the additional redox reaction occurred on the surface layer of the NiO grains. However, its long-term cyclic stability is not good, which is approximately 87.5% of its maximum capacitance after 5000 cycles at current density of 0.49 mA/cm^2 .

Transition metal oxides are the best electrode materials for redox pseudocapacitors. Among the transition metal oxides, RuO_2 is the most promising electrode material due to its high specific capacitance. Due to cost consideration, research in this field is focused on the development of cheaper metal oxides (MnO_2 , NiO , V_2O_5 and other metal oxides) and optimizing the particle size and distribution. However, due to manufacturing consideration, these materials are far from being commercially used in ESs.

2.5.2.2 Conducting Polymers

Conducting polymers are the second group of candidate materials for redox pseudocapacitors due to their fast and reversible oxidation/reduction processes, good electrical conductivity, and relatively low cost. The most commonly used conducting polymers include Polyaniline (PANI), Polypyrrole (PPy), Poly (3,4-ethylenedioxythiophene) (PEDOT), Polythiophene (PTh), and Poly (p-phenylene vinylene) (PPV). They are typically synthesized either through chemical or electrochemical oxidation of the monomer [45], and rendered conductive through a conjugated bond system along the polymer backbone. Two types of charging process are classified: p-doped with anions when oxidized and n-doped with cations when reduced. The simplified equations for these two charging processes are as follow:



the discharge reactions are the reverse of the above equations. Early studies of n-doped materials were performed on polyacetylene and later poly-p-phenylene. These polymers have high impedances upon n-doping and are therefore not suitable for use as negative electrodes [46]. Some conducting polymers, such as PANI and PPy, can only be p-doped due to the very negative potentials required for n-doped, when compared with the reduction potential limit of molecular solvent-based electrolytes [47]. It was reported that p-doped polymers are more stable against degradation than n-doped polymers [48]; hence,

investigations dealing with p-doped polymers are more promising. Table 2-6 [49] gives maximum conductivity and type of doping (n or p) for some common CPs.

Table 2 - 6 Some common conducting polymers properties [49]

Conducting polymer	Conductivity (S cm ⁻²)	Doping type
PA	200-1000	n, p
PPy	40-200	p
PT	10-100	p
PITN	1-50	p
PANI	5	n, p
PPP	500	n, p
PPV	1-1000	p
PPS	3-300	p

PANI is one of the most popular materials for the electrodes of electrochemical supercapacitor due to high electroactivity, a high doping level, excellent stability and a high specific capacitance. In addition, it has good environment stability, controllable electrical conductivity, and can be easily processed [50]. The structure of PANI is illustrated in Figure 2-5 [46]. PANI has been reported to have a wide capacitance value range from 44 to 270 Ah kg⁻¹ [51]. This variation depends on many factors, including synthetic route used, polymer morphology, the amount and type of binders and additives, and the thickness of the electrode [46]. It was reported that the specific capacitance is higher for electrodeposited than for chemically formed PANI. In Ryu's study, PANI was doped by LiPF₆ and achieved a specific capacitance of 107 Fg⁻¹ that decreased to 84 Fg⁻¹ after 9000 cycles. This material was modified to be more stable by forming poly(n-methyl aniline), in which the proton exchange sites are blocked by the methyl groups so that the polymer is stabilised against chemical degradation and made more redox active. However,

there is the most significant disadvantage for PANI; it requires a proton to be properly charged and discharged. Thus, a protic solvent, an acidic solution or a protic ionic liquid is required.

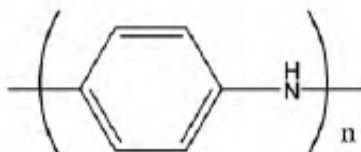


Figure 2 - 5 Polyaniline (PANI) structure [46]

PPy is another promising conducting polymer in view of its high conductivity, stability and ease of synthesis. It offers a greater degree of flexibility in electrochemical processing than most conducting polymers. PPy is typically doped with single-charged anions such as Cl^- , ClO_4^- and SO_3^- but if doped with multiple-charged anions, e.g. SO_4^{2-} , physical crosslinking of the polymer occurs [52]. The cross-linked polymers were reported to have high diffusivity and higher capacitance, presumably due to the greater porosity of the growth. Due to its greater density, PPy has a high capacitance per unit volume (400-500 Fcm^{-3}). However, the dense growth leads to limited access to the interior sites of the polymer for dopant ions, which will reduce the capacitance per gram, especially for thicker coatings on electrodes.

The electropolymerization mechanism is a controversial subject as there have been a number of mechanisms proposed to date. The mechanism described by Diaz and his colleagues [53] is the mechanism encountered most often in the literature. This mechanism can be described by the following stepwise reactions:

Step 1: Oxidation of monomer R to form the cation radical R^+ , as shown in Figure 2-6 [54].



Figure 2 - 6 Formation of cation radical [54]

The several resonance form of this cation are represented in Figure 2-7 [54].

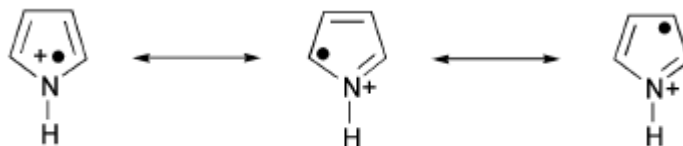


Figure 2 - 7 Resonance form of cation radical [54]

Step 2: the coupling between two radicals results in the formation of a bond between their α -positions and the formation of the dihydromer dication.



Figure 2 - 8 Formation of the dihydromer dication [54]

Step 3: the loss of two protons forms the aromatic dimer (stabilization step) shown in Figure 2-9 [54].

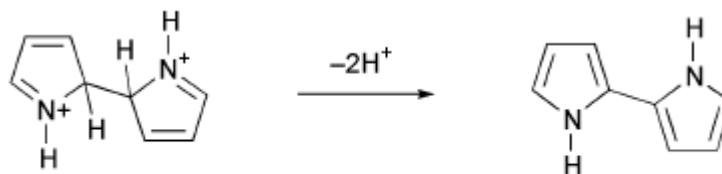


Figure 2 - 9 Formation of the aromatic dimer [54]

Step 4: the polymerization reaction follows the oxidation of the dimer into the cation radical.

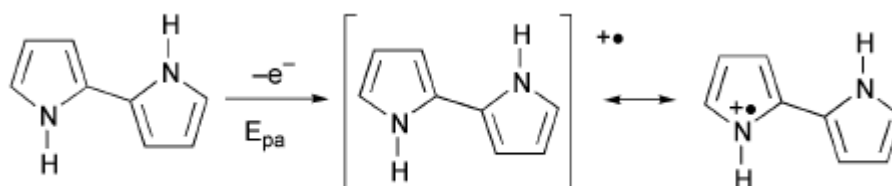


Figure 2 - 10 Formation of cation radical [54]

Step 5: the resonance form of cation radical reacts with a monomer radical cation to form the trimer dication that deprotonates to give the neutral trimer, as shown in Figure 2-11 [54].

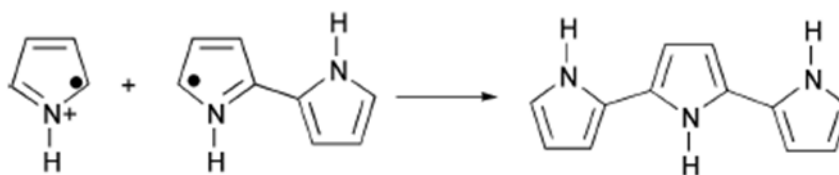


Figure 2 - 11 Formation of trimer [54]

Step 6: The propagation continues in the same sequence: oxidation, coupling and deprotonation until the final polymer product is obtained.

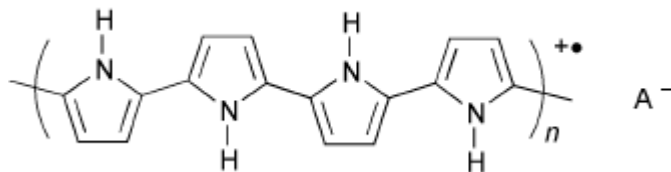


Figure 2 - 12 Formation of final PPy conducting polymer [54]

The electropolymerization does not give the neutral non-conducting PPy but its oxidized conducting form (doped). Actually, the final polymer chain carries a positive charge every 3 to 4 pyrrole units, which is counter-balanced by an anion. It also was noticed that the films obtained consist of about 65% polymer and 35% anion (% in weight).

The stability of CPs is not constant. Generally, there are two distinct types of stability of CPs: extrinsic and intrinsic stability [55]. Extrinsic stability is related to vulnerability to external environmental agents such as oxygen, water that can attack the charged sites of polymers by the nature of nucleophilicity and electrophilicity. For example, in ambient atmosphere, polyheterocyclic polymers, such as PPy and PTh exhibit much higher stability than PA exposed to the oxygen, whilst PTh is more sensitive to water than PPy [56]. Intrinsic stability of CPs is thermodynamic in origin. The degradation of CPs is likely due to the irreversible chemical reaction with main chain dopants or counter ions, leading to a break of conjugation and the loss of conductivity. The nature of dopants or counter-ions with respect to different polymers is the key factor affecting the conduction stability [57], under systematically controlled environmental and thermal conditions. The conduction stability of PPy was found to be significantly better than that of poly(3-alkylthiophenes). PPy doped with arylsulfonates were found to exhibit excellent stability in inert atmosphere but were slightly less stable in the presence of dry

or humid air. PPy samples doped with the tosylate anion were found to be the most stable, while PPy doped with longer side chain substituted benzenesulfonates exhibited lower stability.

The electrical conductivity of polymers comes from the conjugated polymer backbone in the doped form. As a result, conducting polymers are insoluble, infusible and intractable, and their processing presents difficulties. To overcome the processing problems, the structure of the polymer can be modified by attaching long flexible side groups to some separated monomers along the conjugated back bone. An example is copolymer poly(3-octythiophene-co-3-methylthephene) [58]. Another way is to deposit the polymer in desired shape and form. For example, PAN/poly (sulfonated styrene) nanofiber composites were prepared by the interfacial method [59]. PANI nanofiber in the presence of sulfonated polystyrene allows for the growth of PANI 2-D nanostructures embedded in the polymerized sulfonated host. The mechanism for this growth is believed to involve some alignment of the aniline monomer onto the anionic dopant.

As stated earlier, the conducting polymers are cheap, light weight. They have suitable morphology, fast doping-undoping process, and can be relatively easily manufactured into electrochemical supercapacitors. However, the long-term stability during cycling may be a problem. The swelling of electroactive polymers may lead to degradation during cycling [14]. In addition, the charge-storage mechanism in polymer electrodes is still not completely understood. Therefore, the research work of this field is consisted of two different aspects: the first one is to develop the new conductive material and improve the capacitance; the second one is to incorporate the well conductive

material (such as active carbon) with conducting polymers in order to reduce overall resistance [9].

2.5.3 Composite Materials

Aside from the two categories of pure materials (carbon-based material and redox pseudo-capacitive materials), there is a new tendency to synthesize composite materials combining two pure materials for supercapacitors. The strategy for material combination is to utilize the advantages of different materials in the composite material, like the examples presented in Figure 2-13. Carbon-based materials facilitate charge transfer and allow double-layer charge storage with high surface area, which is able to increase the contacting areas between the capacitive materials and electrolyte. Thus, both of energy and power densities of the composite materials are increased.

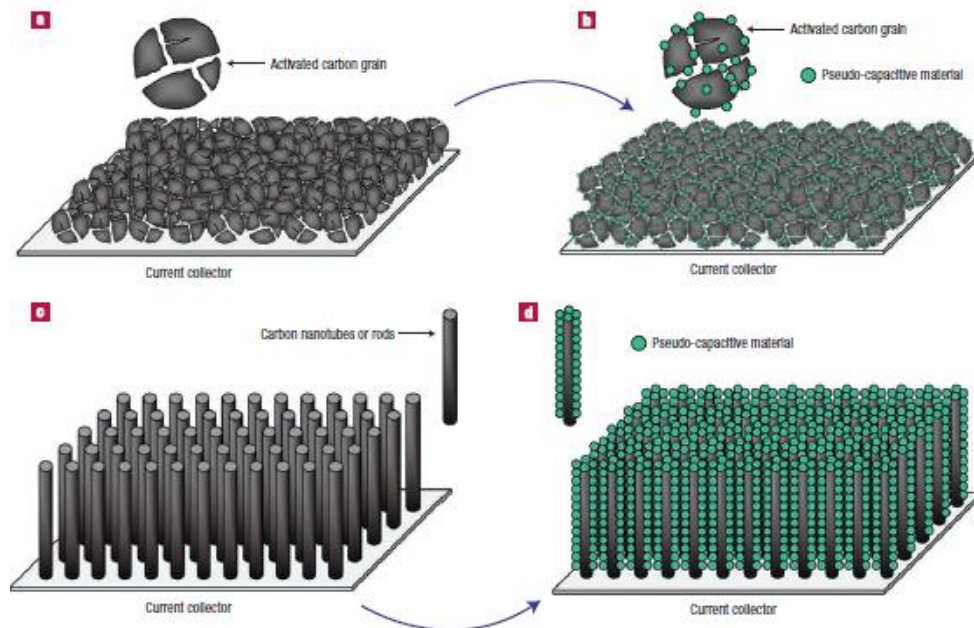


Figure 2 - 13 Composite material to improve both energy and power densities [8]

MnO₂ is one of the most studied materials as a low-cost alternative to RuO₂. The combination of MnO₂ and low-cost carbon system provides high capacitance in neutral aqueous electrolytes with high cell voltages, making it a green alternative to EDLCs using acetonitrile-based solvents and fluorinated salts [8]. A composite electrode material comprised of CNTs and MnO₂ was prepared by Deng et al. [60]. They refluxed the CNTs firstly, and then deposited MnO₂ on the refluxed CNTs. The results show that supercapacitors based on the composite electrode material are characterized by high specific capacitance, high energy density, excellent reversibility and long lifetime. The specific capacitance reaches 134 Fg⁻¹ when MnO₂ mass fraction (the same below) is 65%. The supercapacitors showed good power performance when MnO₂ is less than 50%. Jang et al. [61] used an activated CNT (A-CNT) to prepare a composite of MnO₂/A-CNT by the co-precipitation method, and its physical and electrochemical properties were evaluated for the use in supercapacitors. The specific capacitances of the MnO₂/A-CNT composite electrode, measured using cyclic voltammetry at scan rates of 10 and 100 mVs⁻¹, were found to be 250 and 184 Fg⁻¹, respectively, compared to 215 and 138 Fg⁻¹, respectively, for the MnO₂/CNT composite electrode. Moreover, it showed an improved capacitance and good cycle performance, due to the reduced stress during charge-discharge cycling.

The composites of carbon based materials and conducting polymers are even more interesting and promising since they can combine two relatively cheap materials to gain the large pseudocapacitance of the conducting polymers coupled with the conductivity and mechanical strength of the carbon based materials [22]. For example, Zhang et al. [62]

have studied PPy/AC composite electrode. Using AC as substrate material is being expected as a way to relieve the instabilities because adhesion and charge transfer between the PPy and substrate can be improved. In addition, due to an enlarged active surface area of PPy layer deposited on the surface of AC in the composite electrode, an enhancement of the specific capacitance of PPy is being expected. Moreover, carbon based materials such as CNTs exhibit high mechanical strength properties, when combined with conducting polymers. The composite CP/CNTs structures showed reduced degradation, compared to pure polymer films. In the study of Du et al. [63], the CNTs were used as reinforcing material to overcome the PPy swelling and shrinking during long-term doping-undoping process. The results showed that the capacity of the composite electrode is 30% larger than that of the pure PPy electrode. It can be charged-discharged for over 1000 cycles with only slight capacity loss.

2.6 Electrolytes

Another criteria to classify different electrochemical capacitors is the electrolyte, which is typically one or more solvents containing one or more dissolved ionic species. In many cases, the properties of electrolyte are a key factor in determining the internal resistance of supercapacitor and the power properties. As the equations 2-1 and 2-2 show, the energy and power density are highly dependent on the operating voltage and internal resistance, respectively. These two factors are mainly given by the conductivity and voltage window of the electrolyte. There are two principal factors involved in conductance, which are (1) the concentration of free charge carriers, cations and anions of a given salt or acid solute; and (2) the ionic mobility, or conductance contributions per ion,

of the dissociated ions of the electrolyte solute [5]. Three different types of electrolytes have been currently studied: aqueous, organic and ionic.

2.6.1 Aqueous Electrolytes

The use of aqueous electrolyte for electrochemical capacitors offers the higher conductance (0.8 S/cm for H₂SO₄) or very low ESR, low cost and environmental friendliness of aqueous electrolyte and high solubility of the salts. In addition, purification and drying processes during production are less stringent compared to organic electrolytes. Moreover, in order to avoid electrolyte depletion problem during charging/discharging of the electrochemical capacitors, the electrolyte concentration has to be high. If the electrolyte reservoir is too small the performance of the capacitor is reduced. This problem is particularly important for organic electrolytes where the solubility of salts may be low [14]. However, there is main drawback of aqueous electrolyte, where the unit cell voltage of electrochemical capacitor is limited to 1V, thus reducing the available energy significantly compared to organic electrolytes.

2.6.2 Organic Electrolytes

The main advantage of using organic electrolyte for electrochemical capacitor is the higher operating voltage, due to the larger decomposition limits of such electrolyte solutions. Using an organic electrolyte one can usually achieve voltages in the range of 2-2.5V. The stored energy significantly improved since the energy is proportional to the voltage squared, this is an obvious advantage over aqueous systems. However, the resistivity of organic electrolytes is relatively high (20-60 Ω), which is higher than that of aqueous electrolytes by a factor of at least 20. Such high electrolyte resistance enlarges

the equivalent distributed resistance of the porous layer and consequently reduces the maximum power, although part of the reduction in power is compensated by the higher cell voltage achievable with an organic electrolyte [14]. In addition, the pore size requirements for organic electrolyte are also greater (15-20 Å) due to the large size of organic molecules [17].

2.6.3 Ionic liquid electrolytes

Ionic liquids have desirable electrolyte properties as they usually have high ionic conductivity, low vapour pressure, non-flammability, a wide electrochemical window, and high thermal stability [64, 65]. They are entirely composed of cations and anions, their voltage window stability is thus determined by the electrochemical stability of ions. The ionic conductivity of these liquids is low at room temperature, thus they are mainly used at high temperatures. A number of electrodes have been prepared using ionic liquids with conducting polymers. Balducci et al. [66] prepared a hybrid supercapacitor device based on an activated carbon negative with a PMeT positive electrode and an ionic liquid as the electrolyte, named as N-butyl-N-methyl pyrrolidinium bis-(trifluoromethanesulfonyl) imide. It was reported that the ionic liquid has a low melting temperature, and is hydrophobic and highly cycleable with a voltage window that allows hybrid supercapacitor operation between 3.43 and 1.5 V. The device exhibited a specific energy of 14 Wh kg⁻¹ and power of 1.9 kW kg⁻¹. The device was also cycled 16 000 times. After cycling, the average power was 90% of the initial value and the energy was 40-50% of the original value.

2.7 Problem Formulation

PPy is one of the most promising conductive polymers for energy storage applications. Fabrication of PPy films by electropolymerization is an attractive technique that allows the pyrrole monomer, dissolved in a solvent, containing anionic dopant, to be oxidized at the electrode surface by the applied anodic potential, forming a polymer film [67]. The anionic dopant is incorporated into the polymer to ensure electrical neutrality of the resulting film. One of the major challenges of electrochemical polymerization of pyrrole involves formation of adherent PPy coatings on stainless steel substrates, as oxidation and dissolution of the substrate during electropolymerization occur readily. However, PPy deposition on low-cost stainless steel current collectors is important for the application of PPy films in electrochemical supercapacitors.

Previously, PPy coating were formed on low carbon steels using oxalic acid as an electrolyte [68]. It was shown that steels interacted with oxalic acid to form passive layers, which prevented corrosion of the substrate. However, the formation of the non-conductive and non-capacitive iron oxalate layer results in increasing charge transfer resistance and reduced electrochemical capacitance of the PPy coated electrodes [69]. Recent studies showed that composites containing CNTs in a PPy matrix exhibit improved capacitive behavior compared to pure PPy [70]. However, the electrodeposition of PPy-CNT films on stainless steel presents difficulties related to poor dispersion of CNTs in oxalic acid solutions.

3 Objectives

The objective of this research is to develop advanced electrodes for electrochemical supercapacitors, investigate and optimize the electrochemical performance through following engineering aspects:

- Development of composite polypyrrole-carbon nanotube composite electrode materials for electrochemical supercapacitors on low cost stainless steel substrates.
- Development of advanced anionic additives, which prevent anodic dissolution of stainless steel, promote electron transfer during electropolymerization.
- Development of advanced dispersing agents for electrodeposition of carbon nanotubes (CNT).
- Fabrication of composite materials, investigation of microstructure, adhesion, composition and electrochemical performance for application in electrodes of electrochemical supercapacitors.

4 Approach and Methodology

4.1 Novel Additives

The electropolymerization of PPy on stainless steel is challenging due to the active metal as anode tends to dissolve before the electropolymerization potential of the pyrrole monomer is reached. The oxidation potential of stainless steel is much more negative than pyrrole. Therefore, the dissolution of stainless steel in the electrodeposition prevents the oxidation of pyrrole and impedes the formation of PPy. Thus successful deposition of PPy on stainless steel requires a partial passivation of the metal and reduction the dissolution rate without preventing the formation of PPy. In order to overcome the problems discussed above, the special additives have to serve as the electron transfer mediators during electropolymerization process. Such additives could reduce the over potential required and help to form a passivation layer that can stabilize the interface between the substrate and PPy as well as promote electron transfer without hindering the formation of PPy film on the substrate. In this research, three novel additives (a) gentisic acid sodium salt (GA), (b) 5- sulfosalicylic acid (SSA), (c) pyrocatechol violet (PV) were selected; and the chemical structures are presented in Figure 4-1.

The electrodeposition of PPy-CNT composite films on stainless steel presents another problem due to very poor dispersion of CNT in aqueous solution. In order to co-electrodeposit PPy-CNT composite films, it is assumed that CNTs must be incorporated in PPy during electropolymerization, and must be negatively charged and dispersed without damage. Therefore, the Poly[2,5-bis(3-sulfonato-propoxy)-1,4-

ethynylphenylene-alt-1,4-ethynylphenylene] sodium salt (PPE) was selected as dispersion agent and synthesized according to literature method [71]. Figure 4-2 shows the chemical structure of PPE.

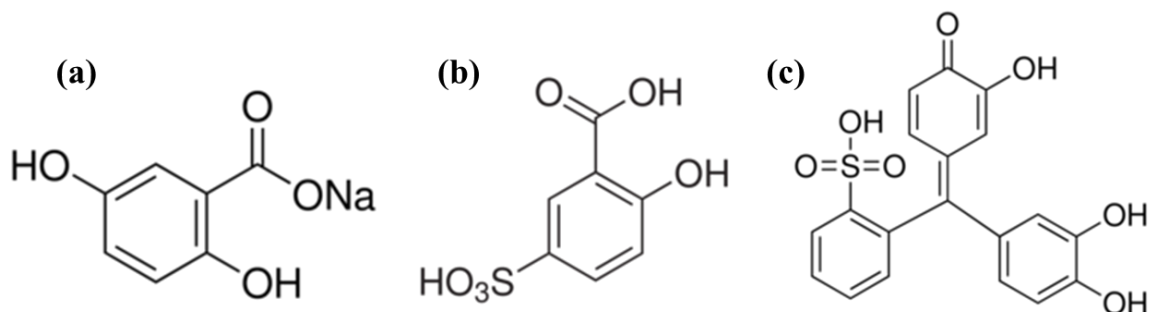


Figure 4 - 1 Chemical structures of novel additives (a) GA, (b) SSA and (c) PV

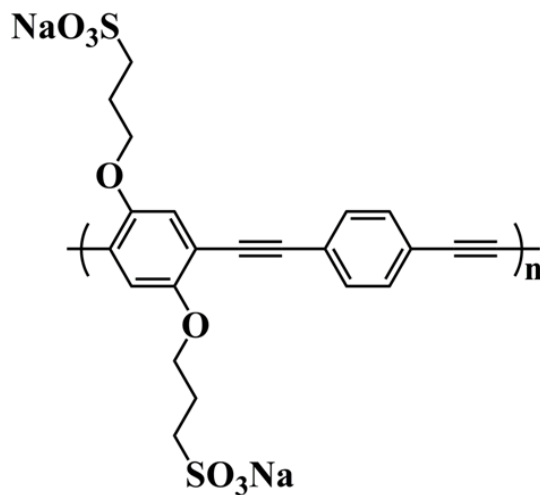


Figure 4 - 2 Chemical structure of PPE polymer

4.2 Suggested Complexation Mechanism

The passivation layer formed between a stainless steel substrate and PPy film is related to the surface complexation of metal atoms by chelating ligands. The chelating ability of the selected novel additives to complex metal atoms is attributed to their function groups, such as adjacent COOH and OH groups bonded to the aromatic ring in GA and SSA, and adjacent OH groups in PV. The suggested mechanisms of complexation is shown in Figure 4-3. The bonding mechanism involved the deprotonation of OH groups. In all of three cases, the chelate complexes form five-membered or six-membered rings, which are thought to be the most stable [72].

PPE polymer containing anionic SO_3^- groups was used for the dispersion, charging and deposition of CNTs. The supramolecular dispersion mechanism [73] is based on the π - π stacking interactions, formation of polymer-CNT complexes and electrostatic stabilization of CNT. The repulsion between the negatively charged side-chains prevented the bundling of CNT, and the resulting polymer-CNT suspensions remained stable indefinitely.

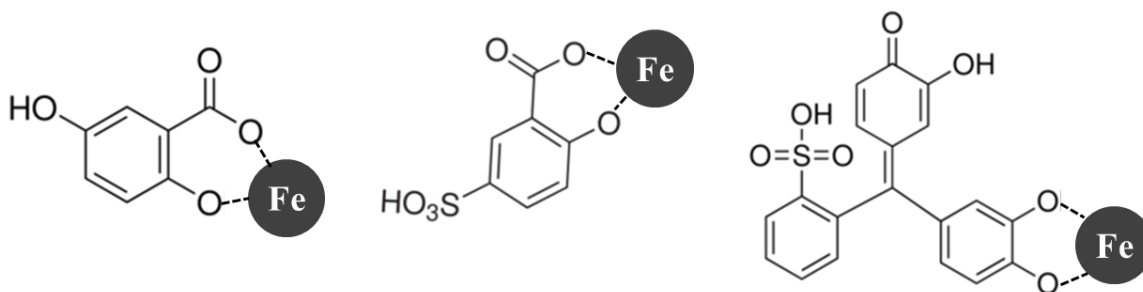


Figure 4 - 3 Chelate complexes formed with Fe^{2+} by (a) GA, (b) SSA and (c) PV

5 Experimental Procedures

5.1 Materials Preparation

GA, SSA, PA and Pyrrole were supplied by Aldrich. PPE polymer was synthesized according to literature method [71]. CNTs were purchased from Carbon Nanotechnologies, Inc. 302/304 annealed stainless steel foil (50 x 30 x 0.05 mm) were purchased from McMaster Carr.

5.2 Electrodeposition Equipments

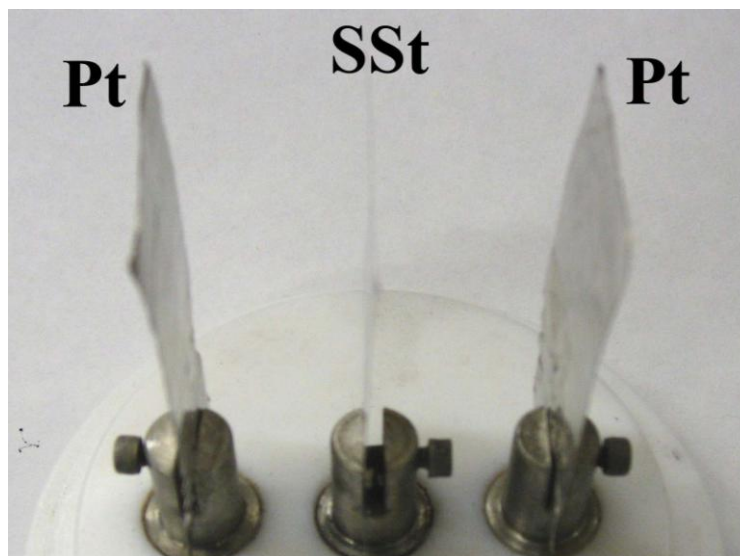


Figure 5 - 1 Electrochemical cell (L: Platinum; M: Stainless steel; R: Platinum)

The electrodeposition was performed by using the electrochemical cell shown in Figure 5-1. It contains a stainless steel foil or nickel plaque as a working electrode and two platinum foils as counter-electrodes. The distance between the anode and cathode was set 20 mm. The power supply Amersham Biosciences EPS 2A200 provided constant

current and Keithley 200 Series Sourcemeter provide pulse current during electrodeposition.

5.3 Electropolymerization procedures

Solution for deposition of PPy was prepared by dissolution of pyrrole in deionized water, adding appropriate concentration of GA, SSA or PV. The aqueous solutions were stirred for 30 minutes before deposition. Anodic deposits were obtained either on stainless steel foils or nickel plaque substrates. The electrodeposition was carried out by either galvanostatic method or pulse deposition method. The deposition time was varied in the range of 1 to 20 minutes. The deposited PPy films were dried at room temperature at least 2 hours. The salient feature of PPy electrodeposition is that polymerization, doping and film processing take place simultaneously. The electropolymerization procedure is shown in Figure 5-2.

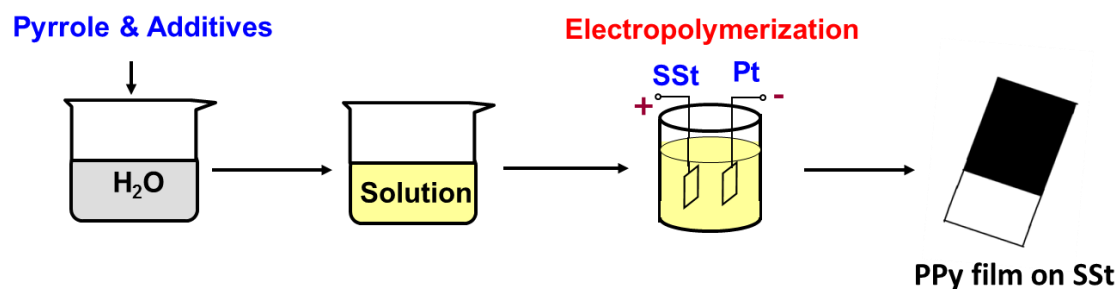


Figure 5 - 2 Scheme of PPy film preparation on SSt

For SSA additive, the procedure for the deposition of PPy/CNT included the formation of aqueous 0.1 g/L PPE solution, adding 0.1 g/L SWCNTs to the solution, stirring during 30 minutes and ultrasonic agitation during 1 hour in order to obtain homogeneous dispersion of SWCNTs. 0.1M pyrrole and 0.01M SSA were added to the

solution, which was then stirred during 30 min and ultrasonically agitated during 30 minutes. Composites were obtained on stainless steel at both constant current and pulse current conditions. The deposition time was varied in the range of 1-10 minutes. The procedure was presented in Figure 5-3.

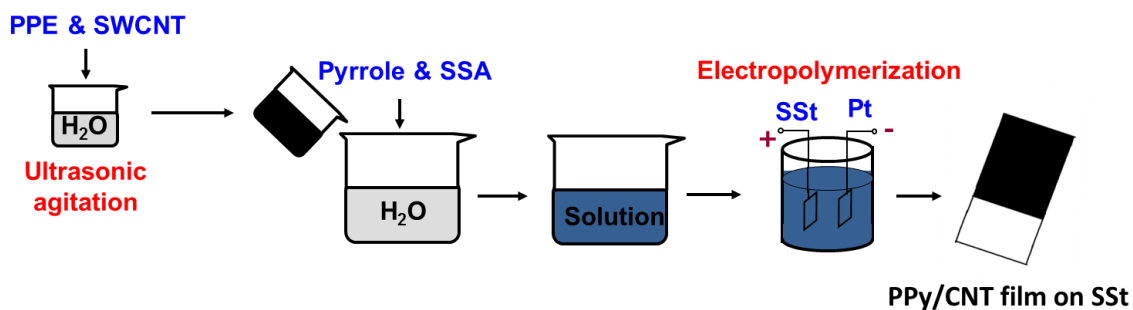


Figure 5 - 3 Scheme of PPy/CNT composite fabrication process by using SSA

For PV additive, the deposition of PPy/CNT composites was performed from aqueous suspensions containing 0.1 – 1 g/L MWCNTs, 0.1M pyrrole and 0.01M PV. The MWCNTs suspension first was ultrasonically agitated for 30 minutes in the presence of PV in water bath, then pyrrole was added into the solution. The mixed solution was stirred 15 minutes before electrodeposition. Composites were deposited on stainless steel and nickel plaque at both constant current and pulse current conditions. The procedure was shown in Figure 5-4.

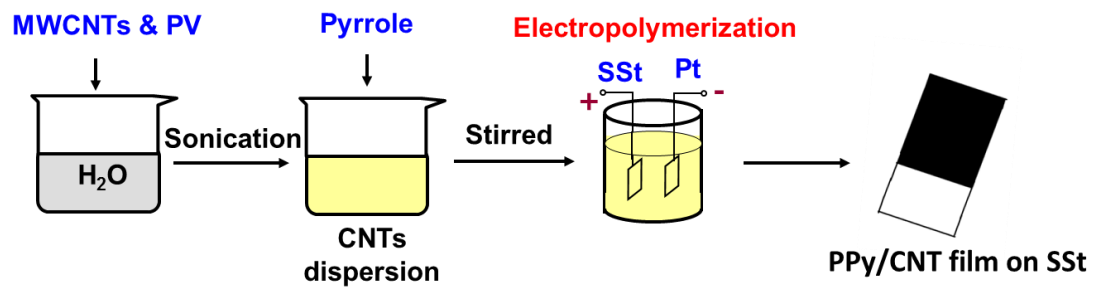


Figure 5 - 4 Scheme of PPy/CNT composite fabrication process by using PV

6 Characterization

6.1 Electrochemical Characterization

The electrochemical characterization of PPy and PPy/CNT films were performed using Potentiostat (PARSTAT 2273, Princeton Applied Research), controlled by the PowerSuite electrochemical software. A standard three electrode electrochemical cell was used in the test. Surface area of the working electrode was 1 cm^2 . The counter electrode was a platinum gauze, and the reference electrode was a standard calomel electrode (SCE). Capacitive behaviour and electrochemical impedance of the films were investigated in 0.5 M Na_2SO_4 aqueous solutions. Cyclic voltammetry (CV) studies were performed within a potential range of -0.5 - +0.4 V versus SCE at scan rates of 2 – 100 mVs^{-1} . The SC was calculated using half the integrated area of the CV curve to obtain the charge (Q), and subsequently dividing the charge by the film mass (mass) and width of the potential window (ΔV):

$$C = \frac{Q}{m\Delta V} \quad (6-1)$$

The materials loading in all films used for electrochemical testing was in a range mass of $100 \mu\text{g cm}^{-2}$ – 1 mg cm^{-2} . Impedance spectroscopy investigations were performed in the frequency range of 0.1 Hz – 100 Hz.

6.2 Investigation of deposition yield

The electrodeposition yield was studied by measuring the deposit weight of deposited coating. In this work, the deposit weight of a deposited coating was obtained by weighing the stainless steel substrate before and after the deposition, followed by drying at room temperature for 2 hours.

6.3 Scanning electron microscopy (SEM)

The SEM is a type of electron microscope that images the morphology of sample surface by scanning it with high-energy beam of electrons in a scan pattern. The electrons interact with the atoms that make up the image producing signals that contain information about the sample's surface topography, composition and other properties.

In this work, the microstructure of the films was investigated using the JEOL JSM-700F SEM.

6.4 Film Adhesion Test

Film adhesion was tested according to the ASTM D3359 standard. This test method is used to establish whether the adhesion of a coating to a substrate is at a generally adequate level. It does not distinguish between higher levels of adhesion for which more sophisticated methods of measurement are required.

In this test, a lattice pattern with six cuts in each direction and the cuts 1 mm apart is made in the film to the substrate, pressure-sensitive tape (Elcometer 1539) is applied over the lattice and then removed, and adhesion is evaluated by comparison with illustration Figure 6-1 [74] provided in the standard.

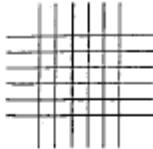
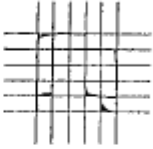

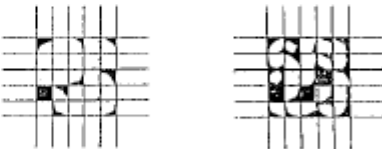
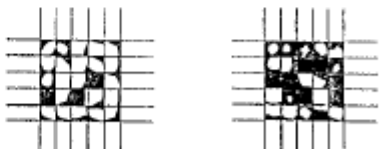
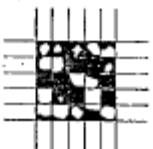
CLASSIFICATION OF ADHESION TEST RESULTS		
CLASSIFICATION	PERCENT AREA REMOVED	SURFACE OF CROSS-CUT AREA FROM WHICH FLAKING HAS OCCURRED FOR SIX PARALLEL CUTS AND ADHESION RANGE BY PERCENT
5B	0% None	
4B	Less than 5%	
3B	5 - 15%	
2B	15 - 35%	
1B	35 - 65%	
0B	Greater than 65%	

Figure 6 - 1 Classification of Adhesion Test results [74]

7 Results and Discussion

7.1 Electropolymerization of PPy using GA as an Anionic Dopant

7.1.1 Deposition Yield

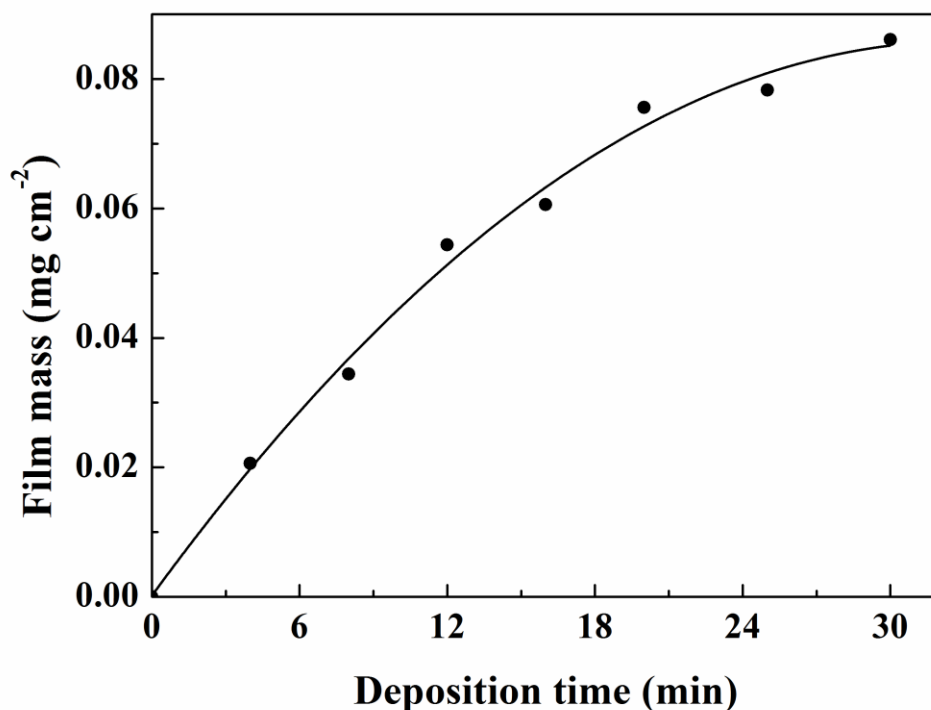


Figure 7 - 1 PPy/GA film mass versus deposition time at 1 mAc^{m-2}

The black uniform PPy films were obtained on the stainless steel substrate by anodic polymerization from a 0.2 M pyrrole aqueous solution containing 0.05 M GA at a constant current density of 1 mAc^{m-2}. The deposit mass versus time dependence presented in Figure 7-1 showed a non-linear behaviour and indicated a continuous film growth. However, due to the non-linear behaviour, it is difficult to control the amount of the deposited materials by varying the deposition time at a constant current density.

7.1.2 Electrochemical Studies

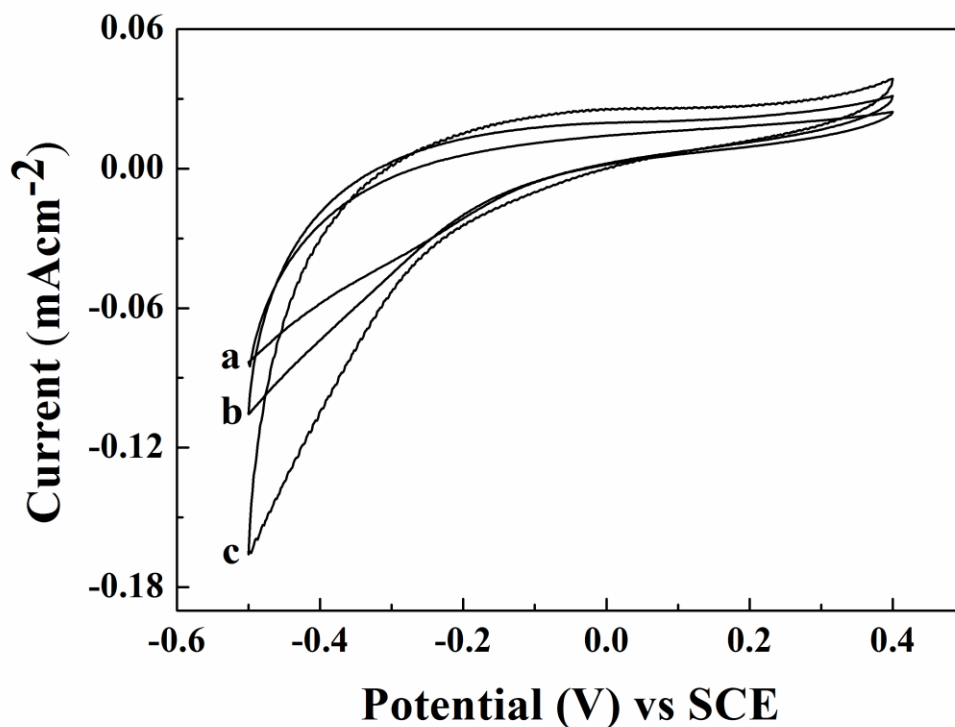


Figure 7 - 2 CV for the 211 μgcm^{-2} film deposited from the 0.2 M pyrrole solution containing 0.05 M GA on stainless steel in 0.5 M Na_2SO_4 electrolyte at scan rate of (a) 2, (b) 5 and (c) 10 mVs^{-1}

The electrochemical properties of the PPy/GA films were studied in 0.5 M Na_2SO_4 solutions using cyclic voltammograms (CV) as shown in Figure 7-2. The film shows capacitive behaviour in the voltage window of 0.9 V. The area of CV increases with increasing scan rate. The CVs show that PPy/GA film exhibits poor capacitive behaviour, as indicated by narrow and small area CVs.

7.1.3 Specific Capacitance

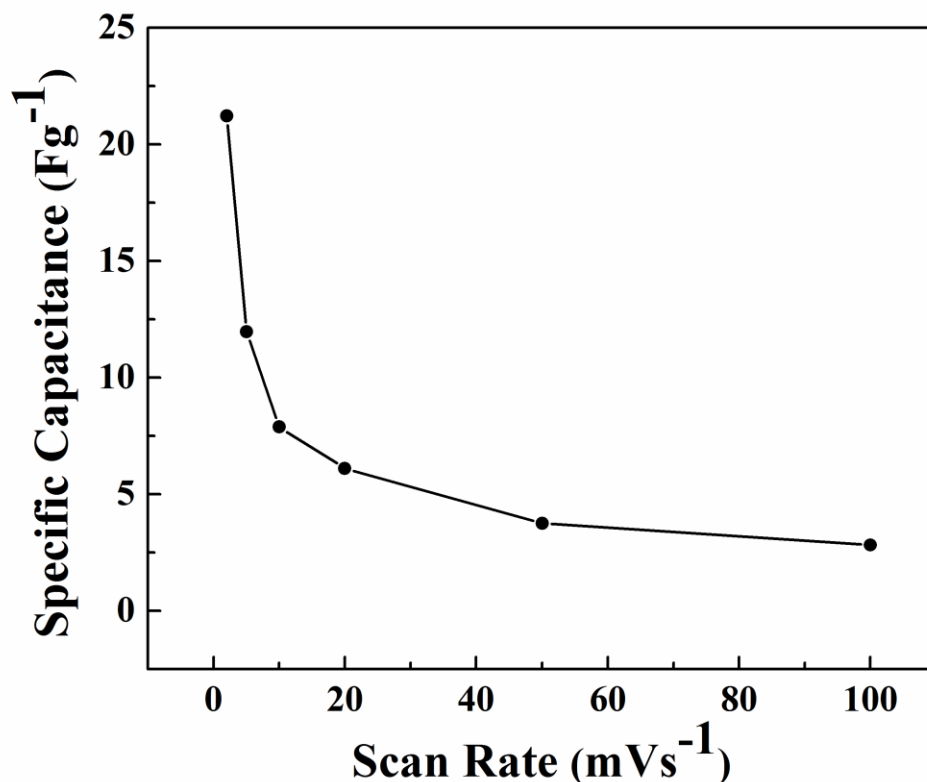


Figure 7 - 3 SC versus scan rates for the 211 μgcm^{-2} film deposited from the 0.2 M pyrrole solution containing 0.05 M GA on a stainless steel

Figure 7-3 shows specific capacitance (SC) versus scan rate for 211 μgcm^{-2} film prepared from the 0.2 M pyrrole solutions containing 0.05 M GA. The highest SC value of 21.2 Fg^{-1} was achieved at 2 mVs^{-1} scan rate, which is much lower than that for PPy doped with tiron (254 Fg^{-1})[75]. The SC decreased with increasing scan rate in the range of 2 – 100 mVs^{-1} . Such decrease is attributed to diffusion limitations of electrolyte in the pores of PPy matrix and low ion mobility within the pores. As the scan rate was increased to 100 mVs^{-1} , practically no capacitive behaviour was observed.

7.2 Electropolymerization of PPy using SSA as an Anionic Dopant

7.2.1 Cyclic Voltammograms for Electropolymerization of PPy

The cyclic voltammograms of the sweeps recorded during the electrodeposition of PPy film on the stainless steel electrode from aqueous solution containing 0.01 M SSA and 0.1 M pyrrole are shown in Figure 7-4.

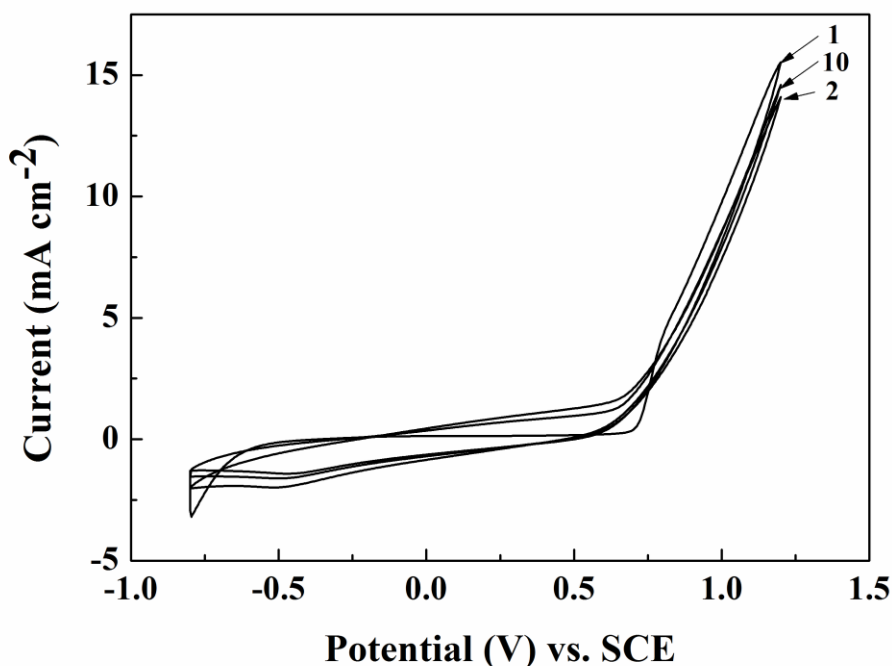


Figure 7 - 4 Cyclic voltammograms at a scan rate of 20 mVs⁻¹ from solution containing 0.01 M SSA and 0.1 M pyrrole

The first positive cycle was characterized by a sharp increase in the anodic current at ~0.7V. A rapid decrease of current was shown in negative sweep. The sharp increase of current after 0.7 V indicated that the PPy generated on the substrate since. Indeed, a black uniform film was observed on the electrode surface. It was also noted that the current

continuously increased when the potential is above 0.7V, which means that the PPy film doped with SSA has a very good conductivity. The deposit was formed as a result to the chain reaction of pyrrole units with cation radicals, and the polymerization on the metal surface. It was noted that the current slightly decreased during cycling. Such decrease can be attributed to film growth at the potentiodynamic condition. It is suggested that the increase in film thickness resulted in increasing film resistance. As a result, the current decreased during cycling. However, such decrease is extremely small compared to published literature [76] . Even after 10 cycles, there is almost no change in current, which indicated excellent conductivity of PPy film doped with SSA.

7.2.2 Galvanostatic Electropolymerization of PPy

The PPy films were obtained on the stainless steel substrate at a constant current of 1 mA cm^{-2} from 0.10 M pyrrole solutions containing 0.01 M SSA. On the other hand, for the purpose of comparison, the deposition was also performed at the same condition in the presence of 0.01 M p-toluenesulfonic acid (PTSA) within the same deposition time of 600s. The galvanostatic behaviour is shown in Figure 7-5, the inset shows corresponding chemical structure of PTSA and SSA.

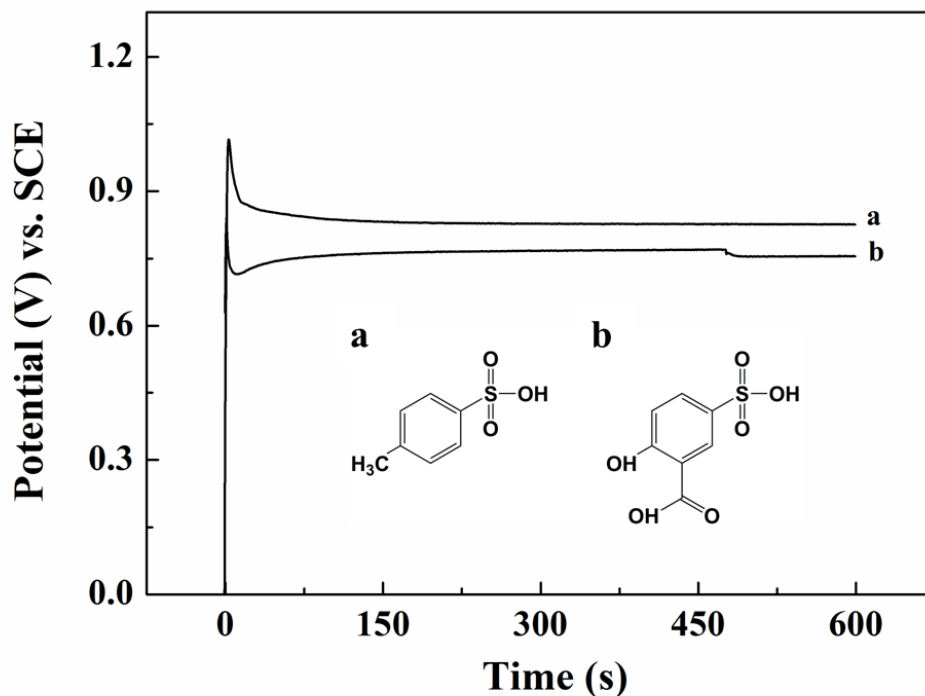


Figure 7 - 5 Galvanostatic behavior of PPy deposit on stainless steel from a 0.10 M pyrrole solution in the presence of 0.01 M (a) PTSA and (b) SSA at a current density of 1 mA cm⁻². Inset shows the chemical structure of (a) PTSA and (b) SSA.

The black thicker uniform and strongly adherent deposit was achieved in the presence of SSA whilst the very thin and non-adherent film was observed in the presence of PTSA, indicating that SSA facilitated a two-stage nucleation and growth process during the electropolymerization of PPy as an electron transfer mediator. It was noticed that in the nucleation stage, the oxidation potential value (peak) of curve b (in the presence of SSA) is lower than curve a (in the presence of PTSA). This can be attributed to the conductive passive layer formed due to the SSA complexation with iron on the

stainless steel substrate. PTSA cannot form such complex with iron on the stainless steel substrate. The comparison of the chemical structures of PTSA and SSA and the experimental data shown in Figure 7-5 indicated that COOH and OH groups of SSA were beneficial for the complexation and application of this material as an additive for PPy electropolymerization on stainless steel substrate. The COOH and OH groups provided chelation of the metal atoms on the substrate surface.

In the electrodeposition process, namely, growth stage of PPy, the potential difference between the working and reference electrode after the peak decreased to a steady value. The deposition potential (plateau region) of curve from the solution containing SSA was 0.1 V lower than that for PTSA. The reduced deposition potential is beneficial for suppressing the substrate dissolution. It was suggested that the adsorbed SSA molecules with conjugated bonds provided efficient charge transfer during electropolymerization, reduced the deposition potential and ensure the electrical neutrality of film. It has previously been shown that salicylates self-assemble on various inorganic substrates, and such adsorbed layers exhibited good chemical stability [77, 78]. The absorption mechanism was related to the surface complexation of metal atoms. The suggested mechanisms of complexation shown in Figure 4-3(b). The bonding mechanism involved the replacement of surface hydroxyl groups with deprotonated salicylate.

7.2.3 Characterizations of PPy Film Prepared Using SSA

7.2.3.1 Deposition Yield

Strongly adherent PPy films were obtained on the stainless steel substrate by anodic polymerization from a 0.1 M pyrrole aqueous solution containing 0.01 M SSA at a

constant current density of 1 mA cm^{-2} . Figure 7-6 shows deposition yield versus time dependence. Nearly linear dependence was obtained, indicating continuous growth without any induction time. Therefore, the amount of the deposited material can be easily controlled by the variation of deposition time at a constant current density.

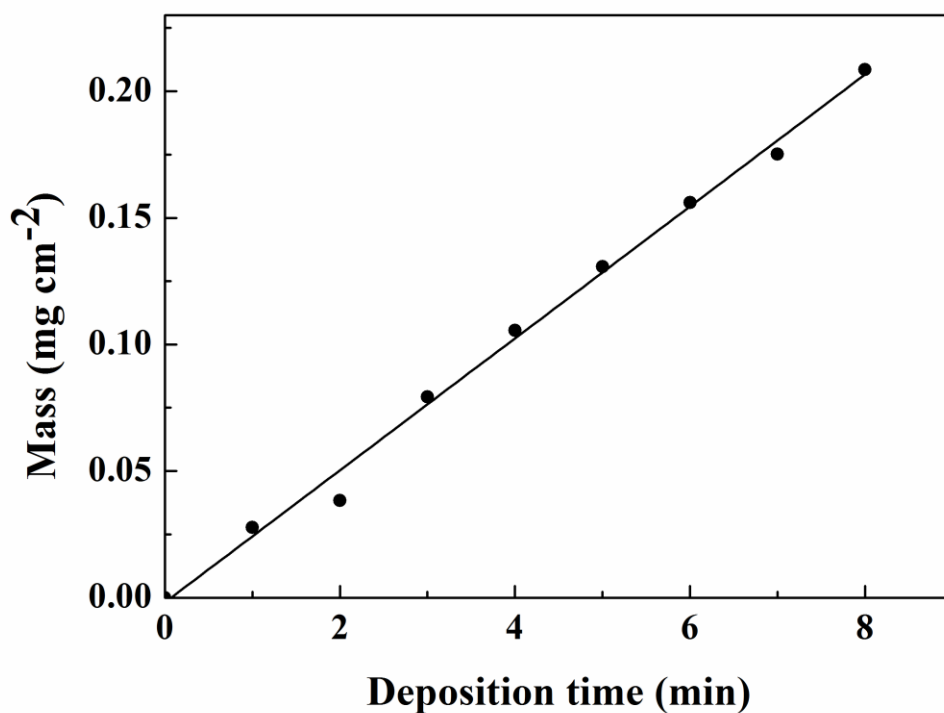


Figure 7 - 6 PPY/SSA film mass versus deposition time at 1 mA cm^{-2}

7.2.3.2 Electrochemical Studies

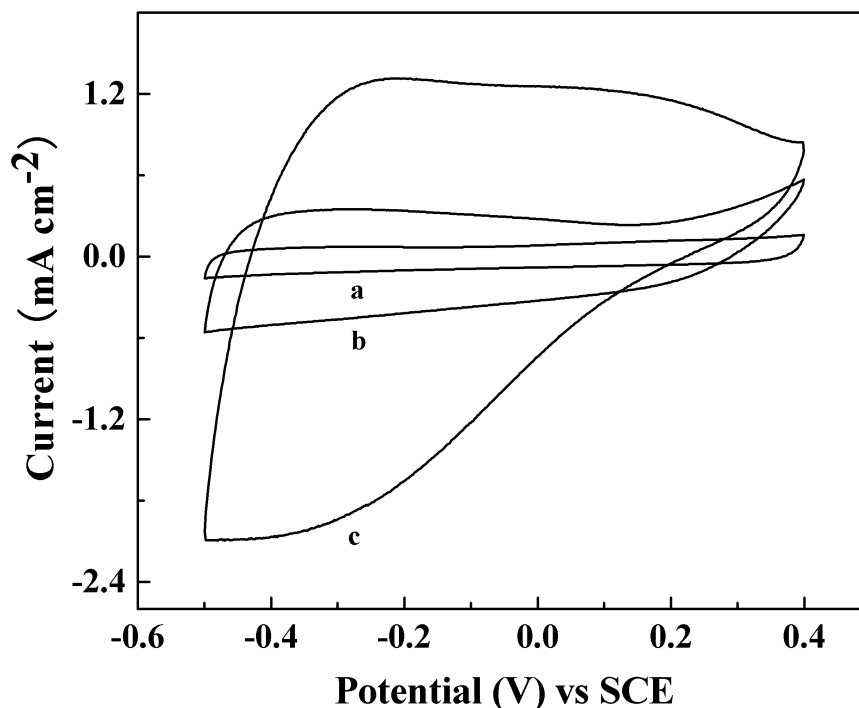
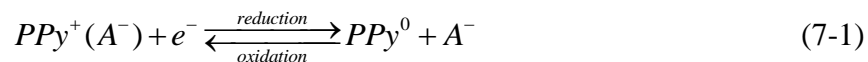


Figure 7 - 7 Cyclic voltammetry data at scan rates of a (a) 2 mV s⁻¹, (b) 10 mV s⁻¹, (c) 50 mV s⁻¹ for 208 $\mu\text{g cm}^{-2}$ film prepared at a current density of 1 mA cm⁻² from 0.1M pyrrole solution containing 0.01 M SSA.

The electrochemical properties of the PPy/SSA films were studied in 0.5 M Na₂SO₄ solutions using cyclic voltammograms (CV) as shown in Figure 7-7. Compared to PPy/GA films, the PPy/SSA films show better capacitive behaviour and box shape CV in a voltage window of 0.9 V between -0.5 V – 0.4 V at low scan rates. The area of CVs increased with increasing scan rate. The CVs show that PPy film exhibits improved

capacitive behaviour in the negative potential window range. The SSA ions participated in the electroactive behaviour by insertion and de-insertion from the matrix during the oxidation and reduction process. The redox reactions of PPy can be expressed as follows:



Where A^- is the counter anion.

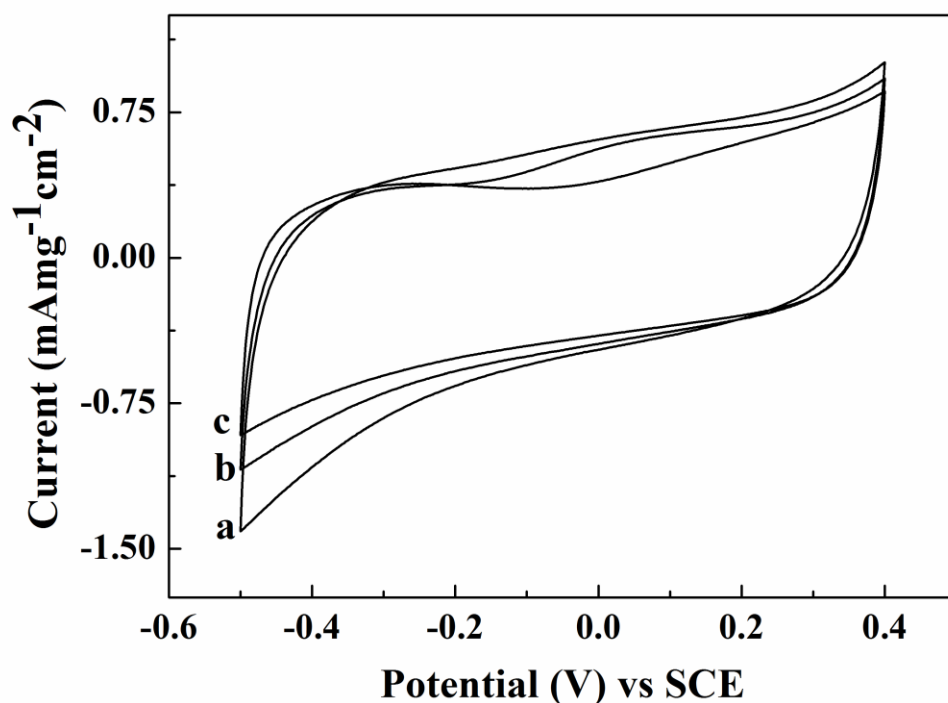


Figure 7 - 8 Cyclic voltammetry data at scan rate of 2 mV s^{-1} for the films of different mass: (a) $108.85 \text{ } \mu\text{g cm}^{-2}$, (b) $160.42 \text{ } \mu\text{g cm}^{-2}$, (c) $263.54 \text{ } \mu\text{g cm}^{-2}$ prepared at a current density of 1 mA cm^{-2} from 0.1 M pyrrole solution containing 0.01 M SSA.

The CVs for PPy films of different mass, prepared from 0.1 M pyrrole solution containing 0.01 M SSA, were studied in a 0.5 M Na₂SO₄ solution as shown in Figure 7-8. All the films showed good capacitive behavior in the voltage window of -0.5 to +0.4 V versus SCE, as indicated by nearly box shape CVs, which did not show any redox peaks. It was also noticed that the area of CV decreases with increasing film thickness. Such decrease was attributed to diffusion limitations of electrolytes in pores. As shown in Figure 7-9, as the film mass increases, the anions penetration into the PPy film is becomes limited.

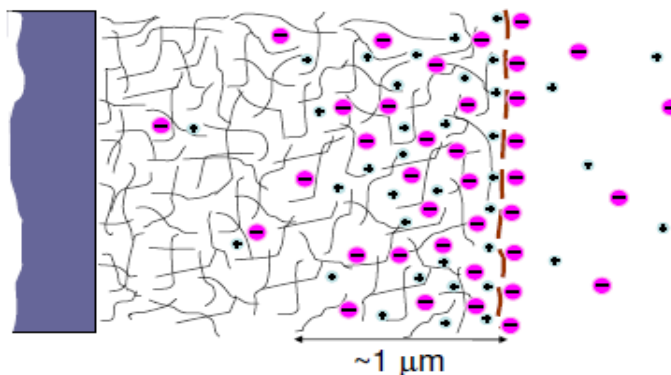


Figure 7 - 9 Limited depth of ion penetration

7.2.3.3 Specific Capacitance

Figure 7-10 shows specific capacitance (SC) versus scan rate for the films of different thickness prepared from the 0.1 M pyrrole solution containing 0.01 M SSA. The films show SC in the range of 200 – 300 F g⁻¹ at a scan rate of 2 mV s⁻¹. The SC decreased with increasing film thickness and increasing scan rate in the range of 2 – 100 mVs⁻¹. Such decrease is attributed to diffusion limitations of electrolyte in pores (Figure 7-9).

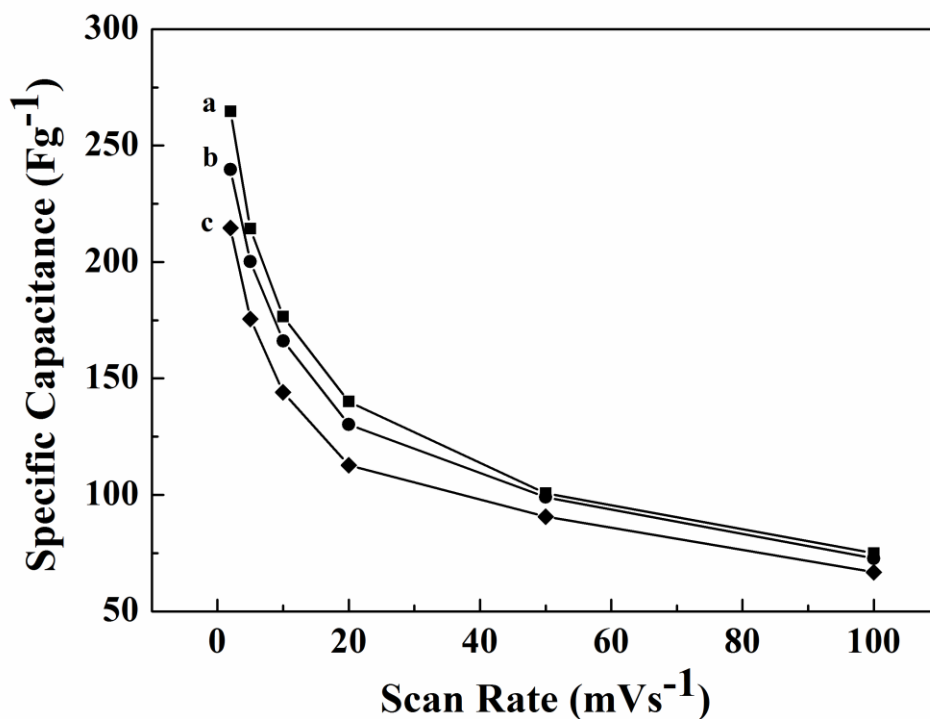


Figure 7 - 10 Specific capacitance versus scan rate for the films of different mass: (a) 108.85 $\mu\text{g cm}^{-2}$, (b) 160.42 $\mu\text{g cm}^{-2}$, (c) 263.54 $\mu\text{g cm}^{-2}$ prepared at current density of 1 mA cm^{-2} from 0.1 M pyrrole solution containing 0.01 M SSA.

7.2.3.4 Morphology Characterization

Figure 7-11 shows surface of the PPy/SSA film deposited on a stainless steel substrate. It showed that the films were crack free, relatively dense and exhibited relatively low porosity. In addition, anodic electropolymerization has also been utilized for the film formation on substrates of complex shapes. As an example, Figure 7-12 shows PPy film coated stainless steel mesh. The high magnification (inset) image of the

mesh surface shows morphology similar to that obtained using a stainless steel foil substrate.

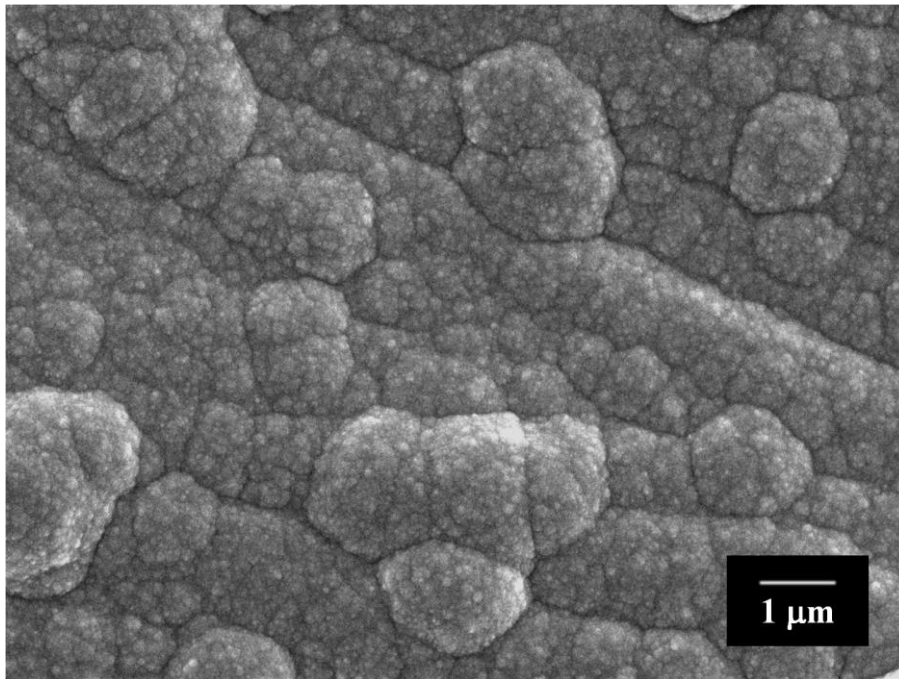


Figure 7 - 11 SEM image of surface for PPy/SSA on stainless steel foil substrate.

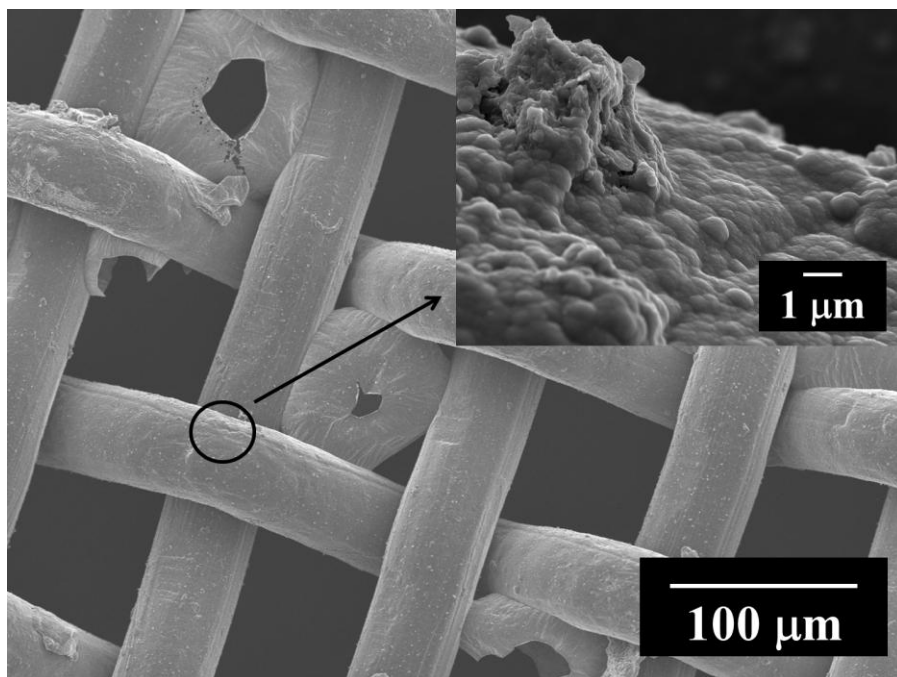


Figure 7 - 12 SEM images for the PPy/SSA film on a stainless steel mesh. Inset is the surface image in the circle area at high magnification.

7.2.4 Corrosion Performance of PPy Coated Stainless Steel

7.2.4.1 Open Circuit Potential (OCP) Measurement

The OCP of PPy coated stainless steel substrate and bare stainless steel immersed in aqueous 0.5 M Na_2SO_4 was measured separately as a function of time and the corresponding plot is presented in Figure 7-13.

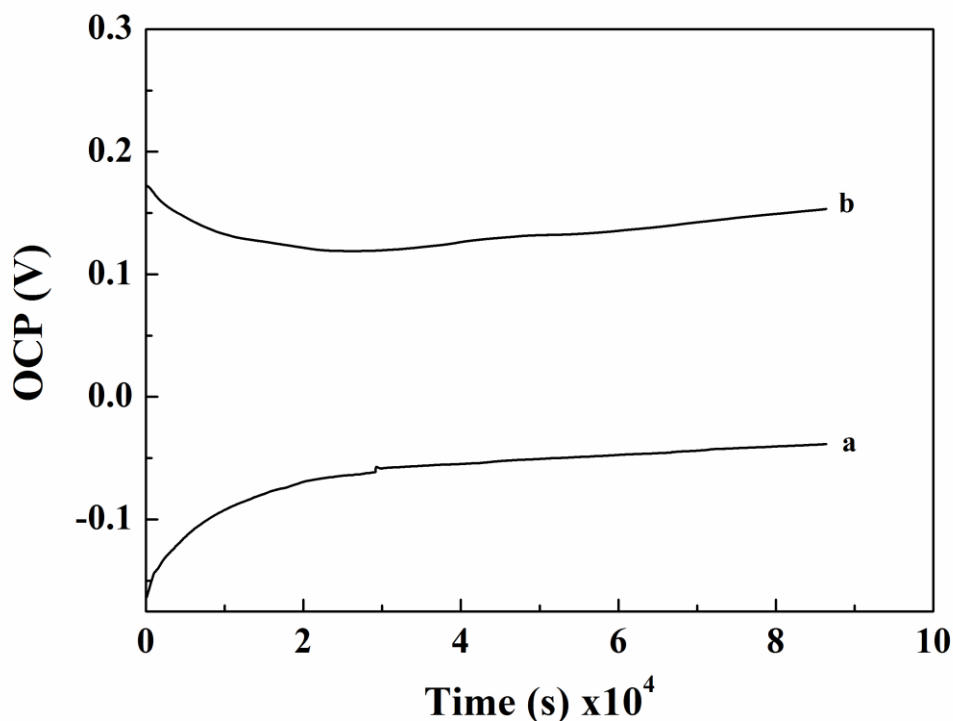


Figure 7 - 13 OCP-time curve recorded for (a) bare stainless steel and (b) PPy coated stainless steel in aqueous 0.5 M Na₂SO₄ solution.

In this figure, curve (a) represents the OCP of bare stainless steel, while curve (b) represents the OCP of PPy coated stainless steel. The initial values of the OCP of PPy coated stainless steel and bare stainless steel in 0.5 M Na₂SO₄ were 0.17 V and -0.16 V, respectively. The E_{ocp} value of PPy coated stainless steel was more positive compared to the bare stainless steel, this indicated that PPy film provided a protective barrier, preventing electrolyte penetration to the substrate surface.

7.2.4.2 Potentiodynamic Polarization

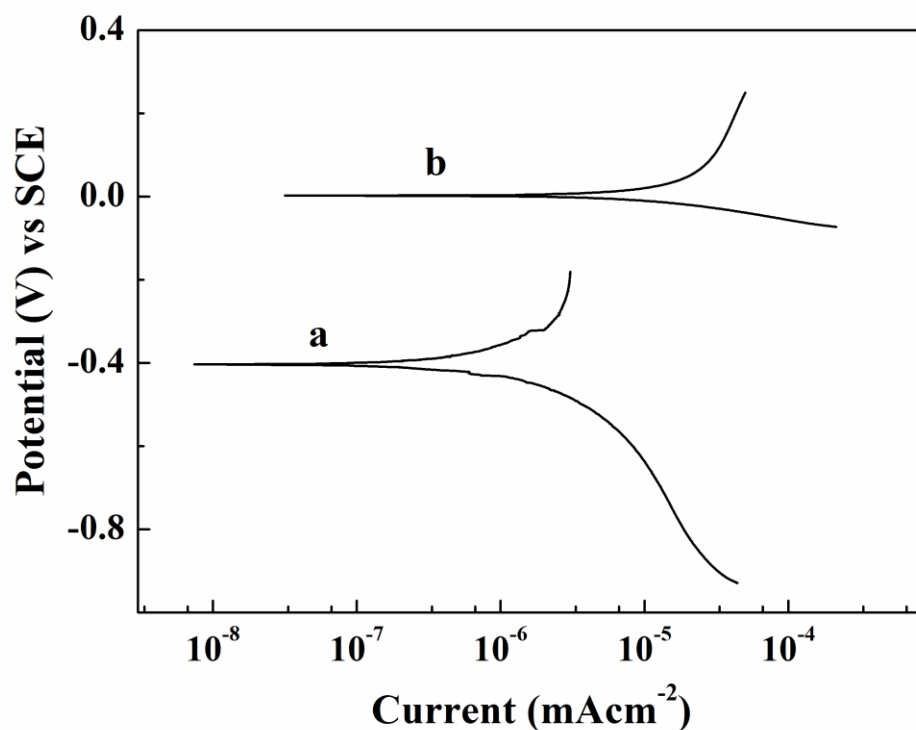


Figure 7 - 14 Potentiodynamic polarization curves for (a) bare stainless steel and (b) PPy coated stainless steel recorded in a 0.5 M Na₂SO₄ solution.

The potentiodynamic polarization curves for bare stainless steel and PPy doped with SSA coated on stainless steel were obtained in a 0.5 M Na₂SO₄ solution (Figure 7-14).

The Tafel plots show that the PPy caused a remarkable potential shift of ~ 0.4 V of the corrosion potential (E_{corr}), relative to the corresponding value of the uncoated stainless steel (~ -0.4 V). The positive shift in E_{corr} confirmed the PPy barrier indicates

corrosion protection of steel, and the Tafel result was in a good agreement with OCP measurements.

7.3 Pulse Deposition of PPy films using SSA as an Anionic Dopant

PPy films were deposited on stainless steel substrates by pulse electropolymerization from pyrrole solutions containing 5-sulfosalicylic acid (SSA) as an anionic additive. The deposition yields at pulse deposition and galvanostatic conditions were compared. The films were investigated using scanning electron microscopy (SEM), cyclic voltammetry (CV), and electrochemical impedance spectroscopy (EIS). The results presented below indicated that the films prepared by pulse deposition method showed finer particle size, lower resistance and higher capacitance compared to the films deposited galvanostatically. The highest specific capacitance (SC) of 545 Fg^{-1} was obtained at a scan rate of 2 mVs^{-1} . The films prepared by the pulse deposition method on stainless steel substrates are promising electrode materials for application in electrochemical supercapacitors.

7.3.1 Deposition Yield

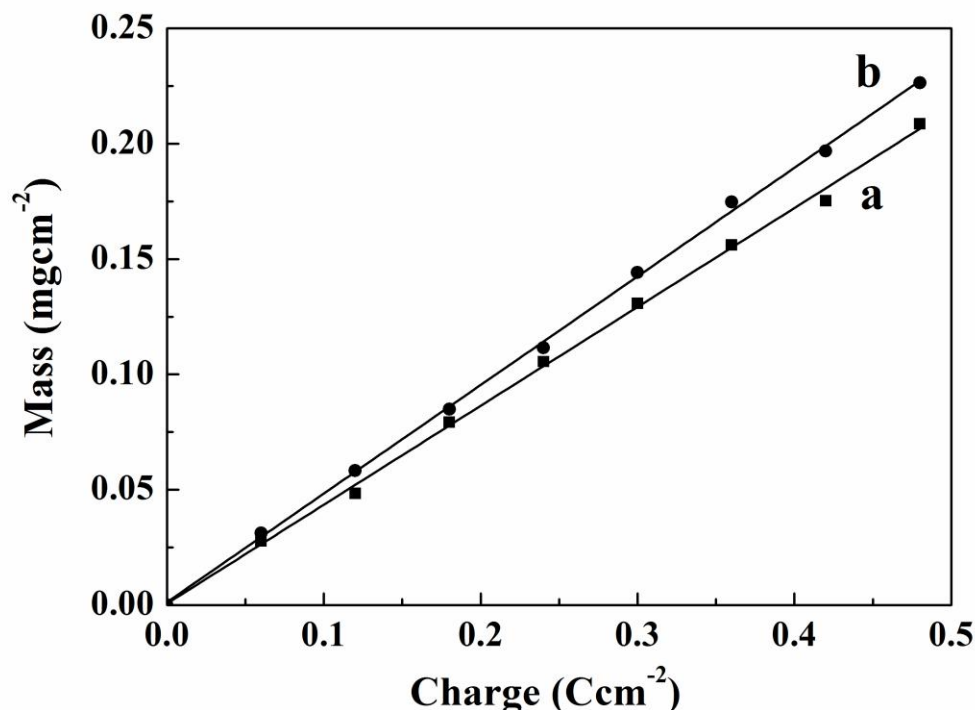


Figure 7 - 15 Deposit mass versus charge passed for deposition from 0.1 M pyrrole solution containing 0.01 M SSA using (a) galvanostatic method, and (b) pulse deposition with ON/OFF times of 0.5 s.

PPy films were prepared using pulse deposition and galvanostatically. Figure 7-15 shows deposition yield as a function of charge passed. The deposition yield measurements showed continuous film growth. Nearly linear dependences were obtained, which indicated film growth without induction time. The deposition yield for the films deposited in the pulse regime was slightly higher than that for the films deposited galvanostatically. It is suggested that pyrrole and SSA consumption in the polymerization reaction led to the reduction of pyrrole and SSA concentration close to the electrode

surface and reduced deposition efficiency. The diffusion during the OFF time in the pulse regime allowed pyrrole and SSA replenishment at the electrode surface, resulting in higher deposition efficiency.

7.3.2 Electrochemical Studies

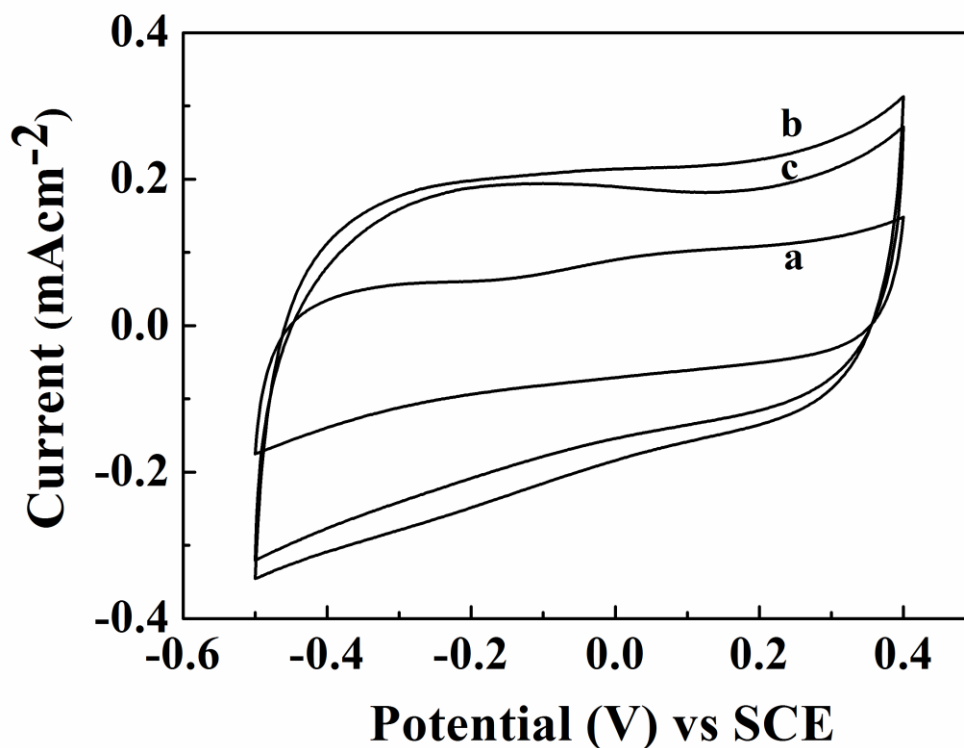


Figure 7 - 16 Cyclic voltammetry data at a scan rate of 2 mVs⁻¹ for 0.2 mg cm⁻² films prepared from 0.1 M pyrrole solution containing 0.01 M SSA using (a) galvanostatic method and (b,c) pulse deposition method with ON/OFF times of (b) 0.5 and (c) 1.5 s.

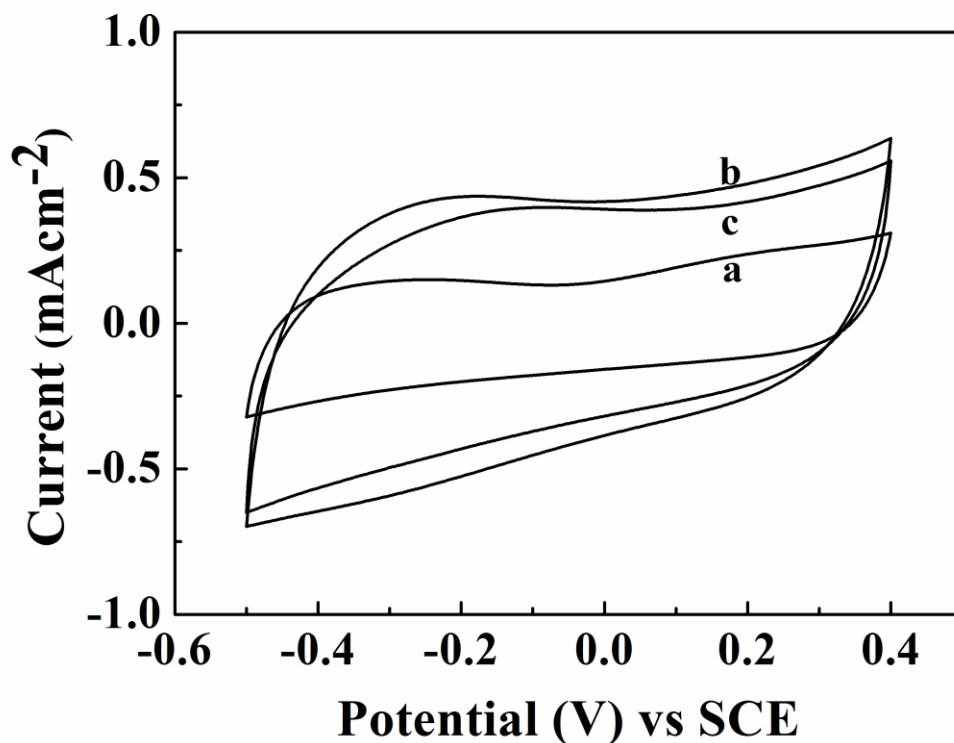


Figure 7 - 17 Cyclic voltammetry data at a scan rate of 5 mVs^{-1} for 0.2 mg cm^{-2} films prepared from 0.1 M pyrrole solution containing 0.01 M SSA using (a) galvanostatic method and (b,c) pulse deposition method with ON/OFF times of (b) 0.5 and (c) 1.5 s .

Figures 7-16, 17, 18, compare CVs for the films prepared galvanostatically and by pulse deposition method. The films showed good capacitive behaviour in the voltage window of -0.5 to $+0.4 \text{ V}$ versus SCE, as indicated by nearly box shape CVs, which did not show any redox peaks. The CV area of the films prepared by pulse deposition was larger than that for the galvanostatically deposited films. The films prepared at pulse duration of 0.5 s showed larger CV area compared to the films prepared at pulse duration of 1.5 s . The larger CV area indicated higher SC for the films of the same mass.

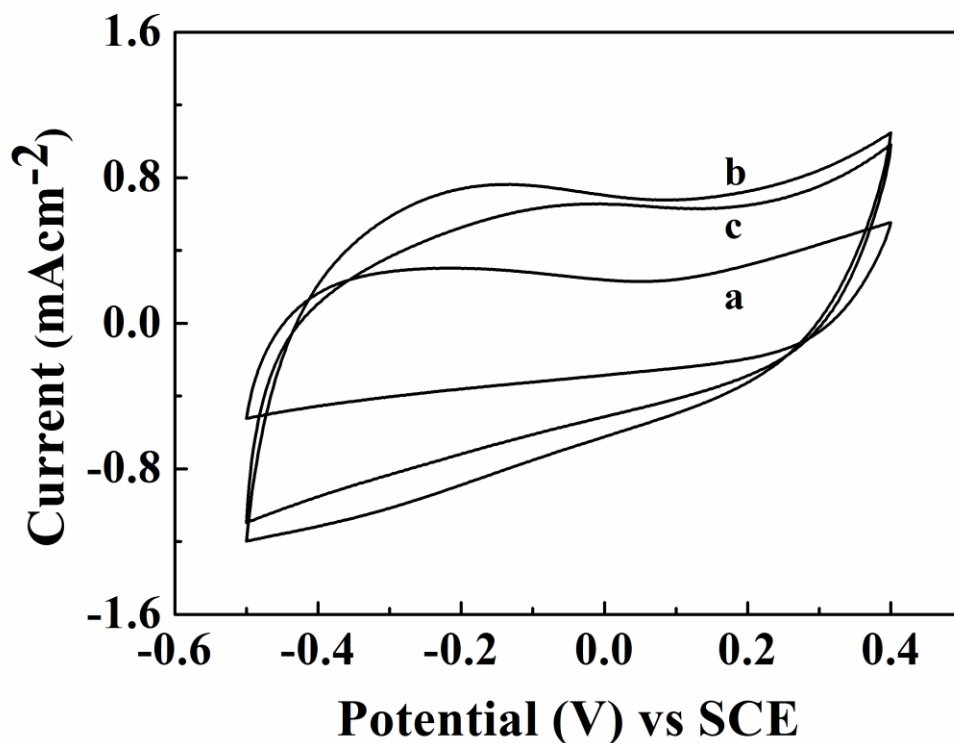


Figure 7 - 18 Cyclic voltammetry data at a scan rate of 10 mVs^{-1} for 0.2 mg cm^{-2} films prepared from 0.1 M pyrrole solution containing 0.01 M SSA using (a) galvanostatic method and (b,c) pulse deposition method with ON/OFF times of (b) 0.5 and (c) 1.5 s .

7.3.3 Specific Capacitance

The SCs calculated from the CV data were plotted versus scan rate in Figure 7-19. The highest capacitance of 545 F g^{-1} was observed for films prepared at pulse duration of 0.5 s at a scan rate of 2 mVs^{-1} . The films prepared at pulse duration of 1.5 s and galvanostatically deposited films showed SCs of 443 and 240 F g^{-1} , respectively, at the same scan rate. The SC decreased with increasing scan rate. Such decrease can be attributed to diffusion limitations of electrolyte in pores of the films.

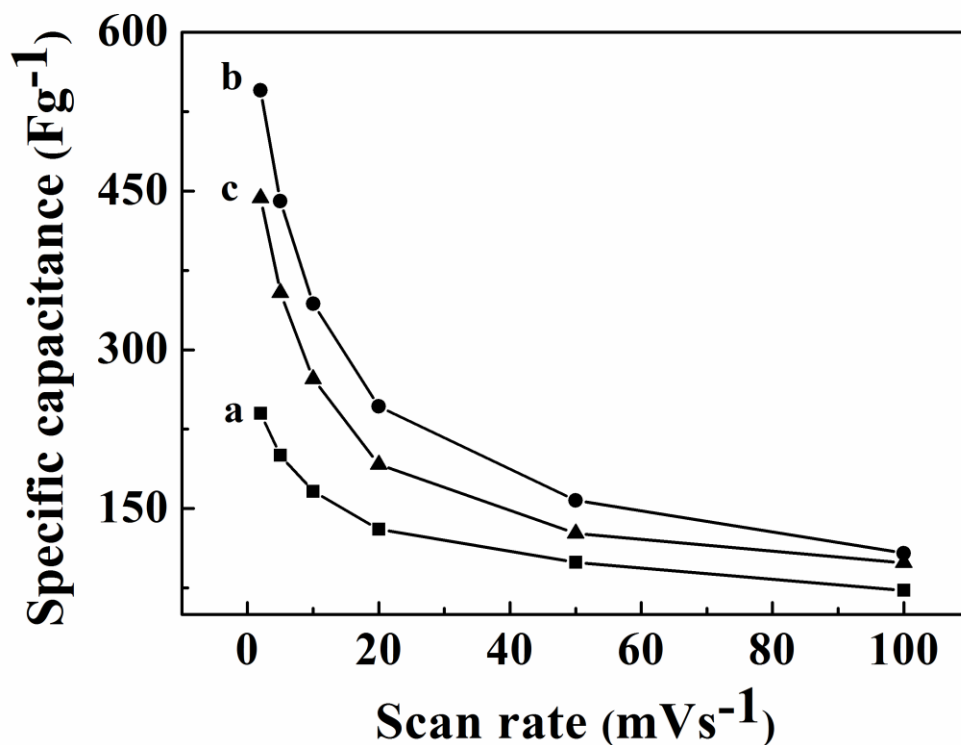


Figure 7 - 19 SC versus scan rate for 0.2 mg cm^{-2} films prepared from 0.1 M pyrrole solution containing 0.01 M SSA using (a) galvanostatic method and (b,c) pulse deposition method with ON/OFF times of (b) 0.5 and (c) 1.5 s .

7.3.4 Morphology Characterization

The films obtained by anodic electropolymerization were studied by SEM. Figure 7-20 compares SEM images of the films prepared in a pulse regime and galvanostatically. The films prepared galvanostatically contained particles with particle size of $\sim 1 \mu\text{m}$. The films prepared using pulse deposition method showed finer particle size. The films prepared by both methods were continuous and crack free.

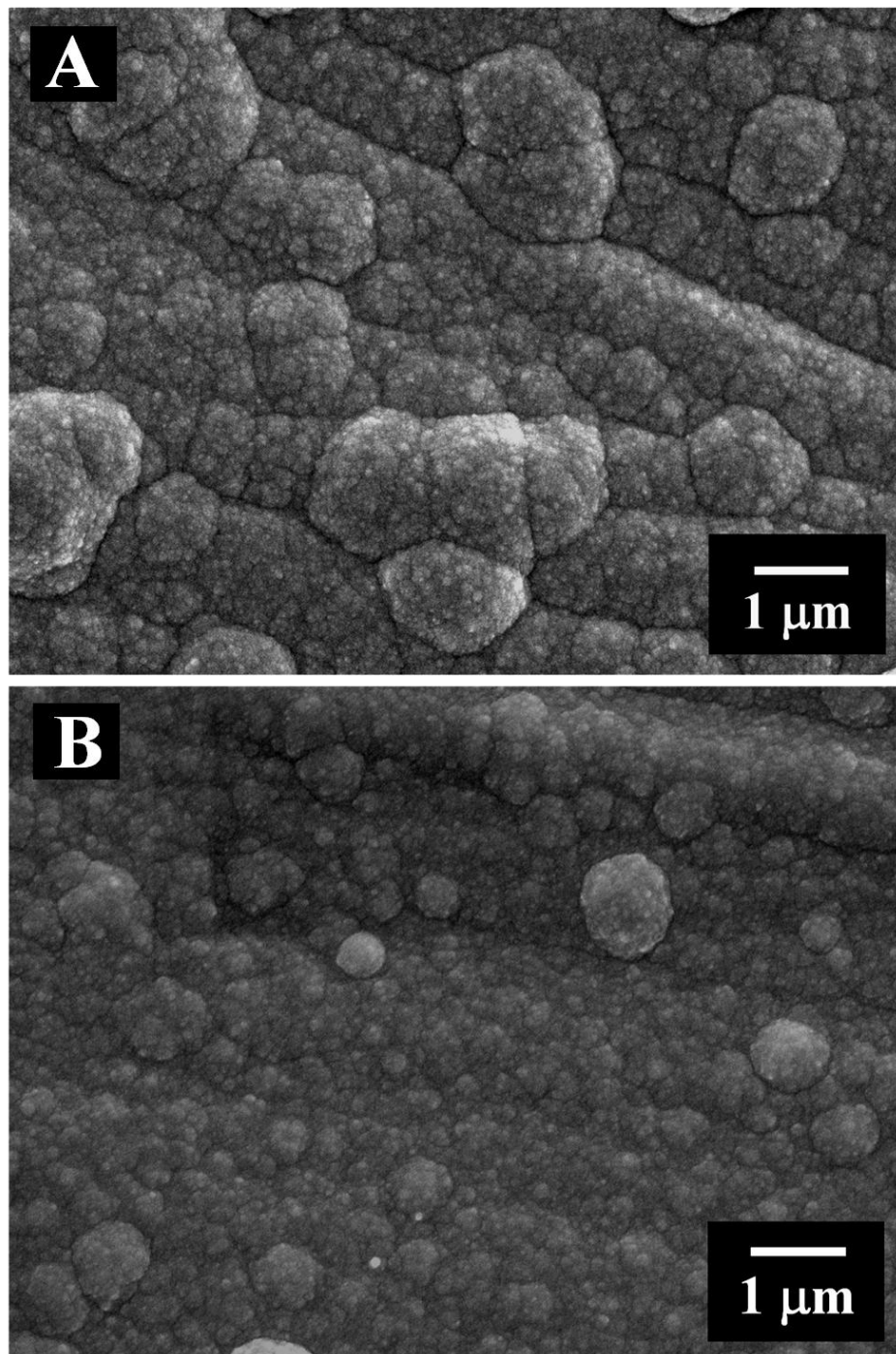


Figure 7 - 20 SEM images of films prepared from 0.1 M pyrrole solution containing 0.01 M SSA using (A) galvanostatic method, and (B) pulse deposition with ON/OFF times of 0.5 s.

7.3.5 Electrochemical Impedance Spectra

Figure 7-21 compares complex impedance $Z=Z'-iZ''$ for the film prepared by pulse and galvanostatic methods. The film prepared by pulse deposition showed lower Z' values, compared to the films deposited galvanostatically. The lower resistance value is beneficial for capacitive behavior. Turning again to the results of SEM investigations it should be noted that films prepared by pulse deposition showed finer particle size. As a result, the films prepared by pulse deposition showed higher SC compared to the films prepared galvanostatically. It should be noted that anodic oxidation of stainless steel usually results in an oxide layer at the film-substrate interface with high impedance and low capacitance. This leads to the low capacitance of the PPy electrode. The problem of anodic dissolution and oxidation of stainless steel current collector can be addressed by the use of SSA. The possibility to achieve high SC for the films deposited on stainless steel substrates paves the way for the application of PPy in advanced ES using low cost stainless steel current collectors.

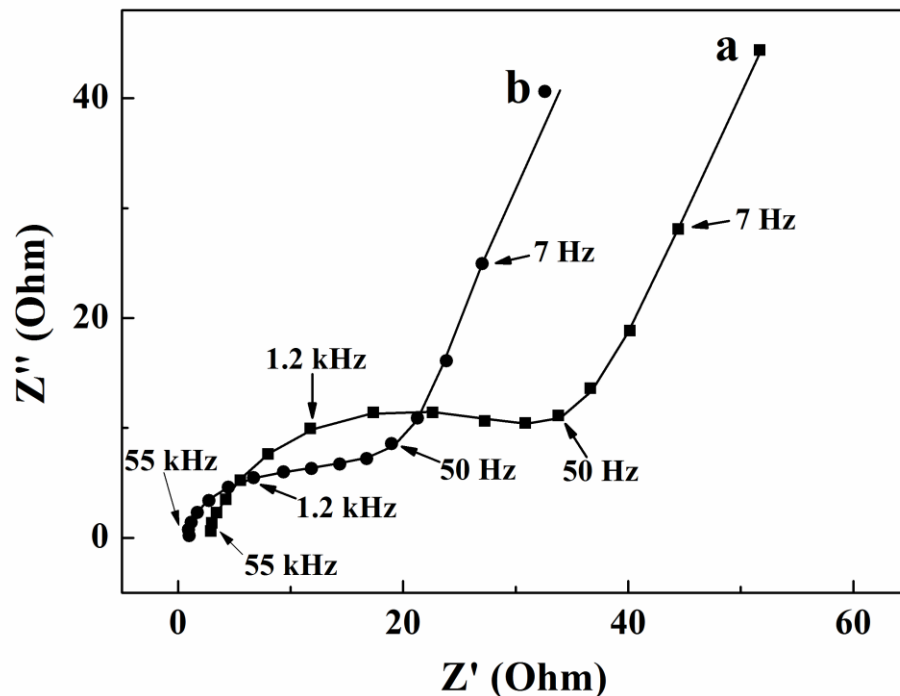


Figure 7 - 21 Nyquist plots of complex impedance $Z^*=Z'-iZ''$ for 0.2 mg cm^{-2} films prepared from 0.1M pyrrole solution containing 0.01 M SSA using (a) galvanostatic method and (b) pulse deposition method with ON/OFF times of 0.5 s.

7.4 Electro-Co-Deposition of PPy/SWCNTs from aqueous SSA/PPE solutions

Polypyrrole (PPy) films were obtained on stainless steel substrates by anodic electropolymerization using sulfosalicylic acid (SSA) as an anionic dopant. SSA adsorption prevented anodic oxidation of stainless steel during electropolymerization, provided efficient charge transfer and enabled the formation of adherent films. It was shown that anionic poly[2,5-bis(3-sulfonatopropoxy)-1,4-ethynylphenylene-alt-1,4-ethynylphenylene] sodium salt (PPE) provided efficient dispersion of single-walled

carbon nanotubes (SWCNT) and allowed the formation of composite PPy- SWCNT films. The PPy-SWCNT films showed improved capacitive behaviour compared to PPy films due to lower resistance and higher porosity. The highest specific capacitance (SC) of 295 Fg^{-1} was obtained at a scan rate of 2 mVs^{-1} . The composite films are promising materials for application in electrochemical supercapacitors (ES).

7.4.1 The Influence of PPE on Dispersion of SWCNTs

Figure 7-22 indicates that PPE provides efficient dispersion of SWCNTs. The supramolecular dispersion mechanism is based on the π - π stacking interactions, formation of polymer-SWNT complexes and electrostatic stabilization of SWCNT. The repulsion between the negatively charged side-chains prevented the bundling of SWCNT, and the resulting polymer-SWCNT suspensions were found to remain stable indefinitely, with no visible SWCNT precipitation over several months. Pristine SWNTs, in the absence of PPE, were not dispersed to any extent.

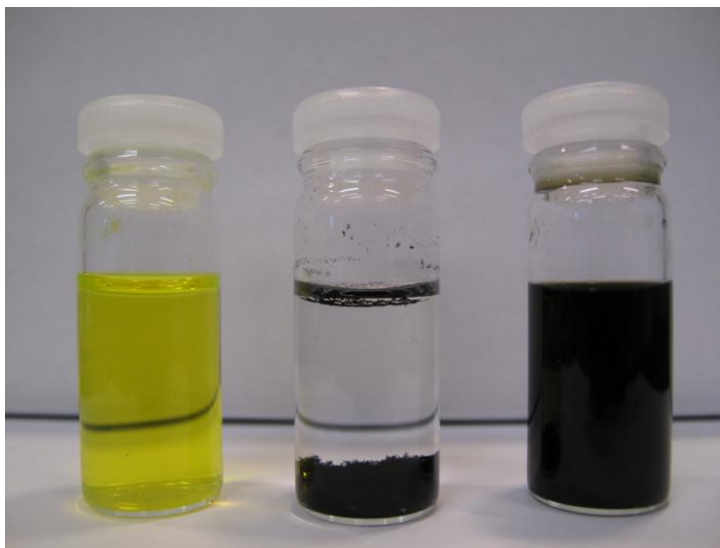


Figure 7 - 22 Aqueous PPE (left), SWCNT (middle), PPE and SWCNT (right).

7.4.2 Electrochemical Studies

The films prepared by the electrochemical polymerization from the pyrrole solutions were investigated for application in ES, and the results obtained for the pure PPy and composite PPy-SWCNT films were compared. The CV data shown in Figure 7-23 indicated the capacitive behaviour of the films in the 0.5 M Na₂SO₄ electrolyte. The comparison of the CV data for the pure PPy and composite PPy-SWCNT electrodes of the same mass showed improved capacitive behaviour of the composite electrode, as indicated by the larger area of the corresponding CV curve. The area of the CV for the pure PPy film was relatively small in the potential range of 0 – 0.4 V(SCE), indicating a poor capacitive behaviour in this range.

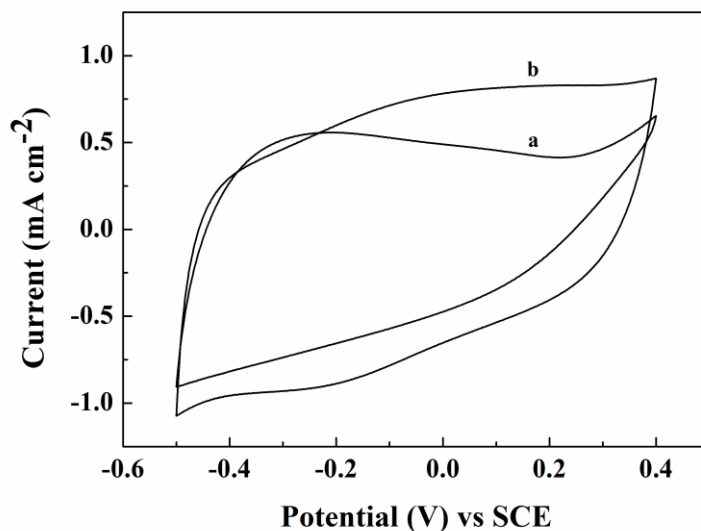


Figure 7 - 23 Cyclic voltammetry data at a scan rate of 20 mVs⁻¹ for 160 µg cm⁻² films prepared at current density of 1 mA cm⁻² from 0.1 M pyrrole solution containing 0.01 M SSA using (a) without additives and (b) containing 0.1 gL⁻¹ PPE and 0.1 gL⁻¹ SWCNTs.

7.4.3 Specific Capacitance

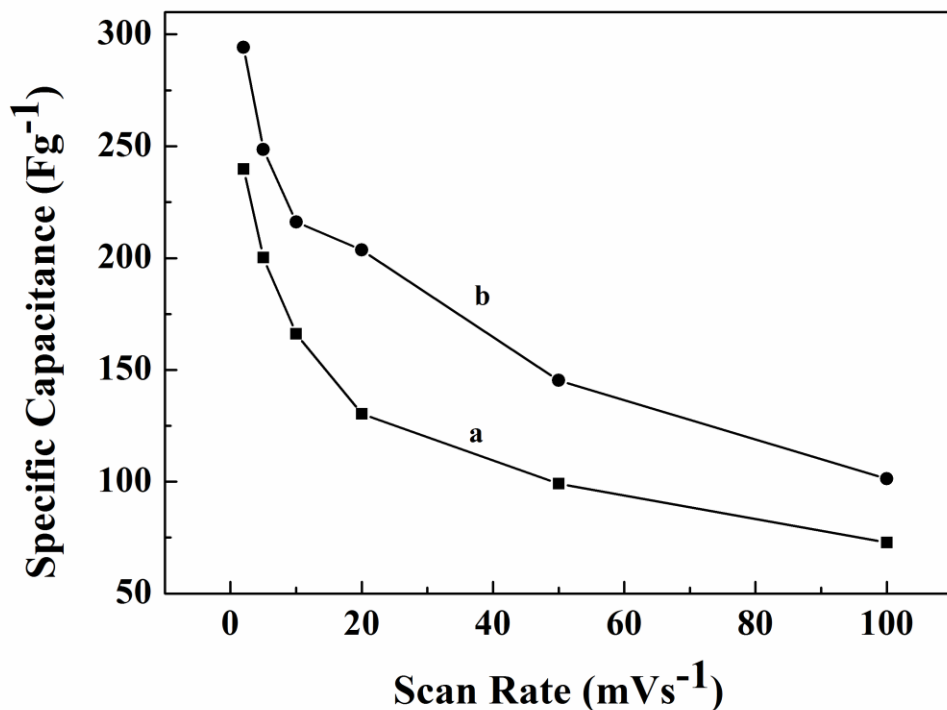


Figure 7 - 24 SC versus scan rate in a 0.5 M Na₂SO₄ solution for 160 $\mu\text{g cm}^{-2}$ films prepared at a current density of 1 mA cm⁻² from 0.1 M pyrrole solution containing 0.01 M SSA: (a) without additives and (b) containing 0.1 gL⁻¹ PPE and 0.1 gL⁻¹ SWCNT.

Figure 7-24 shows SCs calculated from the CV data at different scan rates for the PPy and PPy-SWCNTs films. The SC of PPy films decreased from 240 to 73 F g⁻¹ with an increasing scan rate from 2 to 100 mV s⁻¹. The composite PPy-SWCNTs films showed higher capacitance, compared to the pure PPy films. The highest SC of 294 F g⁻¹ was obtained at a scan rate of 2 mV s⁻¹.

Conductive additives, such as CNTs, are usually used in order to achieve high electronic conductivity in the composite materials. The advantages of CNTs include their good conductivity and high aspect ratio (>1000), which provides percolation effect at very low volume fractions. Moreover, CNTs mechanically reinforce the composite matrix and prevent cracking. However, CNTs possess a rather low SC, typically in the range of $10 - 40 \text{ F g}^{-1}$. Therefore, the amount of CNTs in the composite materials must be minimised, and the CNTs must be well dispersed in the polymer matrix. However, the CNTs show a strong tendency to agglomeration, and their dispersion in the polymer matrix presents difficulties. It is suggested that the method, developed in this investigation, offers processing advantages for the fabrication of composite materials containing CNTs. As pointed out above, PPE provided good dispersion of SWCNTs in the solutions, containing pyrrole monomer. The SWCNTs were incorporated in situ in the polymer matrix formed at the electrode surface. Therefore, the problems of the CNT agglomeration related to the mixing with polymer were diminished.

7.4.4 Morphology Characterization

The improvement in the capacitive behaviour of the composite PPy-SWCNT films compared to the PPy films was attributed to the changes in film morphology and incorporation of SWCNTs into the composited films. SEM investigations (Figure 7-25, 26, 27) showed a higher porosity of the PPy-SWCNT films compared to the pure PPy films. It was suggested that the higher porosity of the PPy-SWCNT films resulted in better electrolyte access to the active materials, whereas the incorporation of SWCNTs into the composite films resulted in an improved electronic conductivity. The SEM image

at high magnification (Figure 7-27) showed that SWCNTs were coated with PPy. It is suggested that the mechanism of film formation involved electrophoresis of anionic SWCNT-PPE complexes and their incorporation into PPy films formed by electropolymerization. It should be noted that PPy and PPy-SWCNT films were prepared at similar conditions, including current density and pyrrole concentration. Therefore, the porosity of PPy-SWCNT was mainly attributed to the incorporation of SWCNT into the PPy matrix. This was in a good agreement with the results of EIS studies.

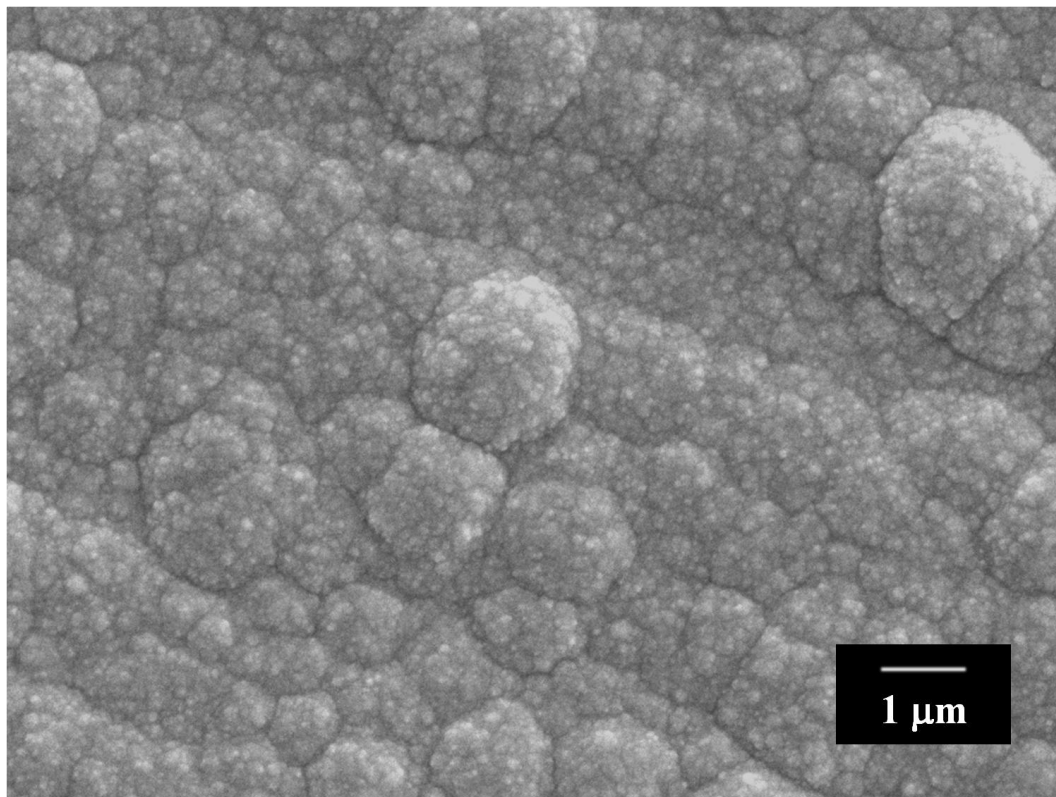


Figure 7 - 25 SEM image of film prepared at a current density of 1 mA cm^{-2} from 0.1 M pyrrole solution containing 0.01 M SSA.

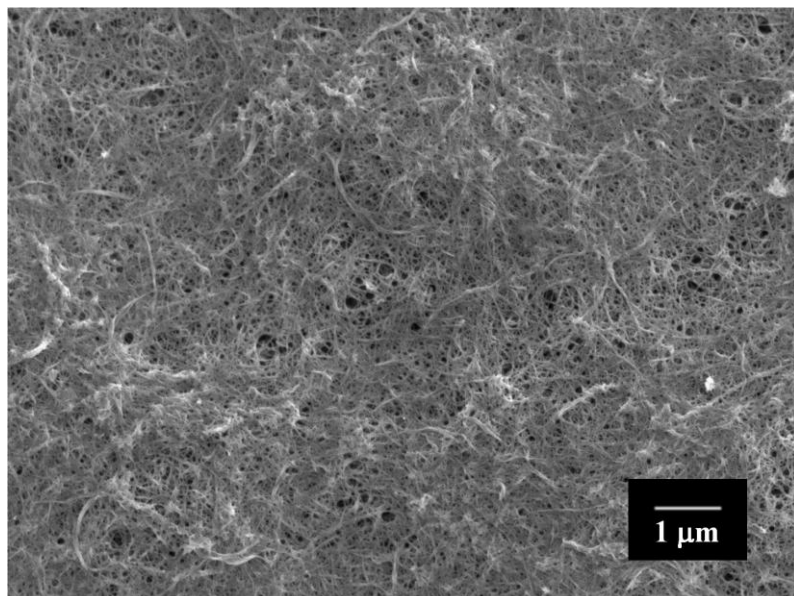


Figure 7 - 26 SEM image of film prepared at a current density of 1 mA cm^{-2} from 0.1 M pyrrole solution containing 0.01 M SSA containing 0.1 gL^{-1} PPE and 0.1 gL^{-1} SWCNT.

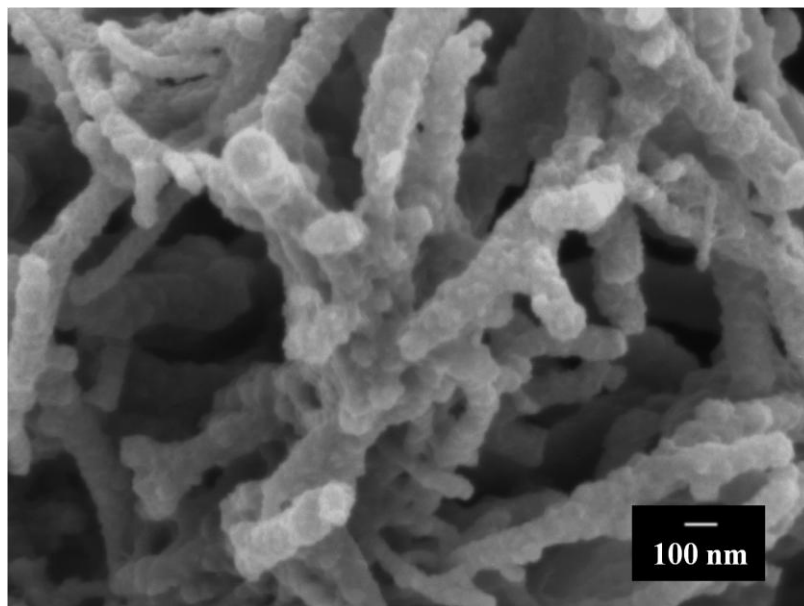


Figure 7 - 27 SEM image of film prepared at a current density of 1 mA cm^{-2} from 0.1 M pyrrole solution containing 0.01 M SSA, 0.1 gL^{-1} PPE and 0.1 gL^{-1} SWCNT at higher magnification.

7.4.5 Electrochemical Impedance Spectra

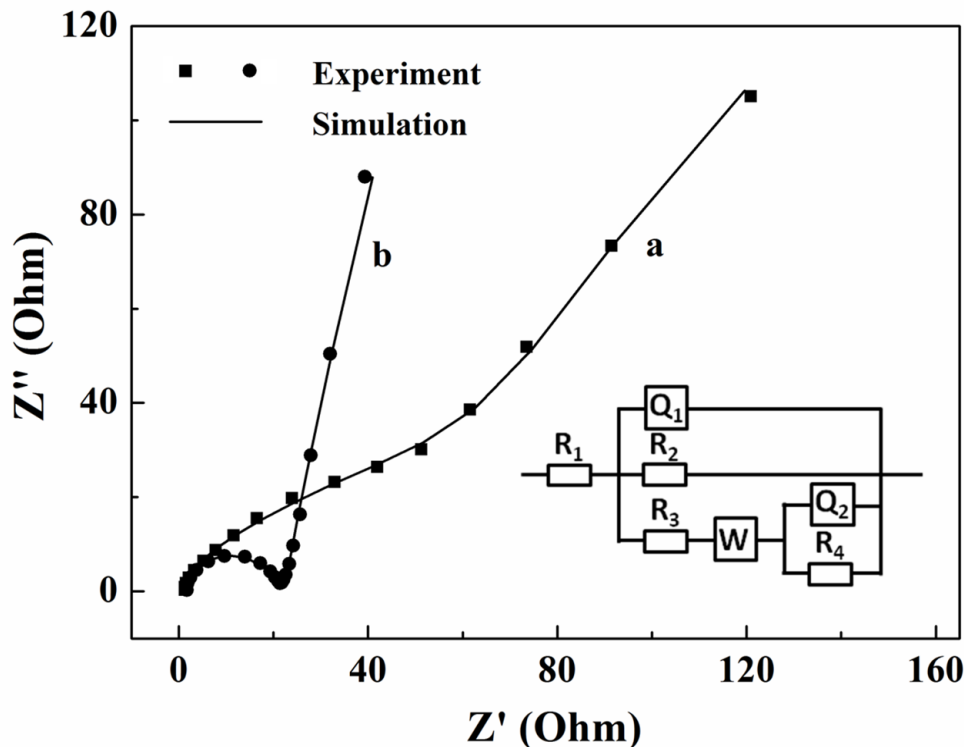


Figure 7 - 28 Nyquist plots for 160 $\mu\text{g cm}^{-2}$ films prepared at a current density of 1 mA cm^{-2} from 0.1 M pyrrole solution containing 0.01 M SSA: (a) without additives (b) containing 0.1 gL^{-1} PPE and 0.1 gL^{-1} SWCNT and an equivalent circuit.

Figure 2-28 compared impedance spectroscopy data for the films. The suggested equivalent circuit contained bulk resistance of electrolyte R_1 , resistance of film material R_2 , resistance of electrolyte R_3 and Warburg impedance W in pores, and charge transfer resistance R_4 . The constant phase elements represented the capacitance of the film material Q_1 and double layer capacitance in pores at the substrate-electrolyte interface Q_2 . The slope of the curve for the pure PPy films at low frequencies was close to 45 ° and

indicated the significant contribution of Warburg impedance. This is in a good agreement with SEM data, which showed low porosity of the films. The addition of SWCNT and increase in film porosity resulted in reduced resistance and improved capacitive behaviour of the composite films.

7.5 Electropolymerization of PPy using PV as an Anionic Dopant

7.5.1 Cyclic Voltammograms for Electropolymerization of PPy

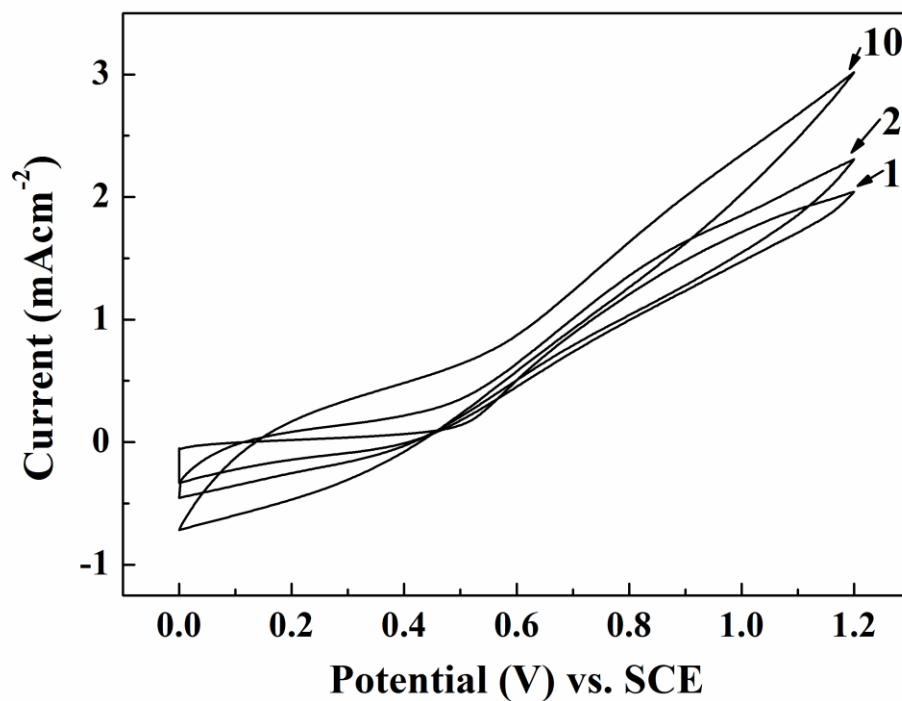


Figure 7 - 29 CV at a scan rate of 20 mVs^{-1} at a current density of 1 mAcm^{-2} for 6.7 gL^{-1} pyrrole solution, containing 0.1 gL^{-1} PV.

Electropolymerization of PPy was performed at potentiodynamic and galvanostatic conditions. The potentiodynamic curves recorded for stainless steel electrode in pyrrole solutions, containing PV, were presented in Figure 7-29. The CV data for the first scan showed that the increase in electrode potential above ~ 0.6 V resulted in increasing current, attributed to electropolymerization of PPy. Indeed, black films were formed at the stainless steel electrode at higher potentials. In the subsequent scans, a slight progressive increase of current was observed, indicating the continuous growth of conductive film without passivation or corrosion [79-82]. Such behaviour also indicates that the electronic conductivity of the film is sufficiently high to consider the ohmic potential drop inside the film as negligible [83, 84]. In contrast, the formation of a passivation layer usually results in the reduction of current with increasing cycle number [85].

7.5.2 Galvanostatic Electropolymerization of PPy

Homogeneous and thick PPy films were also formed under galvanostatic mode using PV additive. The potential versus time dependence at a current density of 1 mA cm^{-2} (Figure 7-30) indicated that there is no induction time for electropolymerization of PPy. At the beginning of the electrodeposition process, the potential difference between the working and reference electrode increased and then slightly decreased to a steady value (Figure 7-30). In contrast, deposition from pyrrole solutions containing oxalic acid (Figure 7-31), revealed the presence of an induction period, related to the dissolution of iron and formation of an iron oxalate layer [69, 86, 87].

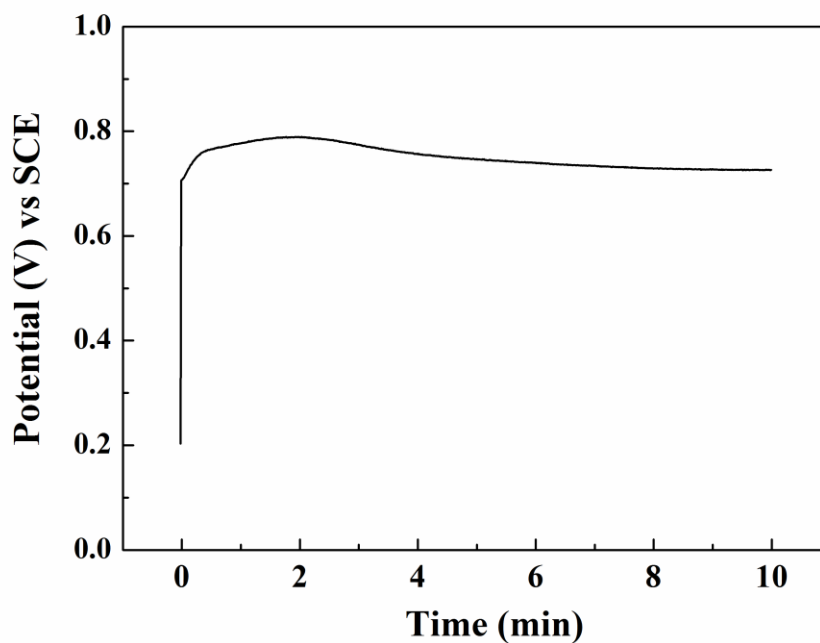


Figure 7 - 30 Potential versus time for 6.7 gL⁻¹ pyrrole solution, containing 0.1 gL⁻¹ PV.

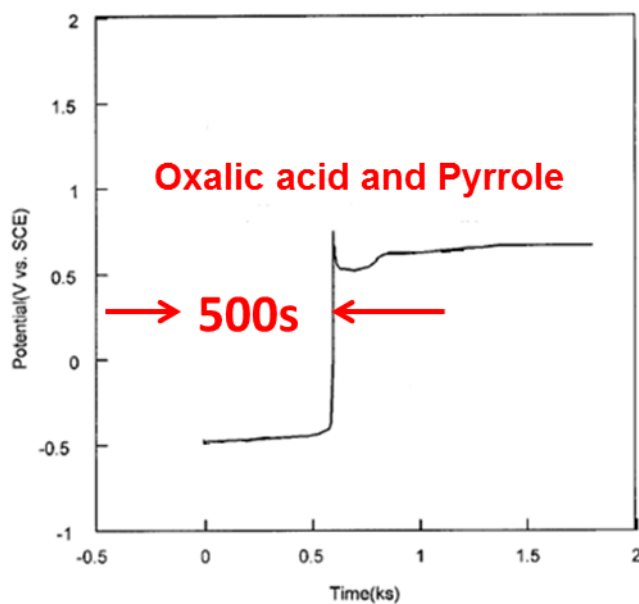


Figure 7 - 31 Potential versus time from pyrrole solution containing oxalic acid [86].

7.5.3 Characterizations of PPy Film Prepared Using PV

7.5.3.1 Chemical Structures Comparison

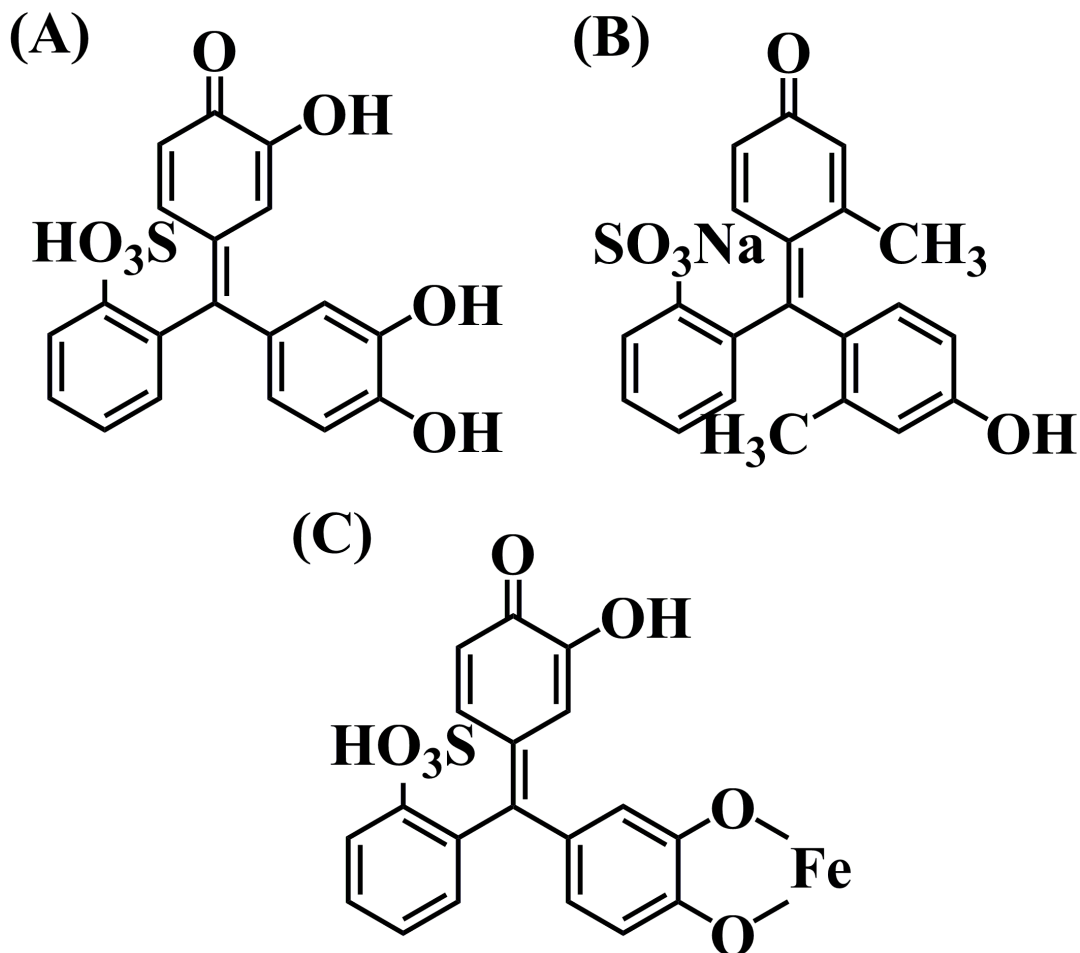


Figure 7 - 32 Chemical structure of (A) Pyrocatechol violet (PV); (B) m-Cresol Purple sodium salt (CP); (C) complex formed by chemisorption of PV on metal (Fe) surface.

Figure 7-32 shows chemical structures of PV and CP molecules used in this investigation. PV and CP are polyaromatic compounds with similar structures. The anionic properties of the molecules are related to their SO_3^- groups. The structures of PV and CP include different number of OH groups bonded to the aromatic rings. PV and CP

were compared as anionic dopants for electropolymerization of PPY and as charging and dispersing agents for the electrodeposition of MWCNT.

7.5.3.2 Deposition Yield

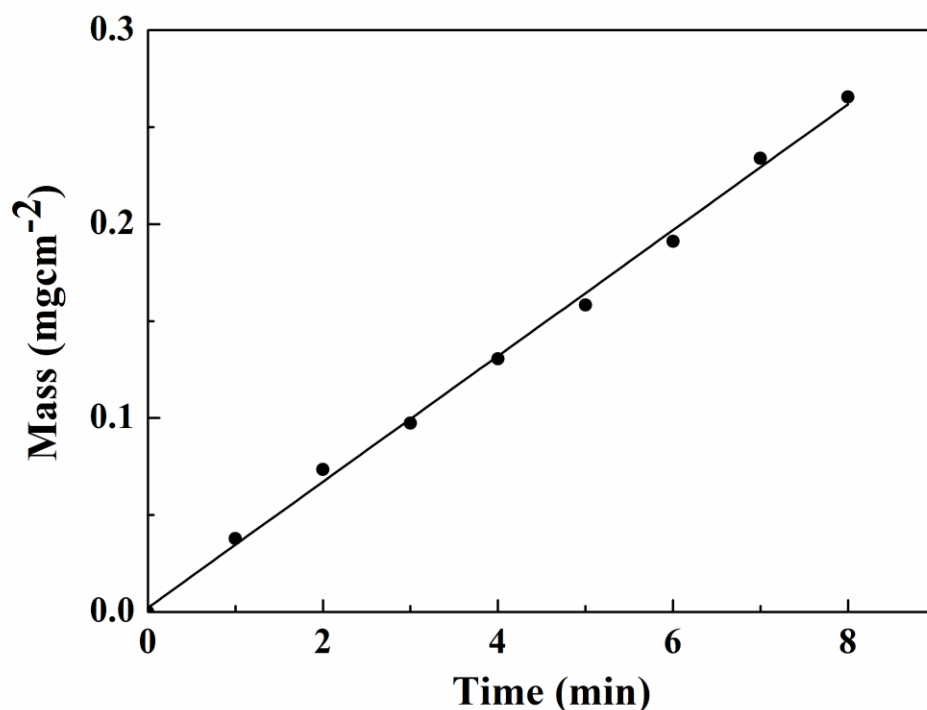


Figure 7 - 33 Deposit mass versus time at a current density of 1 mAcm^{-2} for 6.7 gL^{-1} pyrrole solution, containing 0.1 gL^{-1} PV.

The deposit mass versus time dependence presented in Figure 7-33 was nearly linear and indicated continuous film growth without induction time. The measurements of film adhesion according to the ASTM D3359 standard showed that adhesion strength corresponded to the 4B classification. When CP was used as an anionic dopant for PPY

electropolymerization, patchy deposition was observed. The deposits, prepared using CP, showed poor adhesion.

The comparison of the chemical structures of PV and CP (Figure 7-32 A,B) indicated that OH groups of PV, bonded to adjacent carbon atoms of the aromatic ring, exert influence on the formation of PV doped PPy films on stainless steel substrates. Such groups can provide catecholate type of bonding with metal atoms on the substrate surface and improve film adhesion. The interest in application of molecules from the catechol family for the development of adherent coatings has resulted from the fundamental investigations of biomimetic adhesion [88, 89], which was attributed to the chelation of catecholic amino acid, L-3,4-dihydroxyphenylalanine (DOPA). The remarkable adhesion strength provided by DOPA containing proteins to inorganic surfaces in marine environment has generated significant research activity focused on the development of advanced adhesives with improved stability in aqueous solutions of inorganic salts and novel dispersing agents with strong interfacial adhesion [90-92]. It has been demonstrated that materials from catechol and gallate families, containing OH groups bonded to the adjacent carbon atoms of the aromatic ring, strongly adsorbed on various inorganic materials [91-93]. It is important to note that such bonds improved charge transfer between inorganic and organic materials [93]. Figure 7-32(C) shows the catecholate type bonding mechanism of PV, involving the de-protonation of OH groups and complexation of Fe atoms on the substrate surface.

7.5.3.3 Electrochemical Studies

The electrochemical properties of the films were studied in a 0.5 M Na_2SO_4 solution using CV as shown in Figure 7-34.

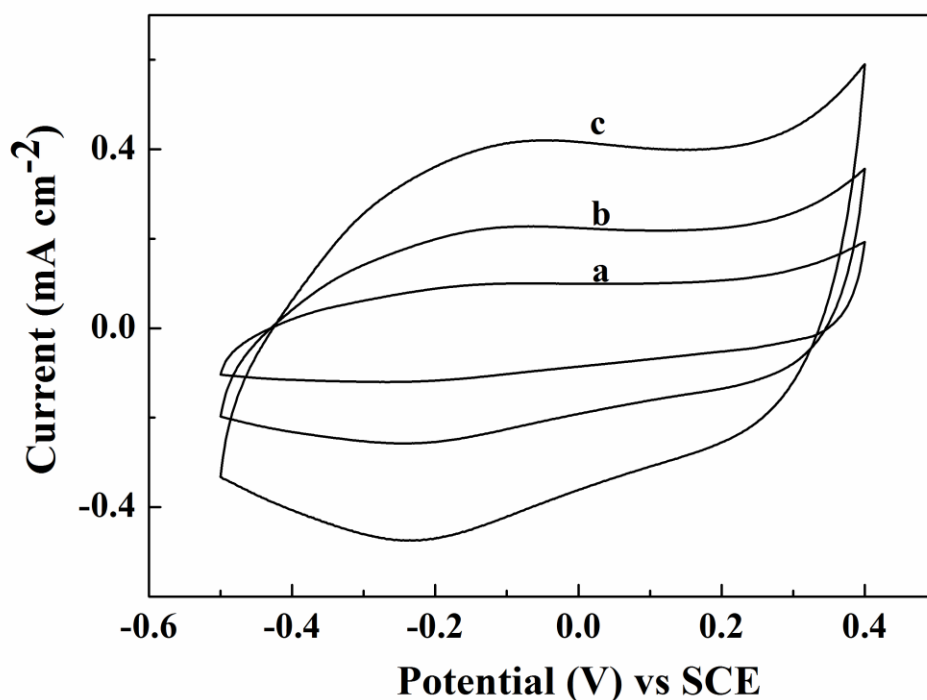


Figure 7 - 34 CV for the $160 \mu\text{g cm}^{-2}$ film deposited from the 6.7 gL^{-1} pyrrole solution containing 1 gL^{-1} PV on a stainless steel substrate at scan rate of (a) 2, (b) 5 and (c) 10 mV s^{-1} .

The film shows capacitive behavior in the voltage window of 0.9 V. The area of CV increases with increasing scan rate. The CVs show that PPy film exhibits better capacitive behavior in the range of negative potentials, as indicated by the larger area of the CVs. Such behavior was similar to the PPy film deposited using SSA additive.

7.5.3.4 Specific Capacitance

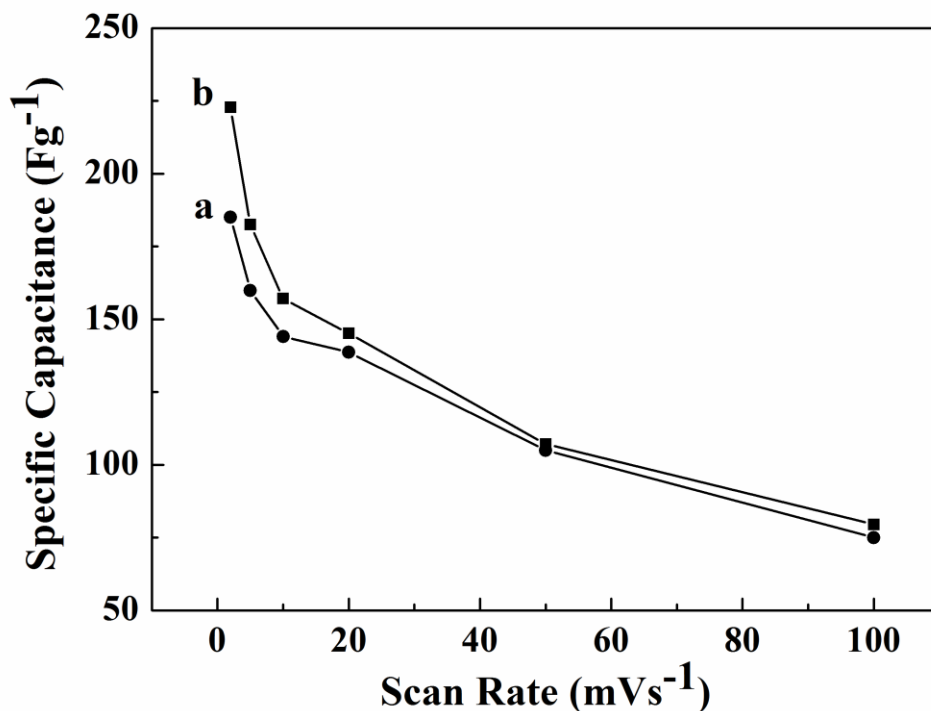


Figure 7 - 35 SC for the (a) $222 \mu\text{g cm}^{-2}$, (b) $160 \mu\text{g cm}^{-2}$ film deposited from the 6.7 gL^{-1} pyrrole solution containing 1 gL^{-1} PV on a stainless steel substrate at current density 1 mA cm^{-2} .

The films deposited on stainless steel substrates showed capacitive behavior in $0.5 \text{ M Na}_2\text{SO}_4$ electrolyte. Figure 7-35 shows SC versus scan rate dependence for $160 \mu\text{g cm}^{-2}$ and $222 \mu\text{g cm}^{-2}$ films. The SC of $160 \mu\text{g cm}^{-2}$ PPy film is higher than the $222 \mu\text{g cm}^{-2}$ film. The SC of 224 Fg^{-1} was obtained at a scan rate of 2 mVs^{-1} for $160 \mu\text{g cm}^{-2}$ PPy film. The SC decreased significantly with increasing scan rate for both films due to diffusion limitation in pores.

7.5.3.5 Electrochemical Impedance Spectra

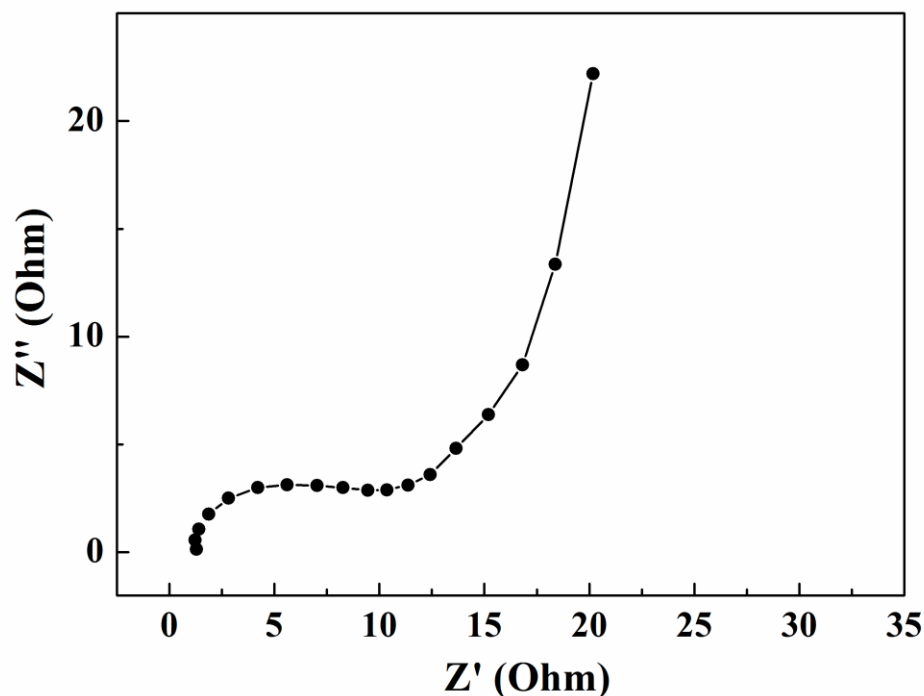


Figure 7 - 36 Nyquist plot in a 0.5M Na₂SO₄ solution for 160 mgcm⁻² film prepared at a current density of 1 mAcm⁻² from 6.7 gL⁻¹ pyrrole solution containing 1 gL⁻¹ PV on SS substrate.

Figure 7-36 shows Nyquist plot for complex impedance $Z^*=Z'-iZ''$. The impedance data for conductive polymer films are usually analyzed using an equivalent circuit [94, 95] including solution resistance, charge transfer resistance and capacitances or constant phase elements representing double layer capacitance and pseudocapacitance. The depressed semicircle [94] at high frequencies indicated the contribution of charge transfer resistance at the interface between the electrolyte and PPY electrode. Similar to

other investigations [94], the low frequency slope deviated from 90° and indicated the contribution of Warburg diffusion.

7.6 Electro-Co-Deposition of PPy/MWCNTs from aqueous PV solutions

In this work a new electrochemical strategy for the fabrication of composite polypyrrole (PPy) – multiwalled carbon nanotube (MWCNT) composites for electrochemical supercapacitors (ES) was introduced. The problem of poor dispersion of MWCNT in aqueous solution is addressed by the use of pyrocatechol violet (PV) dye as an anionic dopant. It was found that PV strongly adsorbs on MWCNT and allows efficient dispersion, charging and controlled electrophoretic deposition (EPD) of MWCNT. The use of PV for electropolymerization of PPy and EPD of MWCNT allows the formation of composite films by combined electrodeposition method.

7.6.1 The Roles of PV in Dispersion of MWCNTs

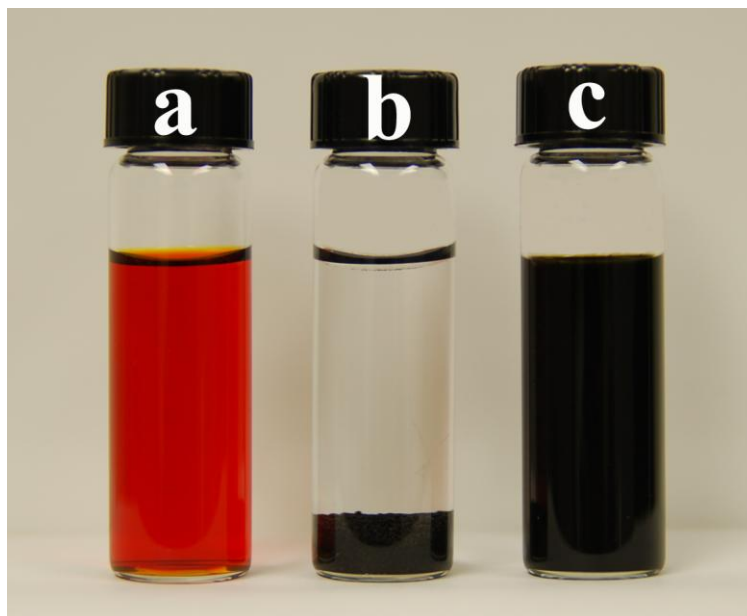


Figure 7 - 37 Aqueous PV (left), MWCNT (middle), PV and MWCNT (right).

Sedimentation experiments revealed excellent colloidal stability of MWCNT suspensions, containing PV. The suspensions with PV/MWCNT mass ratio of 0.2-1.0 were stable for more than 4 months (Figure 7-37). The addition of PV to the MWCNT suspensions allowed the formation of MWCNT films by anodic EPD. The MWCNT films were obtained by constant voltage and constant current deposition methods. It is suggested that PV adsorbed on the surface of MWCNT and provided electrostatic stabilization. Moreover, the adsorbed PV provided a negative charge required for anodic deposition of MWCNT. The mechanism of PV adsorption on MWCNT was related to π - π interactions.

7.6.2 Deposition Yield of MWCNT

Figure 7-38 shows the influence of PV concentration on the deposition yield. It should be noted that the influence of additive concentration on the EPD deposition yield is usually studied at constant voltage conditions [96], because additives can change the suspension conductivity. It is in this regard that EPD involves the motion of charged particles under the influence of an electric field. When EPD is performed in the constant voltage mode, the electric field is the same for suspensions with different additive concentrations [96]. The deposition yield increased with increasing PV concentration (Figure 7-38), showed a maximum and then decreased at PV concentrations above 0.6 gL⁻¹. It should be noted that EPD method is based on the use of stable suspensions of charged particles. Electrophoretic motion results in accumulation of the particles at the electrode surface. Deposit formation is achieved via particle coagulation. Previous investigations

showed that mutual electrostatic repulsions of the charged particles at the electrode surface can reduce the deposition yield or prevent deposit formation [97]. It is suggested that the increase in PV concentration in the suspensions resulted in increased charge of MWCNT, which resulted in enhanced mutual electrostatic repulsions of MWCNT at the electrode surface and reduced deposition yield (Figure 7-38). The deposit mass increased with increasing deposition time. Nearly linear dependence was obtained using a constant current deposition method (Figure 7-39). The results indicated the possibility of controlled deposition of films of different mass and showed relatively high deposition rate.

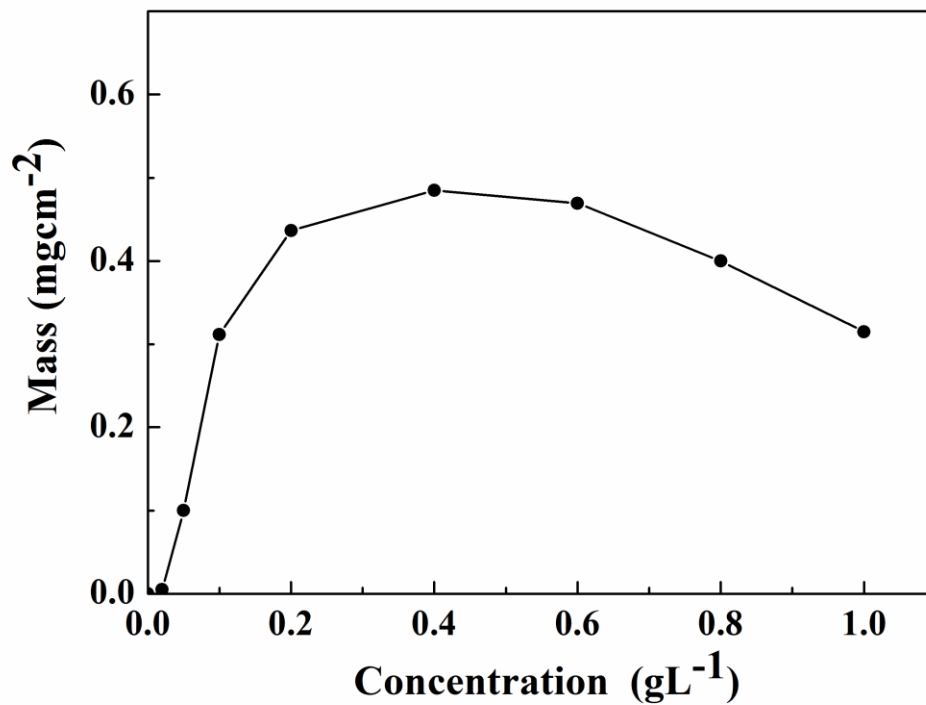


Figure 7 - 38 Deposit mass versus PV concentration in 1g L⁻¹ MWCNT suspension at a deposition voltage of 20V and deposition time of 6 min.

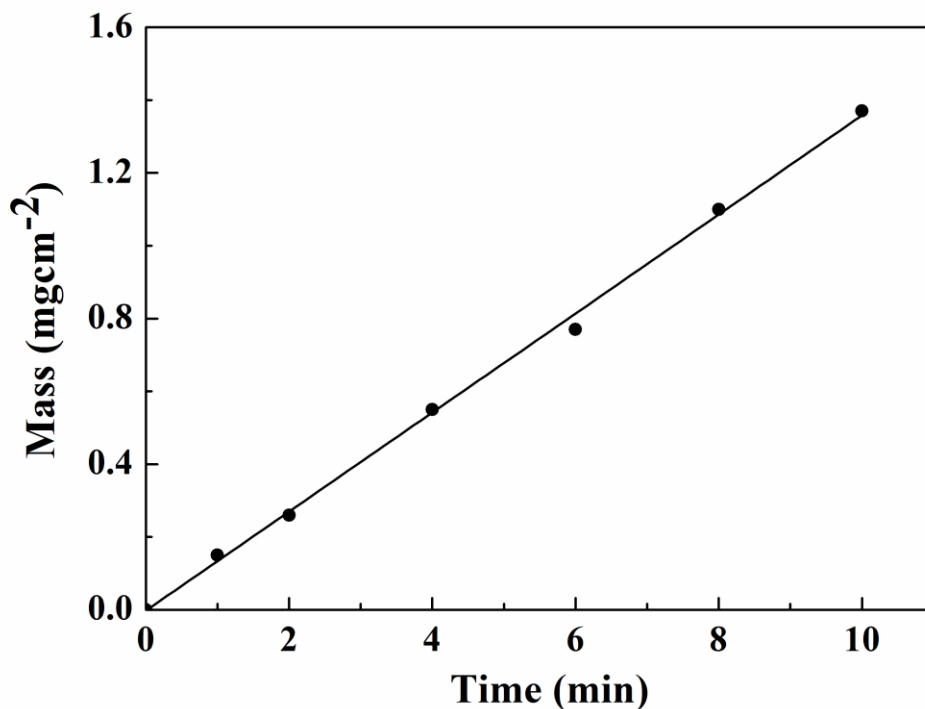


Figure 7 - 39 Deposit mass versus deposition time for 1gL⁻¹ MWCNT suspension, containing 1 gL⁻¹ PV at a current density of 1 mAcm⁻².

The use of PV offers important advantages for the MWCNT dispersion and electrodeposition, such as high suspension stability and high deposition rate. In the previous investigations, various methods were developed for the dispersion and EPD of CNT. It was found that adsorbed anionic and cationic polyelectrolytes provided charging of CNT in suspensions and allowed the formation of anodic or cathodic deposits by EPD [98]. Significant effort has been invested in the development of functionalization strategies, which included both covalent and supramolecular approaches [99-101]. However, polymer “wrapping” and supramolecular dispersion methods often result in the formation of CNT bundles.

The interactions of CNT with charging additives and solvents are especially important for EPD technology [102]. Many attempts have been made to improve wetting properties of carbon nanotubes in solvents by oxidation in strong acids or mixtures of acids [102, 103]. It was shown that under acidic conditions, defective sites in the CNT are attacked, resulting in the formation of fragmented CNT, decorated with carboxylic and other oxygen-containing groups on their surface. These acidic groups electrostatically stabilized the CNT in suspensions and provided a negative charge for EPD. However, the oxidation and functionalization strategies introduce defects on the CNT sidewalls and reduce electronic conductivity of CNT. In another approach, the charging of CNT for EPD was achieved by adsorption of metal ions from added metal salts [102, 104]. It should be noted that the addition of metal salts results in lower suspension stability, attributed to increasing ionic strength of the suspension. The metal ions usually incorporate into the deposits as corresponding hydroxides or oxides and contaminate the deposits.

The dispersion and EPD of CNT using surfactants is of special interest [99]. Sodium dodecyl sulfate (SDS) is one of the most promising anionic surfactants for the fabrication of stable suspensions of CNT [99]. However, relatively large concentration of SDS is required for CNT dispersion and EPD [105]. SDS form micelles, which induce a depletion attraction between the nanotubes [106, 107]. The strength of the attraction increases with increasing micelle concentration [106, 107]. As a result, the increase in SDS concentration results in CNT aggregation. Van der Waals - induced aggregation at low SDS concentration and depletion-induced aggregation at high SDS concentration

define an intermediate concentration range, where CNT can be homogeneously dispersed. The width of this SDS concentration range decreases drastically with increasing CNT concentration preventing the dispersion. It should be noted that the mechanism of PV adsorption on MWCNT is different from the mechanism of SDS adsorption. It is suggested that π - π interactions allow strong adsorption of PV on MWCNT, improved dispersion and EPD of MWCNT films.

7.6.3 Morphology Characterization

The results presented above (Figure 7-33 and Figure 7-39) indicated that PPY and MWCNT can be deposited at similar conditions on stainless steel substrates using PV additive. The use of PV allowed controlled deposition of both materials. These results pave the way for the deposition of composite PPY-MWCNT films from pyrrole solutions containing PV and MWCNT, using PV as an anionic dopant for PPY and dispersing agent for MWCNT. The method for the fabrication of PPY-MWCNT composite films involved electropolymerization of PPY and EPD of MWCNT. Figure 7-40 shows SEM images of PPY, MWCNT and composite PPY-MWCNT films and corresponding pictures of the deposits on stainless steel substrates. The films were continuous and crack free. The SEM image of PPY film (Figure 7-40A) showed that the film contained nanoparticles with size below 100 nm. The film porosity can be attributed to gas evolution during electropolymerization. Figure 7-40B shows the surface morphology of the MWCNT films. The film contained non-agglomerated MWCNT, which formed a continuous network. Figure 7-40C shows nanoparticles of PPY and MWCNT and confirms the formation of composite films. The MWCNT were well dispersed and

formed a conductive network. The PPY nanoparticles were deposited between MWCNT. Moreover, the SEM image showed that some MWCNT were coated with PPY. The film showed enhanced porosity, compared to pure PPY and MWCNT films. The microstructure of the composite film (Figure 7-40C) is beneficial for electrodes of ES, because dispersed MWCNT can provide improved electronic conductivity, whereas film porosity allows electrolyte access to the active material.

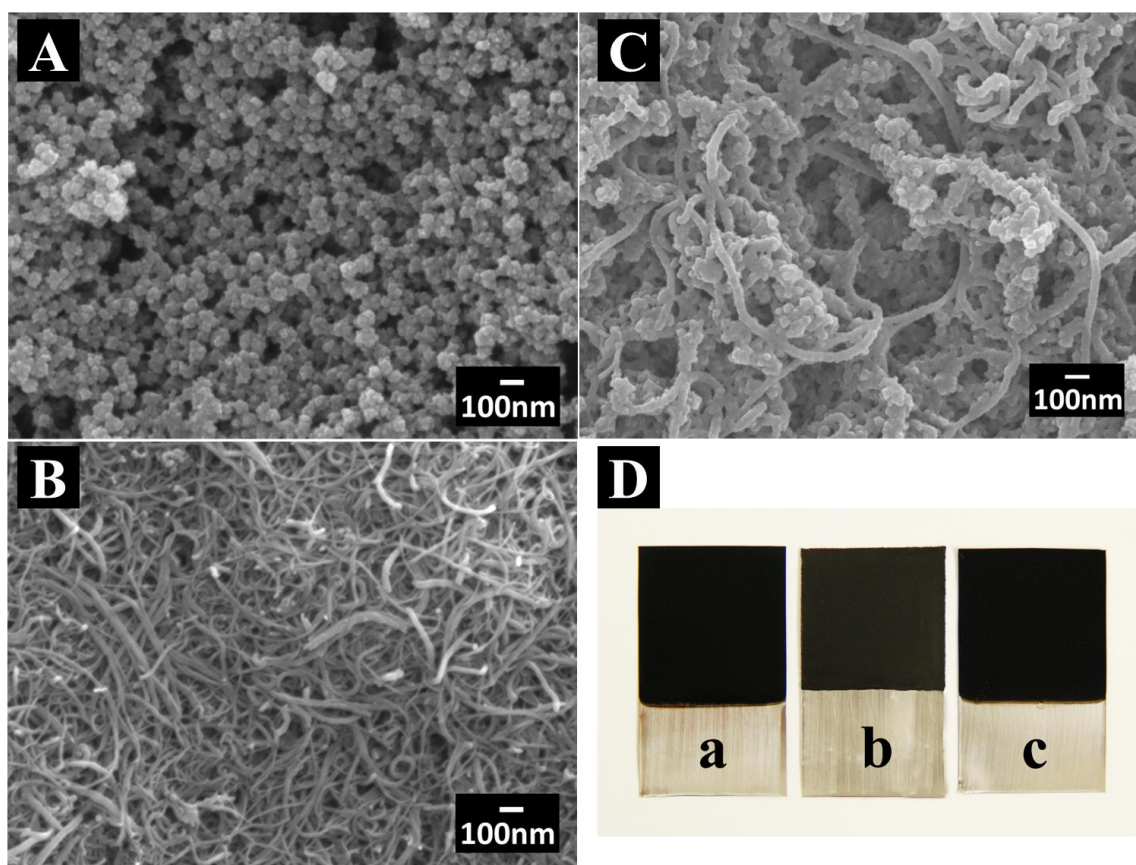


Figure 7 - 40 SEM images of films prepared at a current density of 1mAcm^{-2} : (A) PPY, deposited from 6.7 gL^{-1} pyrrole solution, containing 1 gL^{-1} PV (B) MWCNT, deposited from 1 gL^{-1} MWCNT suspension, containing 1 gL^{-1} PV (C) composite PPY-MWCNT, deposited from 6.7 g L^{-1} pyrrole solution, containing 1 gL^{-1} PV and 0.1 gL^{-1} MWCNT, and corresponding pictures of the films on stainless steel substrates (D)(a) PPY, (b) MWCNT and (c) PPY-MWCNT.

7.7 Electro-Co-Deposition of PPy/MWCNTs from aqueous PV solutions on Nickel plaques

Recent studies [108] highlighted the importance of high active material loadings for the fabrication of efficient ES. However, the increase in material loading usually results in increased resistance, poor electrolyte access to active material and reduced SC. This problem can be addressed by the use of special current collectors, such as Ni foams or plaques [109]. Previous investigations showed that Ni plaques, designed for high power applications, allowed significantly higher SC of MnO₂ electrodes, compared to MnO₂ electrodes based on Ni foams [110]. The advantages of Ni plaque based electrodes were especially important at high charge-discharge rates.

7.7.1 Electrochemical Studies

Figure 7-41 and 7-42 shows the CVs at different scan rate for composite PPy-MWCNT materials with mass of 350 μgcm^{-2} and 660 μgcm^{-2} respectively, electrochemically impregnated into Ni plaques. The films show capacitive behavior in the voltage window of 0.9V. Both of CVs show that PPy-MWCNT film have much better capacitive behavior compared to the PPy-MWCNT on stainless steel substrate (Figure 7-34) as indicated by the larger area of the CVs. Such better behavior was attributed to the high surface area of the nickel plaques substrate.

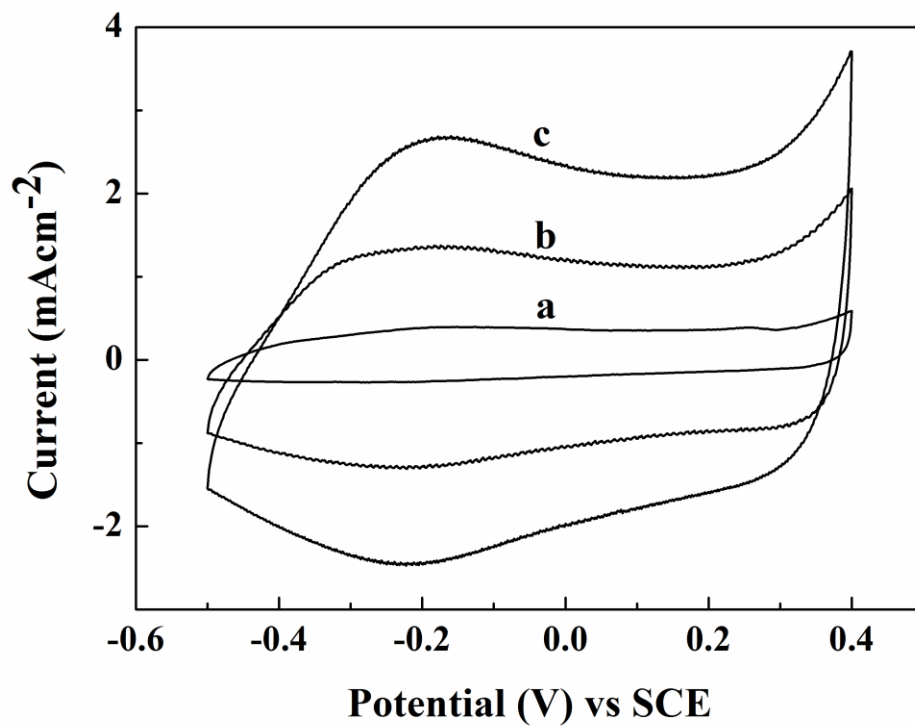


Figure 7 - 41 CVs for 350 mg cm⁻² composite PPy-MWCNT film deposited at a current density of 1 mA cm⁻² from 6.7 gL⁻¹ pyrrole solution containing 1 gL⁻¹ PV and 0.1 gL⁻¹ CNTs on nickel plaque substrate at scan rate of (a) 2, (b) 10 and (c) 20 mV s⁻¹.

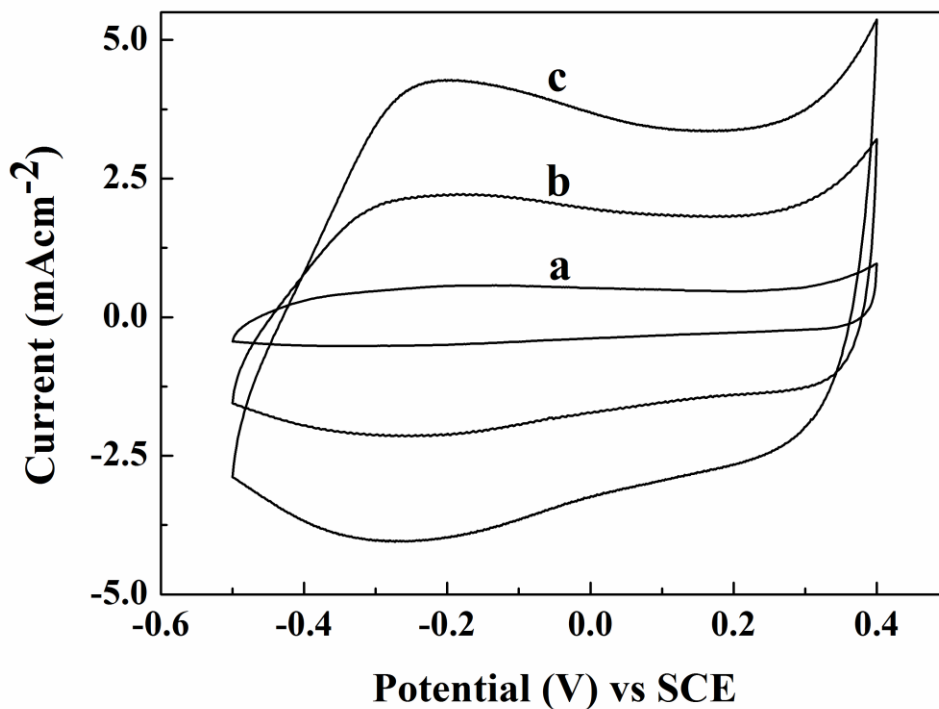


Figure 7 - 42 CVs for $660 \mu\text{g cm}^{-2}$ composite PPy-MWCNT film deposited at a current density of 1 mA cm^{-2} from 6.7 gL^{-1} pyrrole solution containing 1 gL^{-1} PV and 0.1 gL^{-1} CNTs on nickel plaque substrate at scan rate of (a) 2, (b) 10 and (c) 20 mV s^{-1} .

7.7.2 Specific Capacitance

The material loading was increased using Ni plaques as current collectors and higher capacitance can be achieved. Figure 7-43 shows SC versus scan rate for composite PPy-MWCNT materials with mass of 350 and $660 \mu\text{g cm}^{-2}$, electrochemically impregnated into Ni plaques. The electrode with material loading of $350 \mu\text{g cm}^{-2}$, showed a SC of 375 Fg^{-1} at a scan rate of 2 mVs^{-1} . The difference between the electrode formed on stainless steel and Ni plaque current collectors is especially evident at high scan rates.

At a scan rate of 100 mVs^{-1} the Ni plaque based electrode with material loading of $350 \mu\text{gcm}^{-2}$ showed 3 times larger SC compared to the thin film electrode on a stainless substrate with film mass of $160 \mu\text{gcm}^{-2}$.

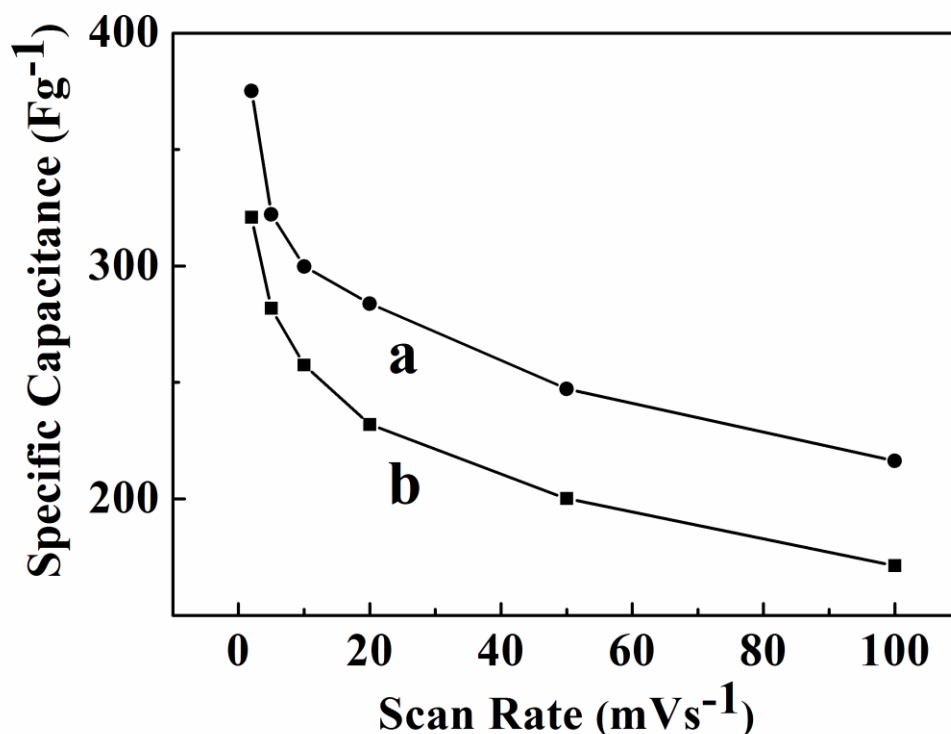


Figure 7 - 43 SC versus scan rate, (a) $350 \mu\text{gcm}^{-2}$, (b) $660 \mu\text{gcm}^{-2}$ films prepared at a current density of 1 mAcm^{-2} from 6.7 gL^{-1} pyrrole solution containing 1 gL^{-1} PV and 0.1 gL^{-1} CNTs on nickel plaque substrate.

7.7.3 Electrochemical Impedance Spectra

The electrochemical impedance (Figure 7-44) of PPy-MWCNT composite films were studied in $0.5 \text{ M Na}_2\text{SO}_4$ solution. The PPy-MWCNT film (Figure 7-44a) with mass of $350 \mu\text{gcm}^{-2}$ showed significantly lower impedance of the Ni plaque based electrode. The

high frequency semicircle practically disappeared, indicating reduced charge transfer resistance. However, the increase in material loading resulted in reduced SC and increased impedance.

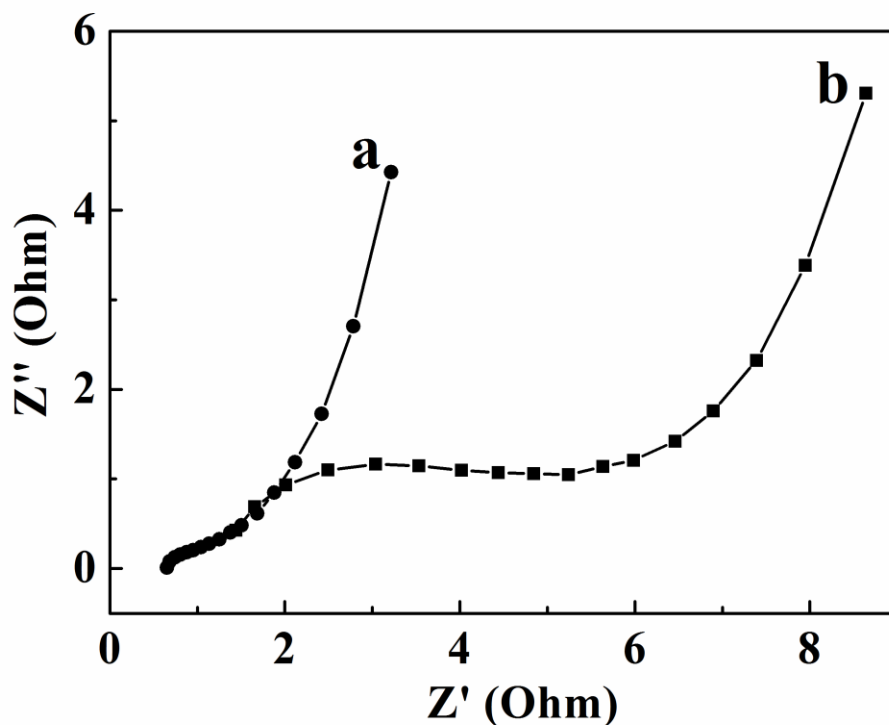


Figure 7 - 44 Nyquist plots in a 0.5M Na₂SO₄ solution for (a)350 μgcm^{-2} , (b) 660 μgcm^{-2} films prepared at a current density of 1 mAcm^{-2} from 6.7 gL^{-1} pyrrole solution containing 1 gL^{-1} PV and 0.1 gL^{-1} CNTs on nickel plaque substrate.

7.7.4 Morphology Characterization

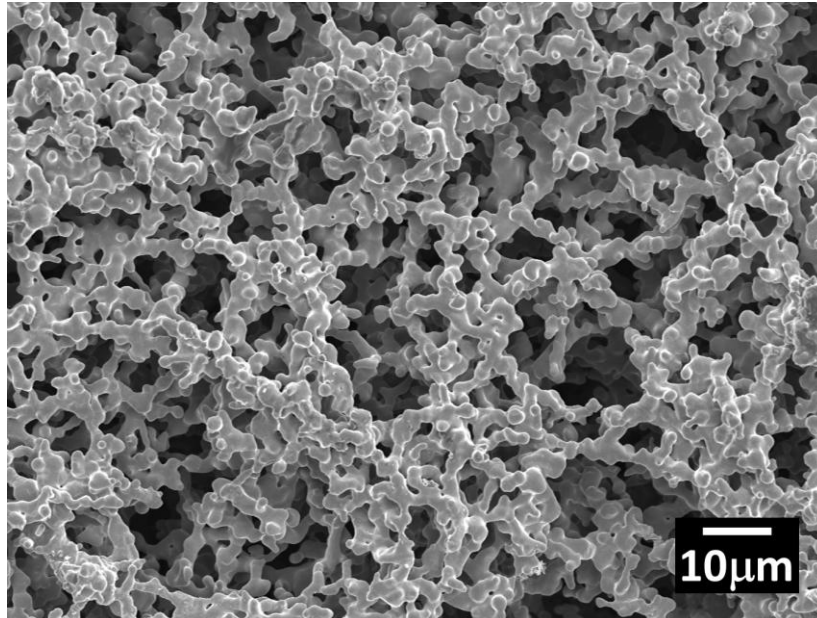


Figure 7 - 45 SEM image at X1000 magnifications of as-received plaques.

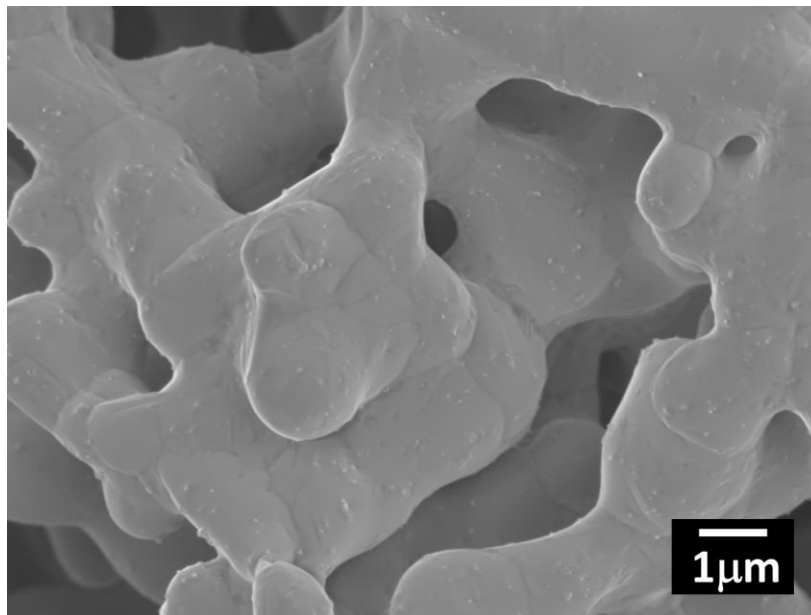


Figure 7 - 46 SEM image at X10000 magnifications of as-received plaques.

The commercial Ni plaques were studied by SEM. The commercial Ni plaques used in this study consisted of a perforated Ni foil and sintered filamentary Ni particles, which formed a porous network. Figure 7-45 and 7-46 show SEM images of the surface of a Ni plaque at different magnifications. The plaques exhibited porous microstructure with pore sizes in the range of 0–20 μm (Figure 7-45). The SEM image obtained at higher magnification (Figure 7-46) showed that the size of Ni particles was in the range of 0.5–2 μm . The porosity and conductivity of commercial Ni plaques are beneficial for their application as current collectors of ES.

7.8 Pulse Deposition of PPy/MWCNTs from aqueous PV solutions on Nickel Plaques

7.8.1 Characterizations of PPy/MWCNTs Film

Further improvement was achieved using a pulse deposition method. Figure 7-45, 7-46 and 7-47 compared capacitive behavior and impedance data for the 1 mgcm^{-2} films prepared by galvanostatic and pulse deposition methods. The film deposited by the pulse method showed SC of 390 and 210 Fg^{-1} at scan rates of 2 and 100 mVs^{-1} , respectively. The film prepared by galvanostatic deposition exhibited much lower capacitance. The comparison of the corresponding impedance data indicated reduced capacitance of the electrode prepared by the pulse deposition method. The analysis of available literature [111, 112] indicated that the PPY films prepared on other substrates by pulse deposition exhibited much higher SC compared to the films prepared galvanostatically. The improved capacitive behavior is usually attributed to higher porosity and lower particle size of the films prepared by pulse deposition method.

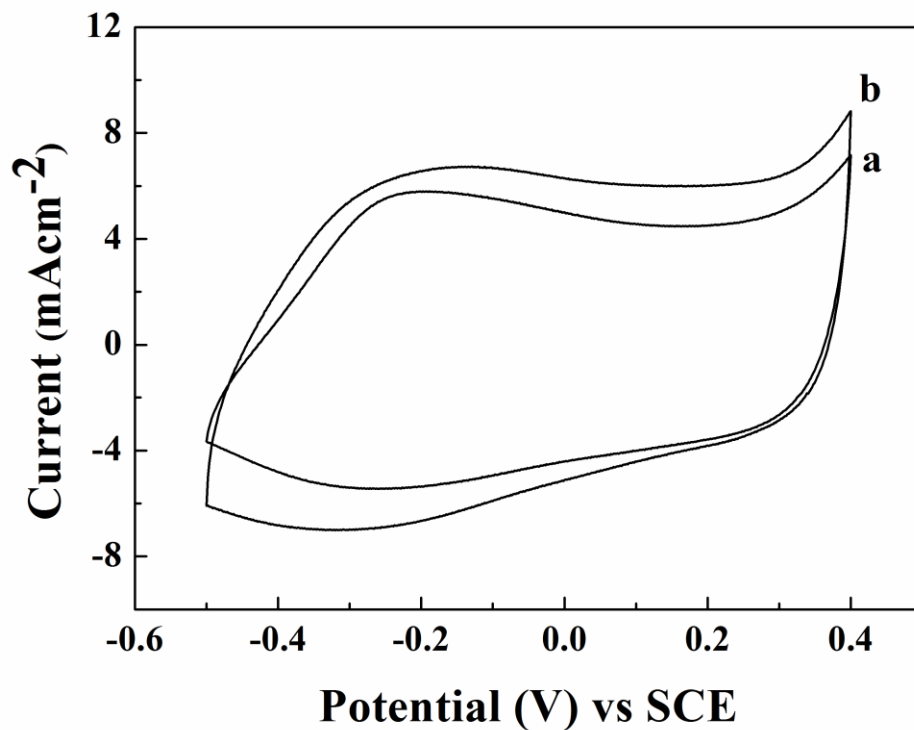


Figure 7 - 47 CVs at a scan rate of 20 mVs⁻¹ for 1 mgcm⁻² PPy-MWCNT films prepared at (a) a constant current density of 1 mAcm⁻² (b) a pulse current density of 1 mAcm⁻² with 0.5s time interval from 6.7 gL⁻¹ pyrrole solution containing 1 gL⁻¹ PV and 0.1 gL⁻¹ CNTs on nickel plaque substrate.

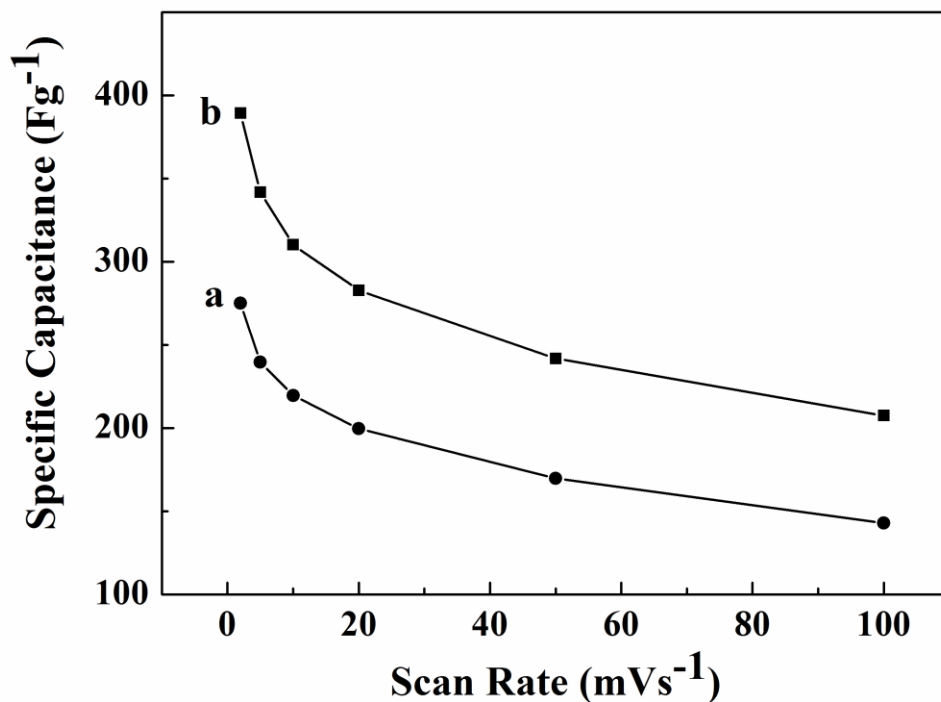


Figure 7 - 48 SC versus scan rate for 1 mgcm⁻² PPy-MWCNT films prepared at (a) a constant current density of 1 mAcm⁻² (b) a pulse current density of 1 mAcm⁻² with 0.5s time interval from 6.7 gL⁻¹ pyrrole solution containing 1 gL⁻¹ PV and 0.1 gL⁻¹ CNTs on nickel plaque substrate.

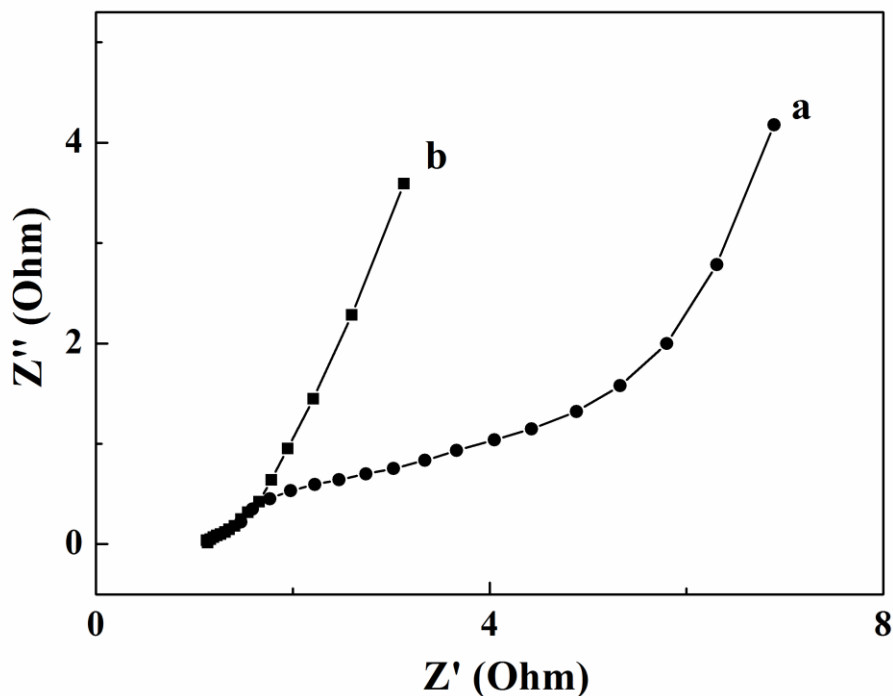


Figure 7 - 49 Nyquist plots for 1 mgcm⁻² PPy-MWCNT films prepared at (a) a constant current density of 1 mAcm⁻² (b) a pulse current density of 1 mAcm⁻² with 0.5s time interval from 6.7 gL⁻¹ pyrrole solution containing 1 gL⁻¹ PV and 0.1 gL⁻¹ CNTs on nickel plaque substrate.

7.8.2 Morphology Characterization

The microstructures of the PPy-MWCNT electrodes, prepared by impregnation of Ni plaques, were studied by SEM. SEM studies showed that plaques were impregnated with composite PPy-MWCNT material. However, in the galvanostatic deposition method, the increase in material loading resulted accumulation of the material on the surface of the Ni plaques. The SEM studies of the impregnated plaques at material loading of 1 mgcm⁻² revealed cracks (Figure 7-50 A, B). It is suggested that some large unfilled pores below

the material, accumulated at the plaque surface, promoted crack formation. In, contrast the SEM images of the plaques impregnated by the pulse method showed crack free morphology. The pulse method allowed improved impregnation of the Ni plaques. The SEM images revealed relatively rough morphology due to the surface roughness of Ni plaques. Some large pores remained open at material loading of 1 mgcm^{-2} . The comparison of the SEM images for the plaques impregnated by galvanostatic and pulse methods revealed relatively large number of MWCNT accumulated at the surface of the galvanostatically impregnated plaques. It is suggested that impregnation was hindered by the MWCNT, accumulated at the plaque surface in the galvanostatic method. The improved impregnation of the Ni plaques in the pulse method resulted in better electrochemical performance. It is in this regard that pulse impregnation method [109] allowed more efficient impregnation of Ni plaques with MnO_2 and provided higher SC, compared to the galvanostatic impregnation method. The PPY-MWCNT loading achieved in this investigation was comparable with loading of MnO_2 reported in the previous investigation [109]. Recent studies highlighted the importance of volume loading of porous current collectors with active material [108]. It is in this regard that PPY and MWCNT have significantly lower density, compared to the density of MnO_2 . It should be noted that Ni plaques are widely used in battery technology. Electrodes are formed by electrosynthesis of Ni(OH)_2 in pores of Ni plaque current collectors [113]. Previous studies showed that electrosynthesis of MnO_2 can be used for the impregnation of Ni plaques and the fabrication of electrodes of ES. The results presented above indicated that Ni plaques, electrochemically impregnated with PPY-MWCNT, are

promising electrodes for ES. However, further investigations are necessary for the optimization of the impregnation method, composition and properties of the electrodes.

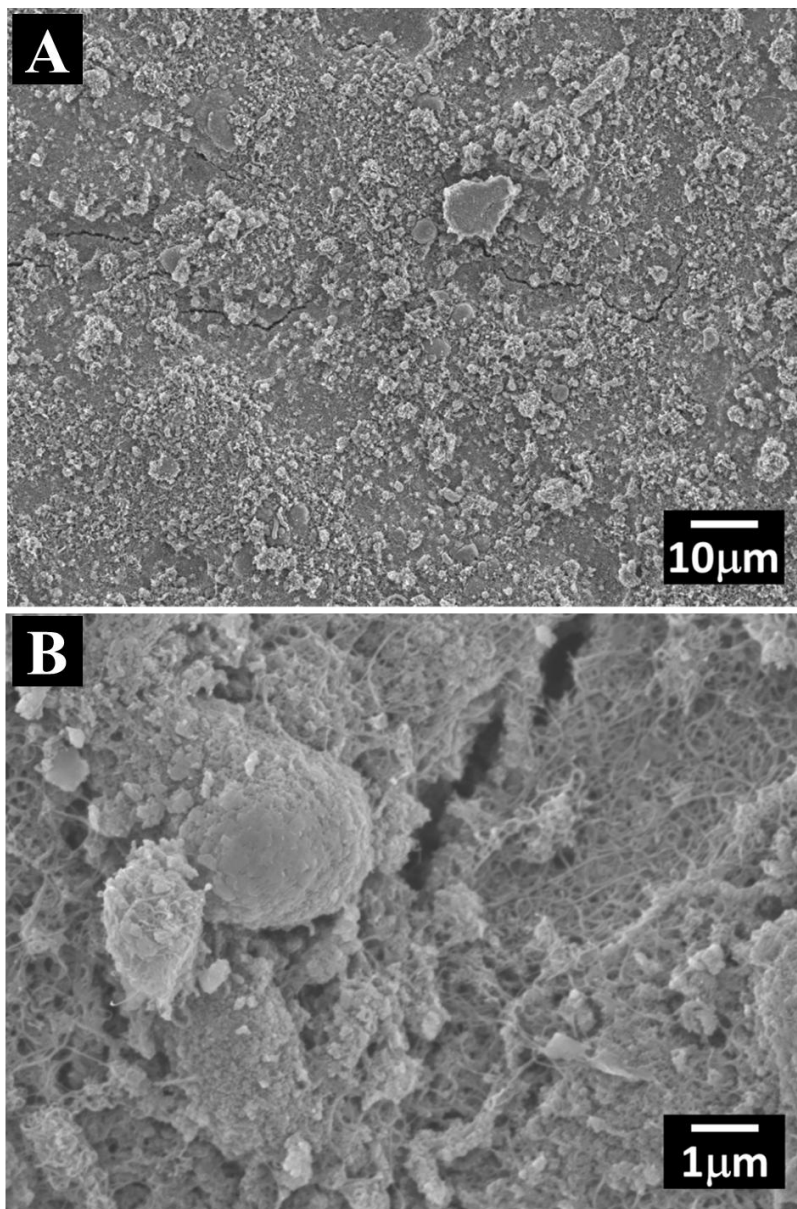


Figure 7 - 50 SEM images of the film prepared on nickel plaques substrates at a constant current density of 1mAcm^{-2} from 0.1M pyrrole solution containing 1g/L Pyrocatechol violet and 0.1g/L CNTs

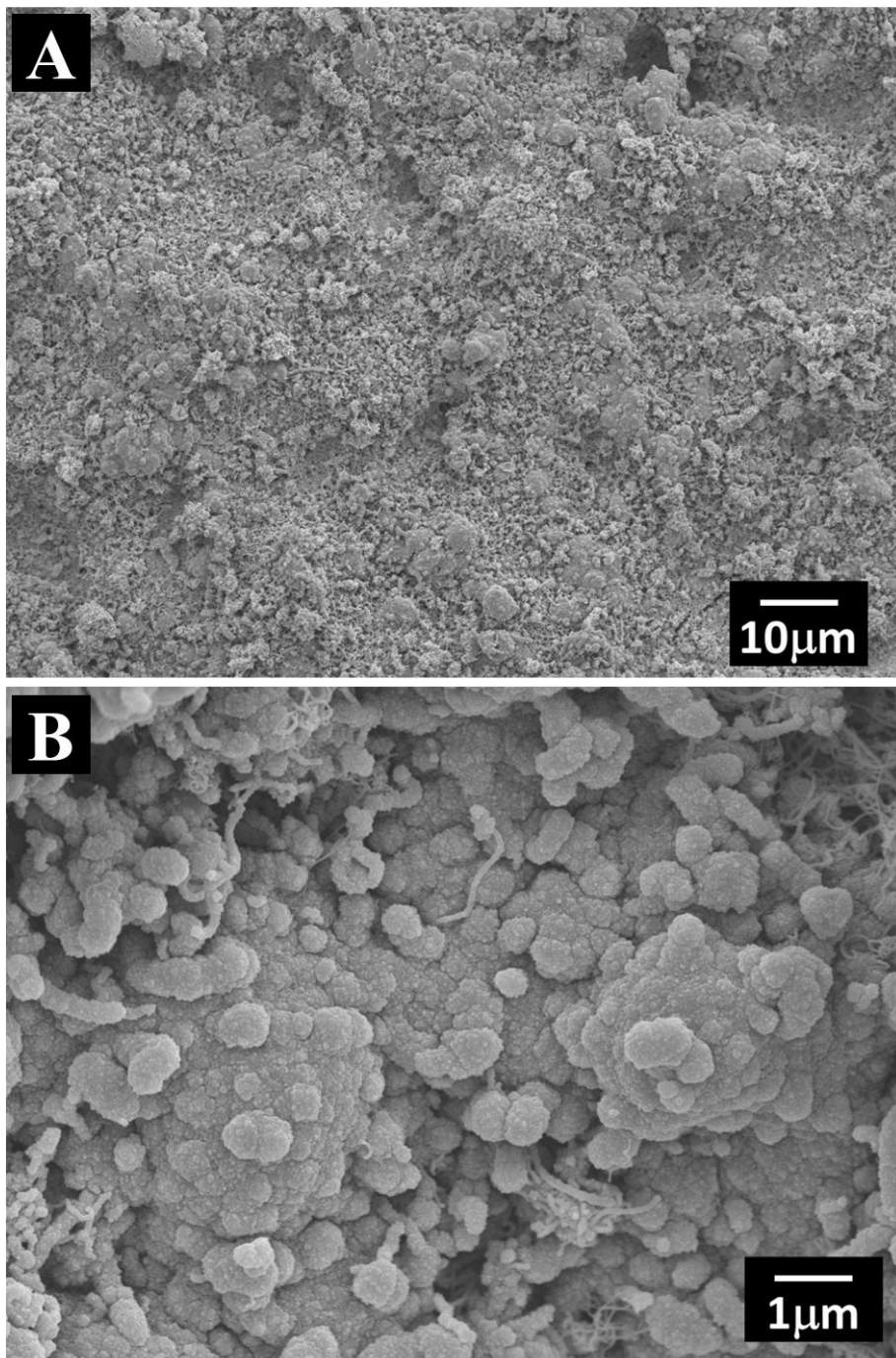


Figure 7 - 51 SEM images of the film prepared on nickel plaques substrates at a pulse current density of 1mAcm^{-2} and 0.5s time interval from 0.1M pyrrole solution containing 1g/L Pyrocatechol violet and 0.1g/L CNTs

8 Conclusions

PPy films were deposited by anodic electropolymerization on stainless steel and Ni plaques substrates from aqueous pyrrole solutions containing GA and SSA additives. Anionic SSA provided charge compensation of PPy during electropolymerization, prevented substrate dissolution, improved charge transfer and enabled the formation of adherent films on stainless steel substrates. The use of an anionic conjugated polymer allowed efficient dispersion of SWCNT in pyrrole solutions, containing SSA and fabrication of composite PPy-SWCNT films. The composite films showed improved capacitive behaviour compared to pure PPy films. The highest SC of 295 Fg^{-1} was obtained at a scan rate of 2 mVs^{-1} . PPy films of controlled mass were also obtained on stainless steel substrates by pulse anodic electropolymerization method using SSA as an anionic additive. The films prepared by pulse deposition showed finer particles size, lower resistance and higher SC compared to the films prepared galvanostatically. The highest SC of 545 Fg^{-1} was obtained at a scan rate of 2 mVs^{-1} for the films prepared at pulse duration of 0.5 s.

Adherent PPY films were also obtained on stainless steel and Ni substrates by electropolymerization, using PV additive from the catechol family as an anionic dopant. The comparison of the experimental data for PV, containing OH groups bonded to adjacent carbon atoms of the aromatic rings, and CV without such groups, showed that the interaction OH groups with metal atoms at the substrate surface promoted film adhesion. It was found that PV allows efficient dispersion, charging and controlled EPD of MWCNT films. Composite PPY-MWCNT films were obtained by a combined

electrodeposition method using PV as an anionic dopant for PPY electropolymerization and as a charged dispersant for EPD of MWCNT. The composite materials deposited as thin film on stainless steel foils or impregnated into Ni-plaque current collectors showed capacitive behavior in 0.5 M Na_2SO_4 electrolyte. Ni plaque based electrodes offer advantages of significantly higher materials loading and superior capacitive behavior compared to thin film electrodes formed on stainless steel current collectors. The electrodes obtained by pulse impregnation show higher specific capacitance compared to the electrodes prepared by galvanostatic impregnation. The highest SC of 390 Fg^{-1} was achieved at a scan rate of 2 mVs^{-1} for 1 mgcm^{-2} electrodes, prepared by pulse impregnation of Ni plaques.

References

1. Yan Wang, Z.S., Yi Huang, Yanfeng Ma, Chengyang Wang, Mingming Chen, Yongsheng Chen, *Supercapacitor Devices Based on Graphene Materials*. The Journal of Physical Chemistry C. 113: p. 13103-13107.
2. Viswanathan, B., *An introduction to energy sources*. Energy sources.
3. H. Ibrahim, A.I., J. Perron, *Energy storage systems - characteristics and comparisons*. Renewable and Sustainable Energy Reviews. 12: p. 1221-1250.
4. M Jayalakshmi, K.B., *Simple Capacitors to Supercapacitors - An Overview*. International Journal of Electrochemical Science. 3: p. 1196-1217.
5. Conway, B.E., *Electrochemical Supercapacitors: Scientific Fundamentals and Technological Applications*. 1999, New York, N.Y.: Kluwer Academic.
6. R. Kotz, M.C., *Principles and applications of electrochemical capacitors*. Electrochimica Acta. 45: p. 2483-2498.
7. Miller, J.R., *Capacitors Overview Encyclopedia of Electrochemical Power Sources*. J: Amsterdam: Elsevier. 587-599.
8. Patrice Simon, Y.G., *Materials for electrochemical capacitors*. Nature materials. 7: p. 845-854.
9. Yong Zhang, H.F., Xingbing Wu, Lizhen Wang, Aiqin Zhang, Tongchi Xia, Huichao Dong, Xiaofeng Li, Linsen Zhang, *Progress of electrochemical capacitor electrode materials: A review*. International Journal of Hydrogen Energy. 34(11): p. 4889-4899.
10. John R. Miller, A.F.B., *Electrochemical Capacitors: Challenges and Opportunities for Real-World Applications*. The Electrochemical Society Interface. 17: p. 53-57.
11. Buell, E. *Development of Lead-Carbon Hybrid Battery/Supercapacitors*. in *Proc. Advanced Capacitor World Summit*. July 17-19, 2006. San Diego, CA.
12. *Superior Tool UltraCut*, www.superiortool.com/UltraCut/35278.htm.
13. Xiaoming Ge, C.F., Siew Hwa Chan, *Double layer capacitance of anode/solid-electrolyte interfaces*. Phys. Chem. Chem. Phys. 13: p. 15134-15142.
14. Kotz R, C.M., *Principles and applications of electrochemical capacitors*. Electrochim. Acta. 45: p. 2483-2498.
15. Zheng, J.P.J., T. R., *High energy and high power density electrochemical capacitors*. J. Power Sources. 62: p. 155-159.
16. B. E. Conway, V.B., J. Wojtowicz, *The role and utilization of pseudocapacitance for energy storage by supercapacitors*. Journal of Power Sources. 66: p. 1-14.
17. Burke, A., *Ultracapacitors: why, how and where is the technology*. Journal of Power Sources. 91: p. 37-50.
18. B. E. Conway, W.G.P., *Double-layer and pseudocapacitance types of electrochemical capacitors and their applications to the development of hybrid devices*. Journal of Solid State Electrochemistry. 7: p. 637-644.
19. Phillips J, X.B., MeneAndez JA., *Calorimetric study of oxygen adsorption on activated carbon*. Thermochim Acta. 312(1-2): p. 87-93.

20. Oliveira LCA, S.C., Yoshida MI, *The effect of H₂ treatment on the activity of activated carbon for the oxidation of organic contaminants in water and the H₂O₂ decomposition*. Carbon. 42(11): p. 2279-2284.
21. Pastor-Villegas J, D.-V.C., *Pore structure of activated carbons prepared by carbon dioxide and steam activation at different temperature from extracted rockrose*. Carbon. 40(3): p. 397-402.
22. Chuang Peng, S.Z., Daniel Jewell, George Z. Chen, *Carbon nanotube and conducting polymer composites for supercapacitors*. Progress in Natural Science. 18(7): p. 777-788.
23. Patrice Simon, A.B., *Nanostructured Carbons: Double-layer Capacitance and More*. The Electrochemical Society Interface. 17: p. 38-43.
24. Chun JH, K.N., Chun JY., *Determination of adsorption isotherms of hydrogen and hydroxide at Pt-Ir alloy electrode interfaces using the phase-shift method and correlation constants*. Int. J. Hydrogen Energy. 33: p. 762-774.
25. Moriguchi I, N.F., Furukawa H, Yamada H, Kudo T., *Colloidal crystal-templated porous carbon as a high performance electrical double-layer capacitor material*. Electrochem. Solid-State Lett. 7: p. A221-223.
26. Zhao Y, Z.M.-B., Cao J-M, Ke X-F, Liu J-S, Chen Y-P, et al., *Easy synthesis of ordered meso/macroporous carbon monolith for use as electrode in electrochemical capacitors*. Mater Lett. 62: p. 548-551.
27. Kim S-U, L.K.-H., *Carbon nanofiber composites for the electrodes of electrochemical capacitors*. Chem. Phys. Letter. 400: p. 253-257.
28. Xu B, W.F., Chen S, Zhang C, Cao G, Yang Y, *Activated carbon fiber cloths as electrodes for high performance electric double layer capacitors*. Electrochim. Acta. 52: p. 4595-4598.
29. Pekala RW, F.J., Alviso CT, Tran TD, Mayer ST, Miller JM, et al., *Carbon aerogels for electrochemical applications*. J. Non-Cryst Solids. 225: p. 74-80.
30. E. Frackowiak, F.B., *Carbon materials for the electrochemical storage of energy in capacitors*. Carbon. 39: p. 937-950.
31. Gross J, S.G., Alviso CT, Pekala RW., *Elastic properties of crosslinked resorcinol-formaldehyde gels and aerogels*. J. Non-Cryst Solids. 211: p. 132-142.
32. A. G. Pandolfo, A.F.H., *Carbon properties and their role in supercapacitors*. Journal of Power Sources. 157: p. 11-27.
33. Cheng, C.L.a.H.M., *Carbon nanotubes for clean energy applications*. Journal of Physics D: Applied Physics. 38: p. R231.
34. Y. Y. Fan, A.K., A. Mukasyan, A. Varma, *Single- and multi-wall carbon nanotubes produced using the floating catalyst method: Synthesis, purification and hydrogen up-take*. Carbon. 44: p. 2160-2170.
35. Iijima, S., *Helical microtubules of graphite carbon*. Nature. 354: p. 56.
36. Reilly, R.M., *Carbon nanotubes: potential benefits and risks of nanotechnology in nuclear medicine*. Journal of Nuclear Medicine. 48: p. 1039-1042.
37. Frackowiak, E., *Nanotubular materials as electrodes for supercapacitors*. Fuel Processing Technology. 77-78: p. 213-219.

38. Wu M. S, H.Y.A., Yang C. H, Jow J. J., *Electrodeposition of nanoporous nickel oxide film for electrochemical capacitors*. Int. J. Hydrogen Energy. 32: p. 4153-4159.
39. Kim I. H, K.K.B., *Electrochemical characterization of hydrous ruthenium oxide thin-film electrodes for electrochemical capacitor applications*. J. Electrochem. Society. 153: p. A383-389.
40. J. P. Zheng, P.J.C., T. R. Jow, J. Electrochem. Society. 142: p. 2699.
41. lee, H.Y., Goodenough, J. B., *Supercapacitor behavior with KCl electrolyte*. J. Solid State Chem. 144: p. 220-223.
42. K. R. Prasad, N.M., Electrochem. Commun. 6: p. 1004.
43. Yang X.H., W.Y.G., Xiong H.M., Xia Y.Y., *Interfacial synthesis of porous MnO₂ and its application in electrochemical capacitor*. Electrochim. Acta. 53: p. 752-757.
44. zhao D.D., B.S.J., Zhou W.J., Li H.L., *Preparation of hexagonal nanoporous nickel hydroxide film and its application for electrochemical capacitor*. Electrochem. Commun. 9: p. 869-874.
45. K. Lota, V.K., E. Frackowiak,, J. Phys. Chem. Solids. 65: p. 295.
46. Graeme A. Snook, P.K., Adam S. Best, *Review conducting-polymer-based supercapacitor devices and electrodes*. Journal of Power Sources. 196: p. 1-12.
47. K. Naoi, S.S., A. Manago, J. Electrochem. Society. 147: p. 420.
48. K.S.Ryu, X.w., Y.G.Lee, S.H.Chang, *Electrochemical capacitor composed of doped polyaniline and polymer eletrolyte membrane*. Joural of Applied Polymer Science. 89: p. 1300-1304.
49. K. Gurunathan, A.V.M., R. Marimuthu, U. P. Mulik, D. P. Amalnerkar, *Electrochemically synthesised conducting polymeric materials for applications towards technology in electronics, optoelectronics and energy storage devices*. Materials Chemistry and Physics. 61: p. 173-191.
50. k.s.Ryu, K.M.K., Y.J.Park, M.G.Kang, S.H.Chang, Solid State Ionics. 152: p. 861.
51. S.R. Sivakkumar, R.S., J. Power Sources. 137: p. 322.
52. S. Suematsu, Y.O., H. Tsujimoto, H. Kanno, K. Naoi, Electrochim. Acta. 45: p. 3813.
53. A.F.Diaz, B.L.F.a., *Organic Electrochemistry: an Introduction and a Guide*, ed. M. Dekker. 1991, New York. 1337.
54. Said Sadki, P.S., Nancy Brodie and Guillanume Sabouraud, *The mechanisms of pyrrole electropolymerization*. Chem. Soc. 29: p. 283-293.
55. Pratt, C., *Conducting polymers*. in Chemistry. 1996, London: Kingston University. 7.
56. N.C. Billingham, P.D.C., P.J.S. Foot, F. Mohammad, *Stability and degradation of some electrically conducting polymers*. Polymer Degradation and Stability. 19: p. 323-341.
57. Y. Wang, M.F.R., L.J. Buckley, *Stability studies of electrically conducting polyheterocycles*. Synthetic metals. 41: p. 1103-1108.

58. Q. Pei, O.I., J.E. Osterholm, J. Laakso, *Electrically conducting copolymers from 3-octylthiophene and 3-methylthiophene*. *Polymer*. 34: p. 247-252.
59. A. R. Hopkins, D.D.S., R. M. Villahermosa, R. A. Lipeles, *Interfacial synthesis of electrically conducting polyaniline nanofiber composites*. *Thin Solid Films*. 469-470: p. 304-308.
60. Bangchao, D.M.Z.Z.a.H.Y.W.B.Y., *Study on carbon nanotubes/manganese dioxide composite electrode materials for supercapacitors*. *Journal of the Chinese Ceramic Society*. 32(4): p. 411-415.
61. Jang Myoun Koa, K.M.K., *Electrochemical properties of MnO₂/activated carbon nanotube composite as an electrode material for supercapacitor*. *Materials Chemistry and Physics*. 114(2-3): p. 837-841.
62. Zhang J., K.L.B., Wang B., Luo Y.C., Kang L., *In-situ electrochemical polymerization of multi-walled carbon nanotube/polyaniline composite films for electrochemical supercapacitors*. *Synth. Met.* 159: p. 260-266.
63. B.Du, Q.J., X.F.Zhao, B.Huang, Y.Zhao, *Preparation of PPy/CNT composite applications for supercapacitor electrode material*. *Materials Science Forum*: p. 502-505.
64. Endres, F., *Chem. Phys. Chem.* 3: p. 144.
65. H. Ohno, K.F., *Electrochemistry*. 76: p. 16.
66. A. Balducci, W.A.H., M. Mastragostino, S. Passerini, P. Simon, F. Soavi, *Electrochem. Acta*. 50: p. 2233.
67. T. Rapecki, M.D., Z. Stojek, *Electrochemistry Communications*. 12: p. 624.
68. W. Su, J.O.I., *Journal of Applied Polymer Science*. 65: p. 417.
69. W.J. Hamer, L.K., J.H.W. De Wit, *Materials and Corrosion*. 55: p. 653.
70. K.H. An, K.K.J., J.K. Heo, S.C. Lim, D.J. Bae, Y.H. Lee, *Journal of The Electrochemical Society*. 149: p. A1058.
71. T. Zhang, H.F., J. Zhou, G. Liu, G. Feng, Q. Jin, *Macromolecules*. 39: p. 7839.
72. Z. Zhang, R.B.J., *Kinetics of dissociation of iron(III) complexes of tiron in aqueous acid*. *Inorganic Chemistry*. 35: p. 1571-1576.
73. F. Cheng, P.I., S. Lazar, G.A. Botton, G. De Silveira, O. Marinov, J. Deen, A. Adronov, *Macromolecules*. 41: p. 9869.
74. *Standard Test Methods for Measuring Adhesion by Tape Test*. ASTM standards. D3359-09.
75. C. Shi, I.Z., *Electrodeposition and Capacitive Behavior of Films for Electrodes of Electrochemical Supercapacitors*. *Nanoscale Res. Lett.*, (5): p. 518-523.
76. Shi, C., *Polypyrrole and Composite Electrodes for Electrochemical Supercapacitors*, in *Material Science and Engineering*. August 2010, McMaster University: Hamilton, ON, Canada.
77. Kallay N, P.T., Markovic J, Kovacevic D., *Colloids Surf A*. 306: p. 40-48.
78. Dobson KD, M.A., *Spectrochim Acta A Mol Biomol Spectrosc*. 56: p. 557-565.
79. L.M. Martins Dos Santos, J.C.L., K.I. Chane-Ching, A. Adenier, L.M. Abrantes, P.C. Lacaze, *Journal of Electroanalytical Chemistry*, (587): p. 67-78.
80. M.B. Gonzalez, S.B.S., *Corrosion Science*, (53): p. 276-282.

81. V. Annibaldi, A.D.R., C.B. Breslin, *Corrosion Science*, (59): p. 179-185.
82. M. Bazzoui, J.I.M., T.C. Reis, E.A. Bazzoui, M.C. Nunes, L. Martins, *Thin Solid Films*, (485): p. 155-159.
83. Mabrouk, P.A., *Synthetic Metals*, (150): p. 101-105.
84. J.P. Correia, M.G., L.M. Abrantes, M.A. Vorotyntsev, *Electrochimica Acta*, (53): p. 1195-1206.
85. M.I. Redondo, C.B.B., *Corrosion Science*, (49): p. 1765-1776.
86. W. Su et al., *J. Elec. Acta*, (46): p. 1-8.
87. A. De Bruyne, J.L.D., R. Winand, *Surface and Coatings Technology*, (99): p. 118-124.
88. L. Haeshin, S.M.D., W.M. Miller, P.B. Messersmith, *Science*, (318): p. 426-430.
89. Waite, J.H., *Nature Materials*, (7): p. 8-9.
90. Y. Sun, M.S.A., I. Zhitomirsky, *Journal of Colloid and Interface Science*, (369): p. 395-401.
91. Y. Wang, I.Z., *Langmuir*, (25): p. 9684-9689.
92. K. Wu, Y.W., I. Zhitomirsky, *Journal of Colloid and Interface Science*, (352): p. 371-378.
93. G.-L. Wang, J.-J.X., H.-Y. Chen, *Biosensors and Bioelectronics*, (24): p. 2494-2498.
94. W. Sun, R.Z., X. Chen, *Journal of Power Sources*, (195): p. 7120-7125.
95. S. Biswas, L.T.D., *Chemistry of Materials*, (22): p. 5667-5671.
96. I. Zhitomirsky, A.P., *Journal of Materials Science*, (39): p. 825-831.
97. I. Zhitomirsky, A.P., *Advances in Colloid and Interface Science*, (97): p. 277-315.
98. K. Grandfield, F.S., M. FitzPatrick, M. Cheong, I. Zhitomirsky, *Surface and Coatings Technology*, (203): p. 1481-1487.
99. L. Vaisman, H.D.W., G. Marom, *Advances in Colloid and Interface Science*, (128-130): p. 37-46.
100. T. Casagrande, G.L., H. Li, J. Wei, A. Adronov, I. Zhitomirsky, *Materials Chemistry and Physics*, (111): p. 42-49.
101. K. Wu, P.I., Y. Sun, X. Pang, A. Adronov, I. Zhitomirsky, *Materials Letters*, (67): p. 248-251.
102. A.R. Boccaccini, J.C., J.A. Roether, B.J.C. Thomas, E. Jane Minay, M.S.P. Shaffer, *Carbon*, (44): p. 3149-3160.
103. K. Esumi, M.I., A. Nakajima, K. Sawada, H. Honda, *Carbon*, (34): p. 279-281.
104. C. Du, N.P., *Nanotechnology*, (17): p. 5314-5318.
105. S. Pei, J.D., Y. Zeng, C. Liu, H.-M. Cheng, *Nanotechnology*, (20): p. 235707.
106. B. Vigolo, A.P., C. Coulon, C. Sauder, R. Paillet, C. Journet, P. Bernier, P. Poulin, *Science*, (290): p. 1331-1334.
107. B. Vigolo, C.C., M. Maugey, C. Zakri, P. Poulin, *Science*, (309): p. 920-923.
108. Y. Gogotsi, P.S., *Science*, (334): p. 917-918.
109. Y. Wang, Q.M.Y., I. Zhitomirsky, *Materials and Manufacturing Processes*, (26): p. 846-854.

- 110. J. Li, Q.M.Y., I. Zhitomirsky, Journal of Power Sources, (185): p. 1569-1574.**
- 111. J. Wang, Y.X., J. Wang, X. Du, F. Xiao, J. Li, Synthetic Metals, (160): p. 1826-1831.**
- 112. R.K. Sharma, A.C.R., S.B. Desu, Electrochemistry Communications, (10): p. 268-272.**
- 113. A.Y. Zaitsev, D.S.W., G.C. Weatherly, T.F. Stephenson, Journal of Power Sources, (123): p. 253-260.**